THE UNIVERSITY *of* EDINBURGH

Protein Crystallisation Using Low-Cost Electric-Field-Assisted Setups for Microbatch, Vapour Diffusion, and In situ Diffraction Studies

Atika Yahya Hamood Al Hasaini

Doctor of Philosophy

The University of Edinburgh

School of Biological Sciences

March 2024

Declaration

I declare that this thesis has been composed solely by myself and that it has not been submitted, in whole or in part, in any previous application for any other awards or qualifications. Except where states otherwise by reference or acknowledgment, the work presented is entirely my own.

Atika Yahya Hamood Al Hasaini

Acknowledgement

First and foremost, I am profoundly grateful to Allah for His endless blessings, guidance, and strength throughout my PhD journey. It is with His grace that I have been able to complete this work.

I would like to express my immense gratitude to my supervisors, Prof. Atlanta Cook and Dr. Norbert Radacsi, for their invaluable guidance, patience, and expertise. Their continuous support and insightful feedback have greatly enriched my academic journey. I send special gratitude for supporting me as a mother during the hard times of the pandemic. I am also thankful to my thesis committee members, Prof. Vasileios Koutsos and Prof. Malcolm Walkinshaw, for their valuable input and feedback. Special thanks to the graduate school administrator, Karen Woodcock, for the always being there when needed.

Thanks to Uma Jayachandran for the technical support in Cook lab and for purifying REMC1 for my experiments. Thanks to Michael Oliver and Gurusaran Manickam for providing purified proteins for my experiments. I also extend my thanks to Ola, Alex, James, Jamilla, Laura, Laurine, Sophie, and David from Cook's lab for the support and fruitful discussions. Thanks to Fergus Dingwall for the technical support and help in the Nanomaterials lab. Thanks to Faraz Fazal for help in 3D printing and to Francisco Javier for help in electrical connections. Thanks to Leyla Altay for her help in data analysis. I extend my thanks to Sakshika, Muhammed, Chiara, Mei, and Lydia from the Nanomaterials lab for their support and fruitful discussions. Thanks to James Sandy from Diamond Light Source for help in XRD studies.

Special Thanks to my husband for his endless support, help, patience, and encouragement throughout my PhD journey. Thanks to my children, Mohriz, Yahya, Nasser, and Ziyad for making my study life joyful and meaningful. Thanks to all members of my family for their love and support and to the soul of my grandmother, who was waiting for this moment, may Allah grant her paradise. Thanks to my niece Aumama for helping with childcare during the pandemic. Thanks to my friends in Oman for always supporting and checking on me. Special thanks to Dr. Muna Al Hinai and Dr. Thurayya Al Hinai for following up with me at every step and listening when I needed to talk.

Special Thanks to my landlords in Edinburgh Jeanette and late Andy Manock, who opened their hearts before their home and showered me with their kindness. Thank you to my beautiful family in Edinburgh, Thurayya, Khaloud, Yusra, Azza, Laila, Muna, Reem, Rawaa, Sakeena, Wasan, Waad, Azhar, Amira, Fatima, Hatham, and Ibtisam, for all the lovely memories we made together, for company at good and hard times, for picnics, road trips, hikes, celebrations, gatherings, and making the abroad life a unique experience. Thank you to the Arab and Muslim community in Edinburgh for making us part of the community and providing support and guidance regarding life in Scotland.

Thanks to the Ministry of Higher Education, Research and Innovation, Oman, for sponsoring my studies and to the Omani Cultural Attaché in London for their continuous support and follow up, especially during the Coronavirus pandemic. Special thanks to the Sector of Research and Innovation in the ministry for supporting my study decision. Thanks to the Welcome Trust for the financial support and to the Diamond Light Source for giving access to the XRD analysis facility.

“And the last of their call will be, "Praise to Allah, Lord of the worlds!"

Yunus (Jonah)10:10, Quran

Abstract

Understanding the molecular structures of proteins is fundamental to elucidating their molecular roles and mechanisms within living organisms. Achieving high-quality protein crystals is essential for successful X-ray crystallography, enabling the determination of protein structures. The efficacy of crystallisation methods directly impacts the physical, chemical, and biological properties of the resulting crystals, highlighting the critical need for precise control over the crystallisation process outcomes. In this thesis, four experimental setups were designed and fabricated using CAD design and 3D printing. These setups allowed the investigation of the effects of electric fields on protein crystallisation employing techniques such as microbatch under oil and vapour diffusion. The influence of the electric field on various aspects of protein crystallisation, including nucleation rates, crystal size, and quality, was analysed using Hen Egg White Lysozyme (HEWL) and previously uncharacterised RNA Editing Mediator Complex 1 (REMC1). The experimental results demonstrated enhanced HEWL nucleation, producing a higher number of crystals with smaller sizes and narrower size distribution when the electric field was applied. This effect was interpreted by modifying the chemical potentials and the diffusion rates in the crystallisation process by the electric field. In addition, HEWL crystals were subjected to in situ X-ray diffraction studies, revealing an enhancement of the internal order of the crystals by electric field. This was evident by the lower mosaic spread and Wilson B-factor, which is attributed to the alignment of molecular dipoles by electric fields, resulting in an enhanced internal lattice order. In contrast, the quality of the REMC1 crystals was not improved noticeably by applying the electric field. This was likely due to the poor intrinsic quality of the crystals. The findings underscore the potential for electric fields to optimise crystallisation processes, offering significant implications for both theoretical understanding and practical applications in fields such as structural biology and pharmaceutical development. The thesis contributes to a deeper understanding of the crystallisation process and opens avenues for advancements in drug design and structural biology research.

Lay Summary

Proteins are unique macromolecules that are essential for living organisms as they regulate biological processes. These molecules are very complex, and to understand how they work, it is essential to determine their three-dimensional structures. Traditionally, scientists use X-ray crystallography to define these structures, which requires creating high-quality protein crystals.

In this research, a new approach was explored to improve the process of growing protein crystals using electric fields. By designing and fabricating four experimental setups, investigating how applying electric fields affects protein crystallisation was carried out, focusing on techniques such as microbatch under oil and vapour diffusion.

The experiments used a commonly studied protein, Hen Egg White Lysozyme (HEWL), and a less studied one, RNA Editing Mediator Complex 1 (REMC1), to analyse how electric fields influence various aspects of protein crystallisation, including the rate of formation, crystal size, and quality. The research discovered that applying an electric field improved the crystallisation of HEWL, resulting in a larger number of smaller, more uniformly sized crystals. This improvement was attributed to changes in chemical potentials and diffusion rates caused by the electric field. Interestingly, the electric field also enhanced the internal order of the HEWL crystals, as seen in X-ray diffraction studies. However, the same approach did not significantly improve the quality of REMC1 crystals.

These findings highlight the potential of using electric fields to optimise the protein crystallisation process, which has significant implications for the fields of structural biology and pharmaceutical development. This research contributes to a better understanding of protein crystallisation and opens new possibilities for advancing drug design and structural biology research.

List of abbreviations

EF	Electric field
HEWL	Hen egg white lysozyme
DC	Direct current
AC	Alternating current
HV	High voltage
CAD	Computer-aided design
3D	Three-dimensional
XRD	X-ray diffraction
DLS	Diamond Light Source
VMXi	Versatile Macromolecular Xtallography *in-situ*
SCXRD	Single crystal X-ray crystallography
SAD	single anomalous dispersion
MAD	multiple anomalous dispersion
PLA	Polylactic Acid

Table of Content

List of Figures

List of Tables

Introduction

1.1. Protein structures and identification methods

1.1.1. Protein structures

Proteins are large and complex biological macromolecules that are vital for biological processes. These molecules are essential for the structure, function, and regulation of cells and tissues in living organisms. They participate in various biological processes, including catalysis, communication, mechanical support, regulation, movement, and transport in cells [1]. Protein functions are encoded in its structure, which is also susceptible to conformational changes [2, 3]. To understand the mechanisms of protein functions in living organisms, it is crucial to determine their structures [4-6].

Proteins are linear polymers with amino acids as building blocks linked together with a peptide bond, a covalent bond between the carboxyl group of one amino acid and the amino group of the adjacent amino acid, making a polypeptide chain [3, 7, 8] (Fig. 1.1). There are twenty common amino acids that are the building blocks of all existing proteins [8]. The sequence of the amino acids in a polypeptide chain is referred to as the primary structure of a protein [7]. As amino acids differ in their side chains, the polypeptide chain is unique for each protein and determines their secondary and tertiary structures [9, 10].

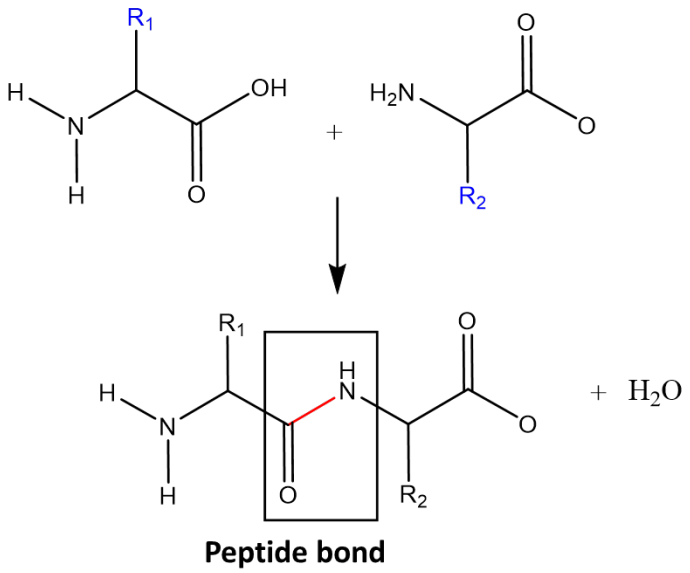

Figure 1.1. The peptide bond formation between two adjacent amino acids. The bond forms between a carboxyl group of one amino acid and the amino group of the adjacent amino acid by removing a water molecule.

A protein's secondary structure is determined by the spatial arrangement of amino acid residues close to each other in a polypeptide chain. Due to the free rotational capacity of the bonds between planar and rigid peptide chain units, these units can align at various angles relative to each other, thereby adopting a multitude of conformations. In addition, intramolecular hydrogen bonds form between the amide hydrogen atom of one peptide unit and the carbonyl oxygen atom of another. These hydrogen bonds give rise to structural formations known as alpha helix and the beta-sheet [10].

In an alpha helix, the structure is defined by a helical shape that is right-handed and stabilised by hydrogen bonds formed between the proton of the N-H group of one amino acid and the oxygen atom of the C=O group of another amino acid in the following turn of the helix. A beta sheet, however, is described by the extended conformation of the polypeptide chain. This structure involves hydrogen bonds between adjacent, fully extended segments, aligning them nearly perpendicular to the chain's long axis, thus forming a beta sheet. Beta sheets are of two types: parallel and antiparallel. In parallel beta-pleated sheets, the C- and N- termini align adjacently, while in antiparallel sheets, they are positioned opposite to each other.

The secondary structures of proteins and their arrangement relative to each other in space determine the features of the tertiary structure of the protein.

The tertiary structure denotes the three-dimensional organisation of the protein molecule [7, 11]. More precisely, it refers to the way in which the secondary components of structure, namely alpha helices and beta sheets, undergo folding and arrangement. The stability of this three-dimensional structure is maintained via a variety of short-range interactions between atoms on the polypeptide chain backbone [12]. These interactions are hydrophobic, hydrogen bonds, ionic interactions, disulfide bridges, salt bridges, and van der Waals interactions [7]. The tertiary structure of a protein is essential for its functionality as it dictates the general conformation and precise locations of functional sites where interactions with other molecules occur [13].

Lastly, the quaternary structure refers to the configuration and interactions of several protein subunits in a single oligomeric protein or several proteins to create a functioning macromolecule [14]. The subunits are held together by hydrogen bonds and van der Waals forces between nonpolar side chains [14]. Figure 1.2 illustrates the four levels of protein structures [11].

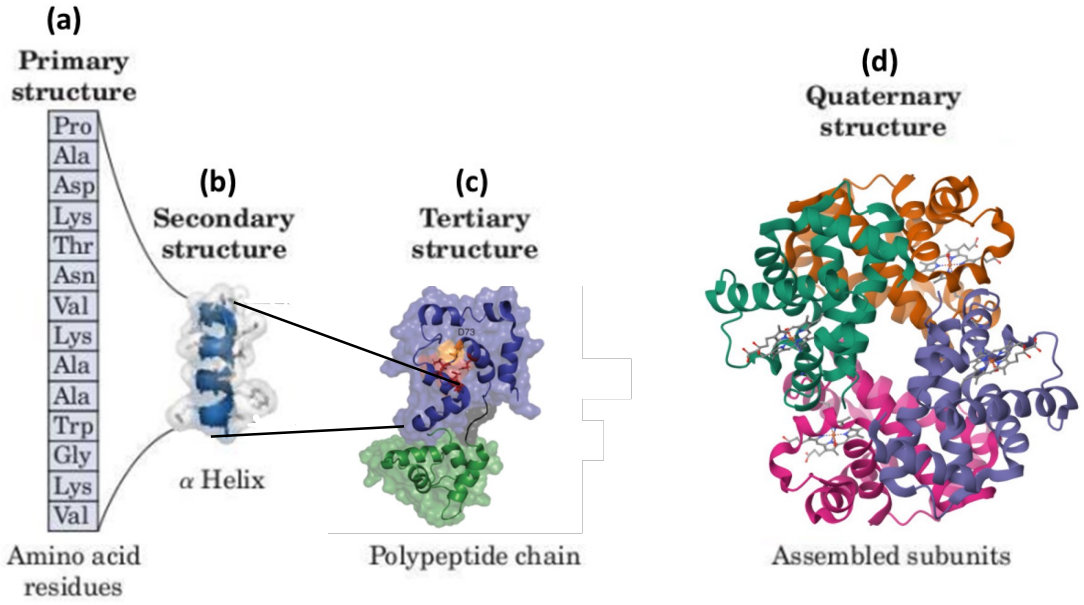

Figure 1.2. The primary, secondary, tertiary, and quaternary structures of a protein (adapted from reference [11]). (a) the primary structure showing the amino acid sequence. (b) the secondary structure showing the spatial arrangements of polypeptide chains. (c) the tertiary structure (F153W Human cardiac troponin C), showing the three-dimensional arrangement of the protein molecule. (d) the quaternary structure (6BB5 Human Oxy-Hemoglobin), illustrating the interactions of several protein subunits.

1.1.2. Crystallography methods for protein structure identification

The binding sites and the nature of a protein's function in a living organism are determined by its tertiary structure, which makes structural identification investigations essential. To date, various methods have been successfully used for protein structure identification, mainly X-ray diffraction (XRD), nuclear magnetic resonance (NMR), and cryo-electron microscopy (cryo-EM), including microcrystal electron diffraction (MicroED) [15]. Moreover, AI-based methods have been recently developed to aid in structural studies using data deposited at the Protein Data Bank (PDB). For example, AphaFold2 program, which uses deep learning to perform protein structure prediction, exhibited exceptional ability to predict the single-chain protein structures [16]. In this chapter, XRD and MicroED diffraction methods are addressed. These methods require high quality crystals to collect high quality diffraction data for atomic resolution structural determination.

1.1.2.1. X-ray crystallography

Protein studies by X-ray crystallography are the most effective structural identification technique [17]. They offers valuable information regarding the overall structure and conformations in protein molecules [18]. X-ray diffraction relies on the principle of the diffraction of X-ray beam when interacting with atoms in a pattern that is related to the protein's three-dimensional structure. However, it requires high quality crystals of appropriate sizes depending on the type of XRD analysis technique.

X-ray diffraction is based on the phenomenon of constructive interference between monochromatic X-rays and a crystalline sample. When the incident rays contact the sample, they create constructive interference and generate a diffracted ray if the conditions meet Bragg's Law. Subsequently, the diffracted X-rays are detected, indexed and integrated, then converted to amplitudes. To achieve all potential diffraction directions of the lattice, one needs to adjust the incident rays, the orientation of the centred crystal, and the detector.

1.1.2.2. Bragg's Law

Bragg's Law explains the relationship between X-ray incidence angles and diffraction by crystal lattice planes, and it serves as a foundation for crystal structure investigation [19]. According to the law, when an X-ray encounters a crystal surface, its angle of incidence, Θ, will reflect with the same angle of scattering, Θ. Constructive interference occurs when the path difference, d, equals a whole number, n, of the wavelength. That is:

$$n\lambda = 2d\ sin\theta \qquad 1.1$$

Where λ denotes the radiation wavelength, d indicates the inter-planar spacing, and Θ represents the angle formed by the incident (or diffracted) ray and the relevant crystal planes.

n is an integer value commonly set to unity and known as the order of diffraction (Fig. 1.3).

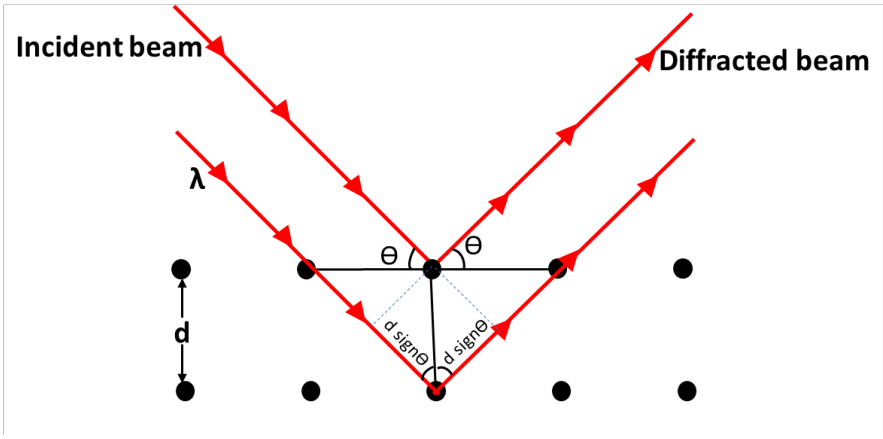

Figure 1.3. Schematic representation of Bragg's law. The distance between the lattice planes is given by d. The X-ray beam is diffracted with the same angle as its angle of incidence (Θ).

1.1.2.3. Micro Electron Diffraction

Micro Electron Diffraction (MicroED) is a new advance in cryo-EM, in which crystals smaller than one micron can give sufficient information to solve the crystal structure using electron diffraction [10, 15, 20, 21]. In contrast to XRD, the crystals are exposed to an electron beam (Fig. 1.4) [15]. The sample stage continuously rotates the crystal throughout the exposure while the data are captured as a movie using a high-speed camera. The camera collects a wedge of reciprocal space within each frame [20]. Thus, MicroED data can be processed to generate 3D models using standard X-ray crystallographic software [15, 20].

Due to the strong scattering of electrons, a submicron-sized crystal is preferred to prevent information loss due to multiple scattering effects. Recent advances in electron diffraction have revealed structures from crystals as small as a few hundred nanometers [22]. In addition, while X-rays provide electron density maps, electrons, being charged particles, can investigate

the electrostatic potential of materials. MicroED allows users to accurately map the charged, electrostatic states of atoms in structures [15, 21].

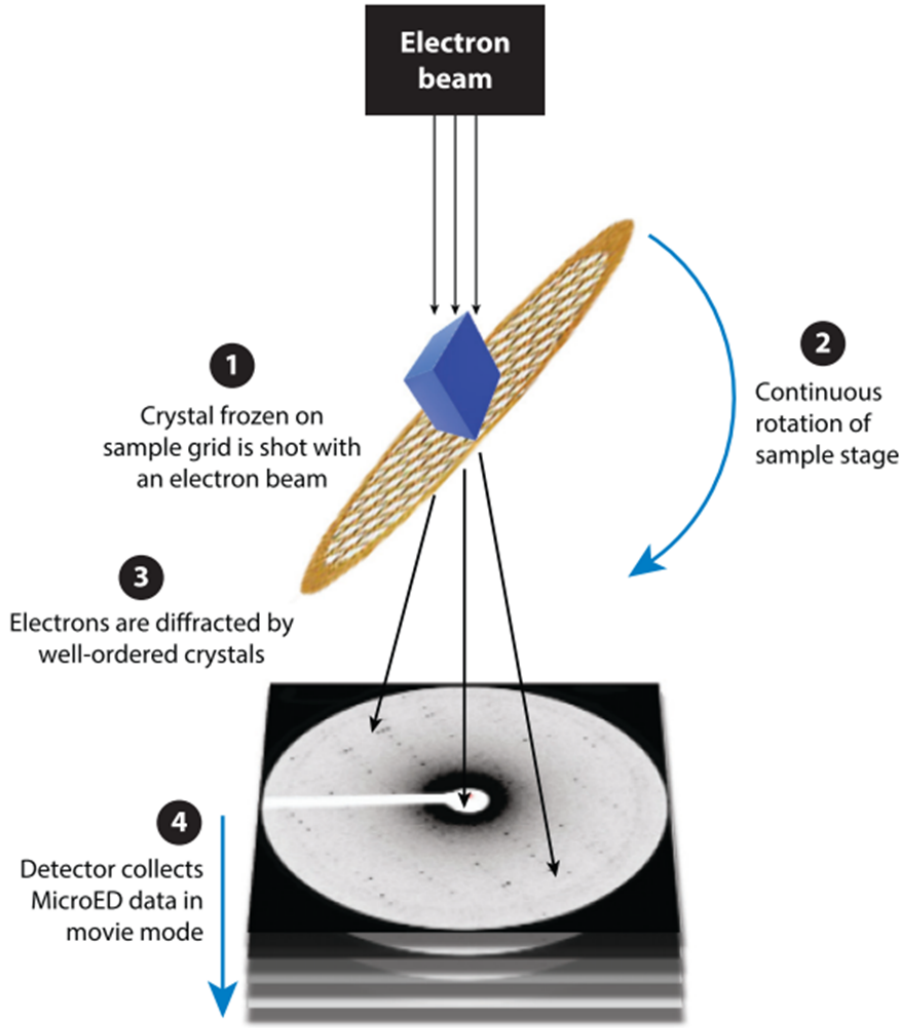

Figure 1.4. A graphical illustration of microcrystal electron diffraction (MicroED) (copied from reference [15]). After the microcrystal is positioned on the sample grid, it is subjected to an electron beam while the sample stage is continuously rotated. The diffraction data are then captured on film using a high-speed camera.

1.2. Crystallography and protein space groups

As various crystallography methods are used to determine the three-dimensional structures of proteins, the precise definition of spatial symmetry and organisation inside crystalline structures, is fundamental.

The core principles of protein crystallography revolve around identifying and describing the symmetry elements present in the crystal lattice. The symmetry elements can include translational shifts, rotational manifestations, mirror-image planes, and inversion centres. The symmetry features of a crystal lattice are concisely described in the space group; for example, the term "$P2_12_12_1$" represents a primitive orthorhombic space group with three perpendicular 2-fold screw axes, which involve rotational along x,y and z axes, in addition to a translation of half the unit cell length along the axes (Figure 1.5).

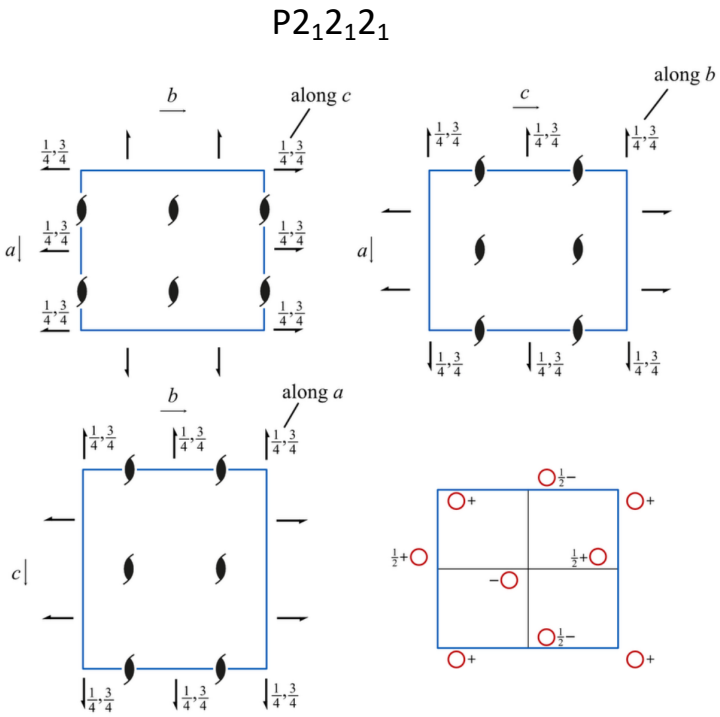

Figure 1.5. A graphical illustration of the symmetry elements of space group $P2_12_12_1$ [23].

The crystal space group significantly influences the crystal diffraction patterns. The symmetry elements in the assigned space group are crucial in determining the intensity and geometrical distribution of diffraction spots on the detector. Accurately interpreting these diffraction patterns relies on the precise determination of the space group [24, 25]. The collection of accurate diffraction data aids in determining the symmetry features of the crystal lattice. Space group identification is crucial in refining and interpreting electron density maps for structural studies [25]. The quality of the electron diffraction pattern is used for accurately positioning the atoms within the crystalline matrix enabling the detailed reconstruction of the three-dimensional protein structure with great precision.

Protein crystals are limited to 65 space groups, compared to the 230 space groups available for combinations of enantiomers [5, 10]. These 65 space groups exhibit some point group symmetries. This is because proteins that make crystal structures are enantiomerically pure, where all the molecules are chiral and contain the same chirality.

1.3. X-ray crystallography data collection methods

Diffraction data are collected using different approaches depending on the experimental setting, the size and number of crystals analysed. These are single X-ray crystallography, serial crystallography and in situ diffraction studies.

1.3.1. Single crystal X-ray crystallography

Single crystal X-ray diffraction is the most accurate and robust method for macromolecular structural studies, where a large, high-quality single crystal is rotated in a beamline while diffraction patterns are collected [26]. Single-crystal X-ray diffraction is an analytical technique offering comprehensive insights into crystalline substances' internal lattice. It reveals precise data such as unit cell parameters, bond lengths, bond angles, and information regarding site ordering.

1.3.2. Serial crystallography

Serial crystallography (SX), whether utilising X-ray free-electron lasers (XFELs) or synchrotron microfocus beamlines, offers a distinct advantage over conventional cryo-crystallography by eliminating the requirement to harvest individual crystals [27]. Instead, several crystals are introduced to the X-ray beam in arbitrary orientations, and a single diffraction image is captured for each crystal during data collection [4, 27]. These images are combined to form a comprehensive dataset to determine the structure. The development of synchrotron radiation allowed diffraction data collection from relatively small crystals with less radiation damage [10, 28].

1.3.3. In situ diffraction studies

Another measure to eliminate the crystal damage is to eliminate the harvesting and cryoprotection steps in the diffraction experiments [28]. The new advancements in synchrotron facilities allow screening and data collection in situ from the crystallisation plates at room temperature [29]. An example of these facilities is the Versatile Macromolecular Xtallography *in-situ* (VMXi) beamline in Dimond Light Source Synchrotron (UK). This beamline is fully automated, allowing remote screening and data collection by users and automated data processing by various programs. The plates are mounted by a robot that enables sample rotation up to 60^{o} [30]. Automated multiplex merging of datasets from numerous crystals allows routine determination of high-quality room temperature structures. It offers information on the diffraction, quality of the crystal, and often the characteristics of the unit-cell and space group. This is applicable even for micro-crystals measuring 10-15 µm, making it a useful tool for selecting and optimizing crystallisation conditions for quality crystals.

1.4. Diffraction studies and crystal quality

Traditionally, the crystals' high quality and large size are the two main features that make successful structural identification by X-ray diffraction. However, with the technical advancement of synchrotron radiation and analysis techniques, structural data can now be obtained from relatively small crystals [5]. Smaller crystals are more likely to have fewer defects and, hence, diffract to a higher resolution. However, they also have fewer unit cells. Thus, a higher X-ray intensity is required to create a measurable diffraction signal. This can result in radiation damage and significant shortening of the crystal lifespan in the beamline [3].

Crystal damage associated with exposure to X-ray radiation is a critical obstacle in crystallography. The primary interactions between the molecules in a crystal and the X-ray beam results in the dissipation of radiation energy through two mechanisms: the generation of heat or thermal vibration of molecules, and the supply of the energy required to break the bonds between atoms within the molecules. The magnitude of this first damage is dependent upon the radiation dosage [31]. Radiation generates reactive radicals in two ways: direct damage to polypeptides and indirect breakdown of a water molecule [31]. Thermal energy facilitates the diffusion of reactive products within the crystal, leading to additional damage known as "secondary" damage [31]. The extent of radiation damage is influenced by both the duration and temperature of exposure.

Using cryoprotectants and flash-cooling the crystals has been an effective method to significantly decrease the secondary radiation damage to the sample during X-ray data collection [5, 31, 32]. This is because most of the solvent free radicals created by incoming radiation have considerably lower diffusion rates at cryotemperatures, which means they do not penetrate the crystal as deeply and do as much damage [31, 32]. In single-crystal diffraction studies, this effect is lower because of the bigger crystal size.

Harvesting the crystals is intrusive and may harm the crystal itself. Additionally, some samples may not withstand the cryocooling procedure [28]. To avoid this, another practice is used to mitigate radiation damage: using lower radiation doses while collecting crystallographic data on multiple crystals at room temperature and subsequently merging them into one integrated dataset. This approach is particularly applicable in serial crystallography and in situ data collection. In these methods, screening crystals for diffraction quality and structure determination is increasingly common, largely because it eliminates the challenging crystal harvesting phase [10].

Many factors govern the collection of diffraction data with high resolution as well as high accuracy and data completeness. By gathering and combining data from multiple crystals, this issue can potentially be resolved; however, if the crystals are not entirely isomorphous (i.e. have the same space group and unit-cell dimensions), the accuracy of the data may once again be compromised [10]. This means that the data collection process involves adjusting the different requirements according to the purpose of the experiment [10].

Only high-quality crystals can be used to generate sufficient datasets for structural determination. Unfortunately, the macroscopic appearance of a crystal does not necessarily correlate with a high diffraction quality [33], so diffraction analysis is the most effective method for evaluating the quality. Well diffracting crystals generally retain good internal order, which can be assessed by the mosaicity and Wilson B factor [34-37].

Mosaicity is a measure of the internal order of a crystal. It occurs when molecules are well-ordered along short-range length scales, but the crystal has some small long-range rotational disorder [10]. In general, protein crystals are not perfect; they exhibit a degree of mosaicity, which means they occur in ordered arrangements with imperfectly aligned blocks [22]. However, higher mosaicity in protein crystals indicates low quality, as it broadens the reflections and reduces their signal-to-noise ratio on the detector [33]. Usually, the larger the crystal size, the higher the mosaicity [8]. Highly mosaic crystals generate diffraction spots that

appear as ellipses and in extreme cases as arcs (Fig. 1.5) and can continue over several successive diffraction images, causing challenges with collecting and processing data [10].

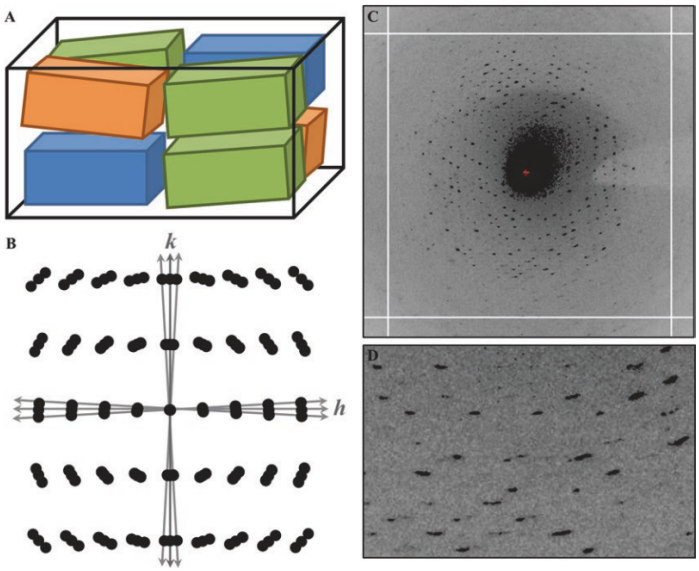

Figure 1.6. Effect of mosaicity in diffraction patterns (copied from Reference [10]). (A) In a mosaic crystal exhibiting short-range order but some long-range disorder, the black line defines the outer edge of a macroscopic crystal, while the individual mosaic domains are illustrated using various colours as minor rotational offset between different domains caused by mosaicity, (B) the influence of crystal mosaicity on X-ray diffraction images, (C, D) show actual diffraction images from a highly mosaic crystal exhibiting arc-like reflections.

Alternatively, one can assess crystal quality using the Wilson B-factor, which measures the average atomic displacement caused by thermal motion or disorder in a crystal lattice [18]. It indicates how the electron density is distributed around the mean atomic locations. It is usually estimated from the slope of a Wilson plot (Fig. 1.6). To get the Wilson plot, Brag intensity is given by [38]:

$$Y = [\,\langle I_{obs}\,(hkl)\rangle\,/\,\textstyle\sum_j f_j^2] = k\exp\left(-2B\,\frac{sin^2\theta}{\lambda^2}\right) \qquad 1.2$$

Where B is the B-factor, λ is the wavelength, Θ is the Bragg angle and k is a constant. The B-factor is obtained by re-writing the equation as follows [38]:

$$\ln(Y) = \ln(k) - 2B\,\frac{sin^2\theta}{\lambda^2} \qquad 1.3$$

The Wilson plot is a plot of ln(Y) against (sin Θ/λ)^2. When the slope of the Wilson plot is small (i.e. small B-factor), the crystal is of good quality and high resolution data are collected.

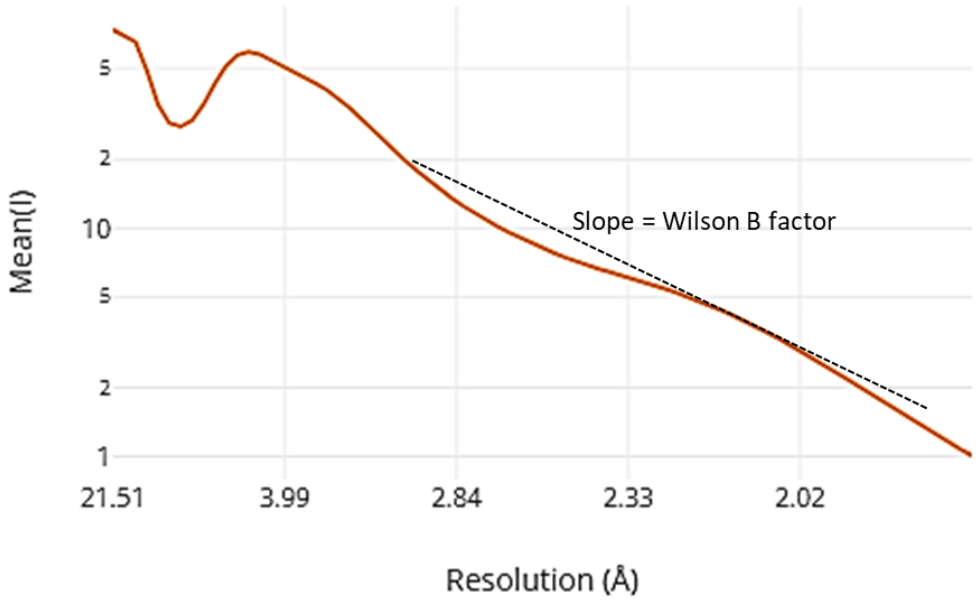

Figure 1.7. Wilson intensity plot. The Wilson B factor is estimated from the slope of the curve. The plot is from XRD data obtained from this research for hen egg lysozyme.

Higher resolution is required for more detailed structural information about the atomic arrangement in a protein crystal. Resolution refers to the shortest distance between crystal lattice planes (given by Bragg's law, equation 1.1) that can be resolved in a diffraction pattern [39]. Although larger crystals often diffract at high resolution due to the higher number of diffracting planes, size is not the ultimate factor affecting crystal quality.

1.5. Phase diagram and nucleation theories

Crystallisation has been described as the bottleneck of structure determination of proteins due to the difficulty of obtaining high quality crystals for diffraction studies [3, 5, 6, 19, 33,

40-42]. Proteins in solution form a complex colloidal system with a diverse spatial structure, many active sites, and conformational flexibility, which make it difficult to establish a highly ordered arrangement of protein molecules in crystalline states [43]. Various methods are currently used to produce high quality crystals.

The crystallisation process involves two steps, nucleation and crystal growth [43], and several theories have been proposed to explain the mechanism of the process. The most common theories are the classical and the non-classical nucleation theories. In general, the nucleation starts when a system overcomes a specific energy barrier.

1.5.1. Classical nucleation theory

Classical nucleation theory involves the spontaneous random aggregation of species from liquid or solution to form stable critical nuclei or clusters [44], allowing them to overcome the energy barrier of the cluster formation [43]. Atomic or molecular attachment then forms a solid crystal structure. The change in the free energy of the system, ΔG, is given by:

$$\Delta G = \frac{i4\pi r^3}{3\upsilon} KT \ln S + 4\pi r^2 \sigma \qquad 1.4$$

In the first term, the contribution to ΔG is represented by the number of molecules in a cluster of radius r, with the volume of a single molecule as υ, and S is the vapour supersaturation ratio. In the second term, the contribution is related to the σ, which is the specific surface energy of the interface between the drop and the surroundings. This means an increase in the nucleus radius r in the first term increases the energy barrier. However, a higher r in the second term decreases the energy barrier (Figure 1.7) [45]. Differentiating the equation with respect to r gives the maximum energy barrier of nucleation:

$$\Delta G^* = \frac{16\pi\sigma^3\upsilon^2}{3K^2T^2 \ln S^2} \qquad 1.5$$

The nucleation rate is given by:

$$J = A\, exp\left[-\frac{\Delta G^*}{KT}\right] \qquad 1.6$$

Substituting the energy from equation 1.5 into equation 1.6 gives the rate of nucleation as follows:

$$J = A\, exp\left[-\frac{16\pi\sigma^3 v^2}{3K^3T^3(\ln S)^2}\right] \qquad 1.7$$

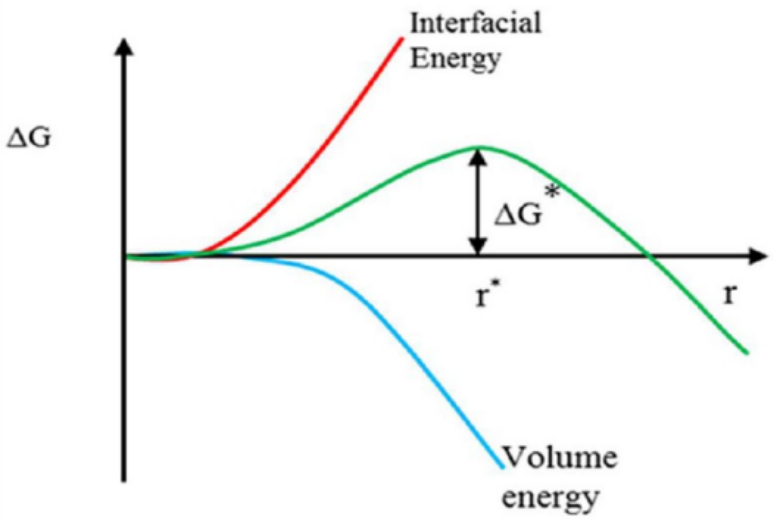

Figure 1.8. A graphical illustration of the nucleation free energy according to the classical nucleation theory (copied from reference [45]). It illustrates the contribution of favourable volume energy and the unfavourable interfacial energy on the nucleation free energy (ΔG*) at the critical nucleus with radius r*.

1.5.2. Non-classical nucleation theory

The second most common theory of nucleation is the non-classical or the two-step theory. In this theory, the nucleation process in solution crystallisation progresses through intermediate stages before reaching a thermodynamically stable phase [43, 45]. The process is considered to undergo two steps towards nucleation; the first step is the production of dense liquid

droplets, known as clusters, caused by density fluctuations or phase separation. The second step is the formation of crystal nuclei due to the structural ordering of molecules [45]. The non-classical approach is preferred when the combined energy barriers in the two-step nucleation process are lower than the energy barrier of classical nucleation theory [45]. The nucleation rate is given by:

$$J = \frac{K_2 C_1 T \exp(-\Delta G_2^* / K_B T)}{\eta\,(C_1,T)\left[1+\frac{U_1}{U_2}\exp\left(\frac{\Delta G_c^*}{K_B T}\right)\right]} \qquad 1.8$$

Where ΔG_2^* is the nucleation energy barrier in the clusters, C_1 is the concentration of the protein in the clusters, η is the viscosity inside the clusters, and U_1 and U_2 are the effective rates of decay and formation of clusters [45].

1.5.3. Phase diagram and crystallisation techniques

To get further insights on understanding the crystallisation process and its dependence on the solution conditions, the protein phase diagram is illustrated in Figure 1.8. The crystallisation process involves two main steps: nucleation and crystal growth [40]. Nucleation is described by the aggregation of single molecules in a supersaturated solution. At very high supersaturation, the protein solubility decreases rapidly, resulting in precipitation to an amorphous solid. At intermediate supersaturation (nucleation zone), nucleation and crystal growth can occur; however, at low supersaturation, only crystal growth is expected [40].

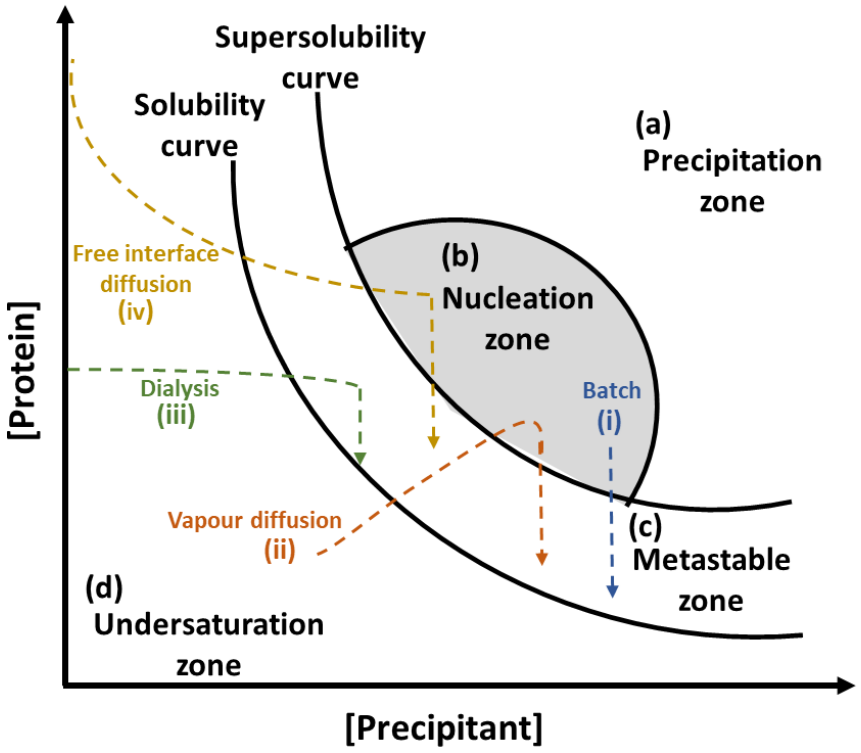

Figure 1.9. The phase diagram of protein crystallisation [42]. (a) is the high supersaturation zone, where precipitation occurs; (b) is the nucleation zone, where nucleation and growth are initiated; (c) is the metastable zone, where the growth of pre-existing crystals occurs; and (d) is the undersaturation zone. The route of reaching the metastable zone in (i) batch crystallisation method, (ii) vapour crystallisation diffusion, (iii) dialysis crystallisation method, and (iv) the free interface diffusion crystallisation method.

After the formation of the nuclei, the protein concentration in the mother liquor decreases slowly, forcing the process into the metastable zone, where the protein solution is supersaturated but unable to form crystals indefinitely [46]. This region is called the "metastable" zone and commonly involves the growth of pre-existing crystal nuclei without an additional crystal nucleation [43]. Regulating the rate of protein crystal growth at a slower pace holds great potential for growing single crystals with better diffraction quality [43]. Additionally, the slower progress of mass transport aids in achieving a more ordered assembly and prevents crystal plane defects. Capillaries, gels, and membranes are currently employed as strategies to decelerate mass movement. In addition, microgravity and magnetic forces have been suggested to mitigate buoyancy-driven convection by shielding the effects of gravity.

Several methods have been used to crystallise proteins, where nucleation and growth are reached by different routes (Figure 1.8) [42]. The two most used techniques for protein crystallisation are the batch and the vapour diffusion methods. In the batch method, the protein and precipitant solutions are mixed at the supersaturation level (nucleation zone), where the nucleation is initiated, followed by a decrease in supersaturation to reach the metastable/ crystal growth zone. Conversely, in the vapour diffusion method, the protein and precipitant are mixed at undersaturation conditions. This is followed by an increase in the concentration due to diffusion until the system reaches the nucleation zone and, eventually, the metastable zone (Figure 1.8) [42].

1.6. Electric-field-assisted crystallisation

Crystallisation is the most challenging step in protein structural studies. Therefore, precise control of the crystallisation process outcomes, such as the degree of crystallinity, polymorphism, crystal size, and crystal quality, is essential due to its effects on the crystals' physical, chemical, and biological properties [47]. The ability to control the crystallisation process can aid in producing large, highly diffracted crystals for the structure determination of new proteins. In addition, suppression of crystallisation can be helpful in many applications, such as food freezing, where smaller ice crystals are desired for enhanced food preservation [48]. Several strategies, such as additives and external forces, have been used to control the crystallisation process.

Additives typically alter the chemical conditions of protein crystallisation, whereas external forces such as magnetic fields, electric fields, ultrasound fields, shear, and light fields produce specific effects on protein crystallisation by introducing physical or chemical interactions or providing significant energy [43]. The impact of external electric fields on protein crystallisation was introduced in the late 1990s and has since demonstrated significant

advancement in its exceptional regulating function within the protein crystallisation process. Many groups have utilised electric fields to enhance crystallisation [34, 36, 47, 49-71].

1.6.1. Theoretical aspects of electric field crystallisation

It has been demonstrated that applying an electric field during the crystallisation of proteins affects the crystallisation outcomes by influencing the chemical potentials of the liquid and solid phases.

When the electric field of strength *E* is applied to a molecule in an *i*th phase, the chemical potential of this phase is given by [72]:

$$\eta_i\,(P,T,E) = \eta_i^0\,(P,T) + U_i\,(E) \qquad 1.9$$

Where, η_i^0 (*P, T*) is the chemical potential in the absence of electric field, *P* and *T* are the pressure and temperature during the electric-field-assisted crystallisation, and $U_i\,(E)$ is the energy of a molecule in the *i*th phase under the influence of an electric field.

The chemical potential of a *j*th species in the liquid and solid phases η_L^j and η_S^j respectively are given by [73]:

$$\eta_L^j = \eta_{0L}^j + RT\ln(\gamma_L^j\,\eta\,X_L^j) + N_A\,z_L^j\,e\phi_L + \frac{1}{2}\,\Omega_L^j\bar{E}_L^2\,\frac{\partial\varepsilon_L}{\partial X_L^j} \qquad 1.10$$

$$\eta_S^j = \eta_{0S}^j + RT\ln(\gamma_S^j\,\eta\,X_S^j) + N_A\,z_S^j\,e\phi_S + \frac{1}{2}\Omega_S^j\bar{E}_S^2\,\frac{\partial\varepsilon_S}{\partial X_S^j} \qquad 1.11$$

Where, η_0^j is the chemical potential in the absence of an electric field, *R* is the gas constant, γ^j is the activity coefficient, X^j is the mole fraction of the concentration, N_A is Avogadro's number, z^j is the valence of the ion, ϕ is a local potential, *E* is the strength of the external electric field, Ω^j is the molar volume and ε is the electrical permittivity.

In these two equations, the second term is a mixed energy term, the third term is the charge potential, and the fourth term is the energy modified by the electric field with respect to the concentration of the j^{th} species. In conclusion, the electric field affects and modifies the chemical potentials of the two phases, affecting the equilibrium state [73].

In addition, electric fields affect the entropy of a crystallisation process; the modified entropy is given by [65, 74]

$$S_{\delta(E)} = S_{\delta(0)} - \frac{1}{2} V_{C\delta} \bar{E}_{\delta}^{2} \frac{\partial \varepsilon_{\delta}}{\partial T} \qquad 1.12$$

Where $S_{\delta(E)}$ is entropy modified by the electric field for δ phase, δ is L or *S* for liquid and solid phases respectively, $S_{\delta(0)}$ is the entropy without electric field, $V_{C\delta}$ is the volume of the δ phase, $\partial\varepsilon_{\delta}$ is the electrical permittivity for the δ phase and *T* is the absolute temperature.

The electrical permittivity difference between the solid and the liquid phases is key to determining whether the electrostatic energy added to the system is larger in the liquid phase [65, 74]. The conservation of dielectric flux at the solid-liquid interface:

$$\varepsilon_L E_L = \varepsilon_s E_s \qquad 1.13$$

Thus, the effect of the electric field is larger on the entropy of the solid if $\varepsilon_L \gg \varepsilon_s$ as $E_L \ll E_s$. If the electric field decreases the entropy of the solid phase, this can lead to imperfections of the crystals associated with the order of the water molecules in the protein crystals [65, 74]. It has been determined that the crystal quality of proteins is correlated with the arrangement of water molecules on their surface [75].

1.6.2. Techniques and setups for electric-field-assisted crystallisation

Electric field effects on crystallisation have been studied in two configurations. When the electrodes are in direct contact with the crystallisation solution, it is called an internal electric field. In contrast, when the electrodes are not in direct contact with the solution, it is called an external electric field [43, 60, 62, 70, 76]. Both direct current (DC) and alternating current (AC) electric fields have been used [49, 70]. DC field strengths ranging from $4.0 \times 10^6 - 2.0 \times 10^7$ V m^{-1} and AC with ~2 to 9 MHz frequency and field strength up to 10^4 V m^{-1} have been used to facilitate crystallisation [77].

Many research groups have used external electric fields to enhance crystallisation, where high potentials are applied (10^3 - 10^5 V m^{-1}). In contrast, relatively lower potentials are used when internal electric fields are applied (as low as 0.13 V m^{-1}) [77, 78]. This was explained by the relatively higher effect of the internal electric fields due to the absence of dielectric media that is present when external electric fields are used [51]. Fewer studies have applied the internal electric fields in the crystallisation process because of electrochemical reactions occurring on the electrodes, which can be enhanced by the presence of the salt/precipitant ions [78]. A recent study showed that a weak internal DC electric field (0.13 V m^{-1}) strength applied uniformly for about 90 min mechanically unfolded the protein, facilitating amorphous aggregation. This dense state of molecules is featured with no tertiary structure, reduced α-helices, and excess β-structures compared to their native state [77].

Several crystallisation techniques have been used to study the effect of the electric field; these include vapour diffusion, microbatch, microfluidics, and gel acupuncture. Vapour diffusion methods have been used by the Aubry [51, 52] and Nanev groups [53, 55], whereas the Koizumi group used microbatch under oil [63, 65, 79]. Although vapour diffusion is known as the standard method for crystallisation experiments, the micro batch-under-oil method is currently attracting a lot of attention due to the very low volumes of proteins and precipitants used and the effect of oil in the nucleation, growth, and stability of the resulting crystal [80].

Electric-field-assisted crystallisation has also been investigated in continuous flow experiments [67, 81]. In 2018, Li et al. designed a novel device for protein separation and purification by continuous flow with the aid of an electric field [67]. Hirao et al. designed an innovative microfluidic device that facilitates the enhancement of protein crystal nucleation, real-time monitoring of protein crystallisation progress, and subsequent analysis of crystal structure [81]. The device tests the effect of electrically stimulating protein microbubbles on the crystallisation outcomes, promoting protein crystallisation [81].

1.6.3. Effects of electric fields on the crystallisation of proteins

To date, previous studies have reported the effects of electric fields on different aspects of crystallisation, namely, the nucleation rate, the size, number, and orientation of crystals, the quality of the crystals, and crystal location.

1.6.3.1. Number and size of Crystals

Several studies have used electric fields to control the size and number of crystals. Due to the importance in traditional single-crystal diffraction studies, the production of larger and fewer crystals was the main focus of many research groups. In 1999, Taleb et al. first attempted to study the effect of an electric field on protein crystals [51]. They observed that HEWL crystals grown under the influence of an external DC electric field are fewer and larger than those grown without the application of an electric field [51].

Al-Haq et al. observed fewer crystals per drop and a larger size of HEWL crystals under the influence of the electric field [60]. Similar results were found by Flores-Hernández [82], who found that the size of lysozyme crystals formed on the cathode was more significant than

those formed on the anode or in the absence of an electric current. Rubin et al. used an external electric field to enhance the size of crystals and reduce nucleation [36].

The larger crystal size produced by applying an electric field was explained by the production of a large protein concentration gradient by an electric field, leading to local supersaturation in the protein solution. An electric field creates a potential difference between the electrodes, facilitating the movement of anions from the precipitating agent and promoting early interactions with protein molecules in solutions. Subsequently, the electric double layer counterions will be a foundation for protein molecules or nuclei with a positive charge, facilitating the crystal's growth on the anode [61].

In addition to pure electric fields, some studies investigated the coupling effect of magnetic and electric fields [37, 58]. Sazaki et al. established a setup to control the number and size of crystals and the homogeneity in crystal size [58]. They found that applying an electric field coupled with a magnetic field decreased the number of crystals produced compared to a pure magnetic field [58]. Similar results were found by Pareja-Rivera et al. [37]. The studies interpreted the large crystal size by the magnetic field's enhanced alignment of protein molecules and the reduced natural convection by the magnetic field opposite to the gravitational force [37].

Contrary to the previously mentioned results, Li et al. observed a larger number of crystals with electric field assisted protein crystallisation in continuous flow [67]. This was explained by the effect of convective transport of impurities and the solute under forced solution flow, leading to restricted crystal growth compared to batch experiments [67]. Li et al. found that applying an electric field in continuous flow also produces a higher number of smaller crystals, which is required in specific applications such as seeding [67].

1.6.3.2. Crystal Quality

Investigations on the effect of electric field on crystal quality have revealed that electric fields led to higher crystal quality. For instance, Taleb et al. observed an improved quality of lysozyme crystal when an electric field was applied by measuring the width of rocking curves [51]. Rocking curves measure the broadening of diffraction peaks, which could be caused by the increased mosaicity or strain in the crystal or the limited layer thickness in the unit cell. The width of rocking curves was found to decrease on average when the electric field was applied [51]. A similar result of crystal quality enhancement by AC electric field was found by Koizumi et al., which was proved by the smaller X-ray diffraction rocking curve measurement of HEWL crystals at optimum frequency [74, 83, 84].

Rubin et al observed enhanced quality glucose isomerase crystals when an external DC electric field was applied, which was indicated by the lower mosaicity and higher resolution of the crystals [36]. Flores-Hernández et al. also observed a better X-ray diffraction pattern of 2TEL–lysozyme (a synthetic protein comprised of a lysozyme moiety connected to two tandem alpha helix motifs) crystals grown under an electric field with a larger number of well-defined signals (diffraction spots), indicating an improved crystal packing [82].

In opposition to these findings, Nanev et al. found that a rough crystal morphology sometimes appears at 0 ^{o}C [53]. This observation was explained by the strain arising due to the nucleation at low temperatures, which affects the crystal quality. They also found that the strain relaxes when the electric field is turned off, and the temperature increases [53].

1.6.3.3. Concentration gradient and crystallisation location

Taleb et al. proved that a local supersaturation is produced in the crystallisation system due to a concentration gradient introduced by the external electric field [51]. In a later study, they

investigated the effects of the electric field on lysozyme concentration in the absence of salt at the cathode and the anode sides of the protein drop [52]. It was observed that the concentration gap between the two electrodes increases in the presence of the electric field, favouring the cathode.

As highlighted by Taleb et al. study, the effect of electric field on the crystallisation depends on the isoelectric point (PI) of the proteins and the experimental conditions. For example, at low pH, lysozyme (PI = 11.1) retains an overall positive charge, therefore, its crystals tend to grow closer to the cathode. This is due to the electromigration of positively charged protein molecules from the anode side to the cathode side [52]. Koizumi and colleagues also observed that lysozyme crystals grow closer to the cathode electrode due to its overall positive charge at acidic experimental conditions [53].

Moreover, it was found that, as the ionic strength of the precipitant increases, the concentration variations between the two electrodes are reduced. In addition, the crystallisation is favoured at a pH far from the isoelectric point of the protein [52]. Koizumi and colleagues also observed that lysozyme crystals grow closer to the cathode electrode due to the overall positive charge of the protein molecules [53]. However, previous research has not focused on the effect of EF on the crystallisation of proteins with different isoelectric points.

1.6.3.4. Orientation of crystals

Nanev et al. studied the effect of the external electric field on the orientation of lysozyme crystals relative to temperature [53, 55]. The lysozyme crystals grown under the electric field exhibited a preferred c-axis orientation normal to the glass support [53, 55]. This was explained by the large dipole created by the electric field transforming the charge on the protein molecules. The dipole-dipole interactions cause the c-axis orientation to predominate

[53, 55]. Moreno and coworkers have studied the internal electric field effect in the orientation of lysozyme crystals using the gel-acupuncture method and found that crystals grow in a preferred orientation towards the cathode [78].

1.6.3.5. Nucleation rate and nucleation time

The effect of electric fields on the nucleation rate has been investigated. Koizumi et al. observed an increase in the nucleation rate of porcine insulin [65]. In another study, Koizumi claimed that the nucleation rate can be either decreased or increased by applying the AC field with different frequencies [63]. Also, several studies have found that the nucleation time is reduced when an electric field is used [51, 78, 82, 85, 86].

1.7. Applications of electric-field-assisted crystallisation

Crystallisation is one of the most effective techniques for structural studies of proteins and macromolecules [17]. Protein structure data is a crucial resource in molecular biology for precisely understanding biological processes and conducting rational drug design [43]. Moreover, protein crystallisation can potentially emerge as a significant purification technique for producing protein-based drugs in future years. This is because crystallisation is crucial in enhancing the effectiveness of drug preparation processes such as separation and preparative purification [43, 87].

However, crystallised protein drugs provide favourable characteristics such as exceptional stability and purity, the capacity to control the release of therapeutic effects, and the concentrated biopharmaceutical dosage [43]. The growing use of protein crystallisation requires the precise management of protein crystals to facilitate additional improvements.

The control of crystallisation using electric fields has been used in several applications, depending on the desired crystal size and morphology. For instance, in the food industry, small-sized ice crystals can be produced in the presence of electric fields, resulting in less freeze damage. Thus, freezing under a static electric field can minimise cell disruption, reduce drip loss, lessen protein denaturation, and preserve the fresh food's texture after thawing [88].

Also, electric field may improve the homogeneity in crystal size and produce smaller size crystals favoured for diffraction studies using the MicroED method. MicroED method enables a fast and precise determination of the structures of proteins at a high resolution using much smaller crystals compared to X-ray diffraction [20, 89].

1.8. Challenges and gaps

Several studies revealed the effect of electric field on the crystallisation of proteins. However, due to its complexity, the mechanism of the electric field effect on the phase behaviour of proteins phase is still poorly understood. As proteins are large and complex biomolecules with heterogeneous and dynamic structures and conformations [90], assembling these molecules to form crystals involves decreased mobility and freedom in the system and, thus, entropy loss. In addition, protein crystallisation is sensitive to many factors, such as temperature, pH, ionic strength, and type of precipitant, which interact differently with the application of an electric field [4]. Only few studies investigated the effect of the electric field at varying experimental conditions on the number, sizes and quality of protein crystals.

In addition, several experimental setups have been used to study the effect of electric field on the crystallisation outcomes, which primarily involve the design of new crystallisation substrates or plates with either one or few experimental conditions to be used at a time and minor consideration of real-time monitoring. Moreover, only few studies highlighted the

effect of the electric field on the quality of the crystals, and none utilised in situ diffraction studies to avoid the effect of crystal handling.

1.9. Objectives of the research

- Designing, fabricating, and testing several low-cost experimental setups using computer-aided design (CAD) and 3D printing for microbatch and vapour diffusion electric-field-assisted protein crystallisation.
- Investigating the effect of direct current (DC) external electric field at different polarities and configurations on the crystallisation of (HEWL).
- Studying the effect of varying experimental conditions such as pH, protein and precipitant concentration and high voltage polarity on crystallisation outcomes of HEWL.
- Designing and validating an experimental setup for the investigation of the effect of electric field on HEWL and REMC1 crystal quality using in situ macromolecular crystallography (vMXi)
- Understanding the phase behaviour of proteins and the mechanism of their nucleation and growth under the effect of electric field.

Electric-field-assisted microbatch crystallisation setup

2.1. Introduction

Batch crystallisation is the oldest, most reliable, and well-characterized method of crystallisation, which was mainly used as a purification method in large-scale and industrial applications [91]. Over time, the technique was modified for low amounts of protein or macromolecules and became an efficient crystallisation techniques [91].

The microbatch under-oil technique has been used to crystallise a wide range of proteins, producing high-quality crystals using low volumes of proteins [92]. This technique uses oil as an inert sealant where protein and precipitant mixture droplets are dispensed under the oil [92]. This means that the protein and precipitant solution are mixed at their supersaturation concentration, and the concentration should be constant throughout the crystallisation experiment [93]. In contrast, in vapour diffusion trials, the droplet is initially under-saturated, and due to diffusion, equilibrium is reached sometime after mixing [80].

Depending on the type of oil used in the microbatch method, there is an extent of diffusion of water molecules out of the crystallisation droplet. Three types of oil have been used in microbatch experiments: paraffin, silicone, and a mixture of the two (known as Al's oil). Paraffin oil allows minimum or no diffusion of water molecules, whereas silicone oil can diffuse oil through it and dry out quickly. To control the rate of diffusion, different ratios of the two oils (paraffin and silicone) can be used to regulate the extent of diffusion of water

molecules. Using the mixture of oils can lead to the crystallisation of proteins in a short time compared to using paraffin oil only.

A different approach, the containerless crystallisation technique, is used to prevent contact between the crystallisation drop and the surface and walls of the container [80, 94-96]. This technique uses two types of oils with different densities, and the crystallisation droplet is dispensed at the interface between the two oil layers [80, 96]. It has been reported that fewer crystals were produced when the containerless technique was used [96].

Another way of controlling the microbatch-under-oil technique is to use a thin layer of oil, and as the protein starts to crystallise, another layer of oil is applied to prevent the droplets from drying out. This technique can avoid the occurrence of shock nucleation, which is caused by high concentrations of the protein or the precipitant [80].

Batch techniques have been used to study the effect of electric field on protein crystallisation. In 2007, Al-Haq et al. studied the impact of electric field on the crystallisation of hen egg white lysozyme (HEWL) and thaumatin using the microbatch under-oil technique [60]. They fabricated a device using a low-cost plastic tray to crystallise proteins under a layer of paraffin oil. Crystallisation of HEWL resulted in fewer crystals when a DC electric field was applied [60].

Koizumi et al. used the batch method to investigate the effect of external AC fields on the nucleation rate, crystal quality, and crystallisation kinetics [74, 83, 84, 97, 98]. They also used the containerless batch method, where a crystallisation drop is suspended between two oils of different densities [63, 79, 99]. They applied the external DC field to study its effect on HEWL crystallisation and external AC to control the rate of nucleation [63, 79]. The results showed a higher effect of the electric field on the nucleation rate when a higher concentration of precipitant is used, which suggested that the thickness of the electric double layer at the inner surface of the drop is dependent on the type and ionic strength of the precipitant.

Another device was designed by Rubin et al. for external DC microbatch crystallisation, which consists of two copper electrode plates fixed at the bottom and the top of a microbatch crystallisation plate and connected to a DC power supply [36]. They studied the effect of electric field on the crystallisation outcomes of glucose isomers using the microbatch technique, which resulted in increased size and quality of the resulting crystals [10].

Studies on the effect of the electric field on crystallisation involved the development of new crystallisation platforms, and often, these are limited to a few experimental conditions. Due to the nature of electric field and the stochasticity of the crystallisation process, a broader range of experimental condition in addition to the ability to replicate these conditions is essential.

In this chapter, a new device is designed using the CAD design and 3D printing to allow the study of electric field effect on HEWL crystallisation without modifying the crystallisation plate. The device allows multiple conditions to be used concurrently while monitoring the experiments in real-time.

2.2. Materials and methods

2.2.1. Materials

HEWL was purchased as a crystallisation kit (Hampton Research, UK), which contains 12 vials of 20 mg HEWL lyophilized powder and 12 vials of 1.0 mL Sodium acetate trihydrate (0.02 M, pH 4.6) (solubilization buffer). The HEWL working solution (20 mg mL^{-1}) was prepared by mixing the buffer with the protein powder and gently rocking the solution at room temperature. Sodium acetate buffer (0.1 M) was prepared by dissolving 13.6 g sodium acetate tetrahydrate in 50 mL Milli-Q water and adjusting to the desired pH with acetic acid. The solution was diluted to 100 mL and filtered using a 0.22 µm syringe filter. Sodium chloride solution (5 M) was prepared by dissolving 29.2 g of sodium chloride salt in 80 mL Milli-Q water,

making up to 100 mL, then filtered using a 0.24 µm syringe filter. The 5 M NaCl solution is used as a stock solution for further dilutions.

$REMC1_{100\text{-}525}$ (clone number: MRO 029), was obtained as frozen aliquots (50 mg mL^{-1} in 50 mM Tris pH 8, 250 mM NaCl) and diluted further to the desired concentrations. 1M solution of Tris-HCl buffer was prepared by dissolving 12.1 g of Tris base (Sigma Aldrich) in 80 mL of distilled water, adjusting the pH to 8.0 using HCL (Fisher Scientific UK Ltd) and adjusting the volume to 100 mL with milli-Q water. Precipitant solutions (600 and 900 mM) are prepared by dissolving the $MgSO_4$ (Fisher Scientific UK Ltd) in Tris-HCl (0.1 M, pH 8.0) buffer at the desired concentration. The protein was screened at different concentrations (50, 37.5, 31.25, 25 and 18.75 mg mL^{-1}) using the microbatch under-oil crystallisation technique. All crystallisation trials were performed using paraffin oil (Molecular Dimensions, UK). The wells are filled with the oil before the crystallisation droplets (2 + 2 µL) are infused.

Paraffin oil and mineral oil (Molecular Dimensions) were used without further processing. All the microbatch crystallisation experiments were performed in Greiner microbatch 72 well plates (Hampton Research, UK). The plates were air dusted, and the desired wells were covered with paraffin oil. The crystallisation droplet was dispensed under the oil by pipetting 1 µL of the precipitant solution followed by 1 µL of protein. Extra oil was dispensed on the plate to fully seal the wells. The plate was then positioned on the electrodes inside the setup, and the setup was covered with the glass plate and secured with screws. In each experiment, a control experiment was prepared to compare the outcomes, and due to the stochastic nature of the experiments, each experiment was repeated 4-5 times for statistical data collection.

2.2.2. Methods

2.2.2.1. The experimental setup

The experimental setup was designed using a CAD design software (Solid Edge, 2019), and the main part was printed with 2.85 mm polylactic acid (PLA) filament material (Ultimaker, The Netherlands). The visualization plates were made of clear annealed glass (3 mm thick, Edinburgh Stained Glass House, UK). The electrodes were made of single-core copper wire (0.87 mm diameter, RS PRO, UK) and connected to the high-voltage power source via high-voltage cables (22 AWG, 40 kV, 4.76 mm diameter, China).

High voltage was applied using two power supplies (Mirion Technologies, CANBERRA UK Limited). For positive polarity, a USB high voltage power supply (CAEN, DT5470P, +5 kV/ 200 µA, 1 W max) was used, whereas for negative polarity, a USB high voltage power supply (CAEN, DT5471N, -3 kV/500 µA, 1 W max) was used. The power supplies were controlled using software provided by the supplier. An electric field ranging from 2-4 x 10^5 V m^{-1} was applied for 48 hrs. The experiments were monitored in real-time using a USB digital eyepiece microscope camera (MD500, Amscope, USA) operated by a computer using imaging software provided by the manufacturer.

2.2.2.2. Image analysis

The experiments were monitored in real-time for the first 48 hrs and then once a week for up to 5 weeks. Images of the crystallisation drops were collected at different focal lengths and analyzed using image analysis software (imageJ 1.53t, and Amscope, v4.8), where the extended depth of focus (EDF) was used to merge images of different depths in one image. Crystal counting, size measurements, and other analysis were performed manually.

2.2.2.3. XRD studies

The crystals obtained from the electric-field-assisted microbatch crystallisation of REMC1 were harvested and cryoprotected for single crystal diffraction analysis by adding 1 mL of a cryosolution containing 70% (v/v) reservoir solution, 30% (v/v) glycerol to the crystallisation droplet and then immediately harvesting a crystal from the drop. The crystals were flash-cooled in liquid nitrogen, stored and shipped to the Diamond synchrotron facility.

2.2.3. Design and fabrication of the microbatch under oil electric field-assisted crystallisation setup.

2.2.3.1. The design

A novel experimental setup was designed and fabricated for microbatch crystallisation under oil (Fig. 2.1). It consists of a 3D-printed case and a pair of clear-glass plates at the top and bottom of the case. The bottom glass plate is equipped with a set of copper electrode arrays. The main parts of the setup were designed in Solid Edge 2019. The 3D-printed part was used as a compartment for the crystallisation experiment, as it encapsulates the electrode arrays and the crystallisation tray and works as an insulating case. Its outer dimensions are 150 × 150 × 40 mm, and the inner dimensions are 120 × 120 × 35 mm. A small protrusion is added at the bottom, where a clear glass plate (3 mm thick) is fixed using silicon glue. This glass plate is equipped with a set of copper electrode arrays connected to a high-voltage power source. The top of the case is designed to hold a second glass plate, which is fixed using four plastic screws for easy installation and removal of the crystallisation plates. These two glass plates provide aid in visualizing and monitoring the crystallisation process under an optical microscope in addition to setup insulation.

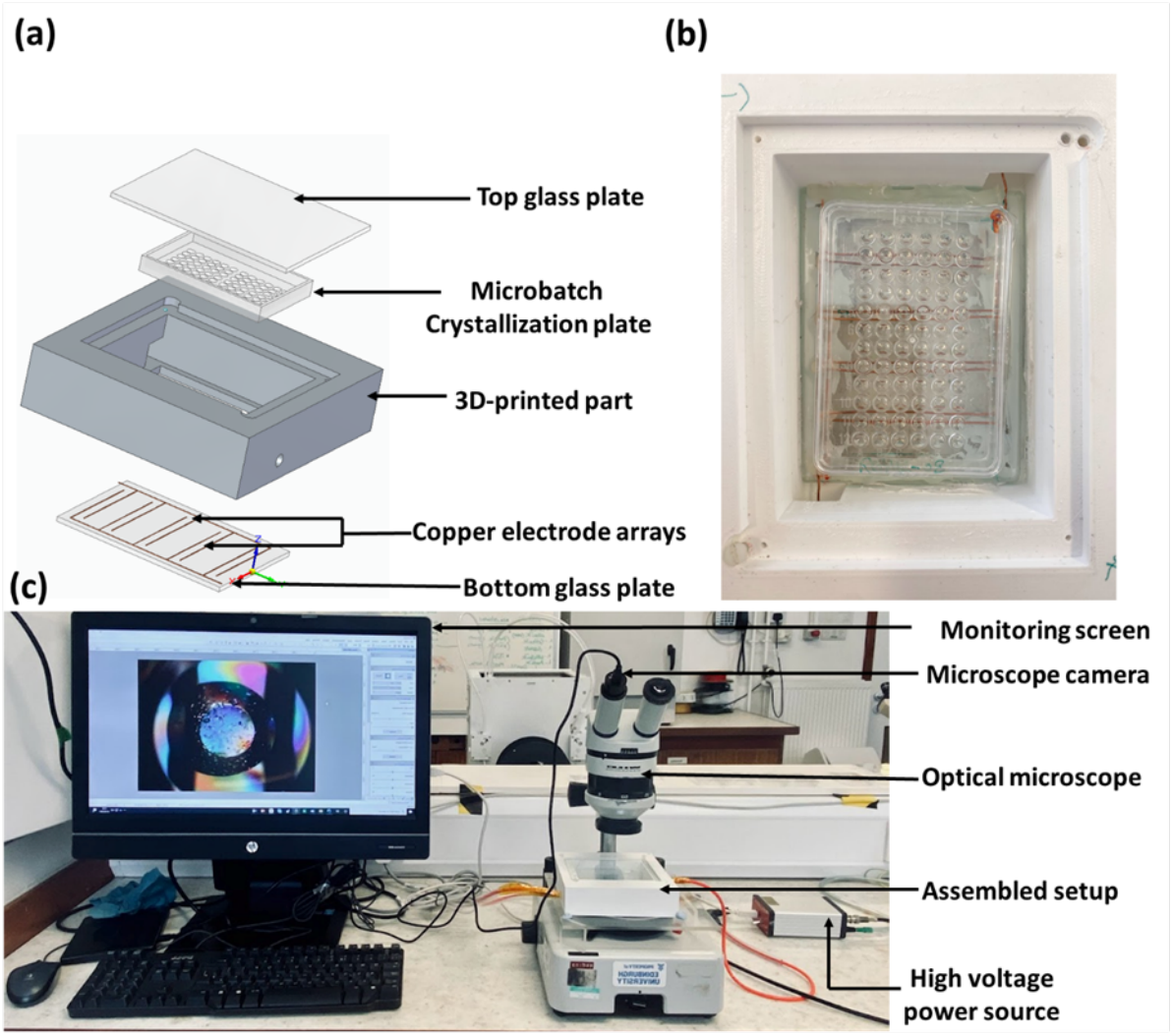

Figure 2.1. The CAD model and the corresponding photographs of the electric-field-assisted microbatch crystallisation setup (Setup I). (a) The CAD model of the crystallisation setup, (b) a photograph of the 3D-printed casing equipped with the electrode arrays and the crystallisation plate, (c) a photograph of the whole setup connected to the high voltage power source and placed under the microscope for continuous monitoring.

2.2.3.2. 3D printing

Ultimaker3 (Ultimaker, the Netherlands) 3D printer was used to print the main parts. The stl files from Solid Edge software are converted to GCODE file format using Ultimaker Cura (4.13.1). The parameters used for printing are shown in Table S2.

2.2.3.3. High-voltage electrodes and connection

The electrode arrays were designed so that each well of the four active rows (2, 5, 8, and 11) falls between a positive and a negative electrode. For an electrode array, four pieces of copper wire (0.87 mm diameter, 6 cm length) were attached to a main copper wire electrode (12 cm) using the soldering technique (Fig. 2.2). The two electrode arrays were then placed and fixed on the bottom glass plate of the setup using hot glue. The distance between each pair of electrodes is approximately 2 mm.

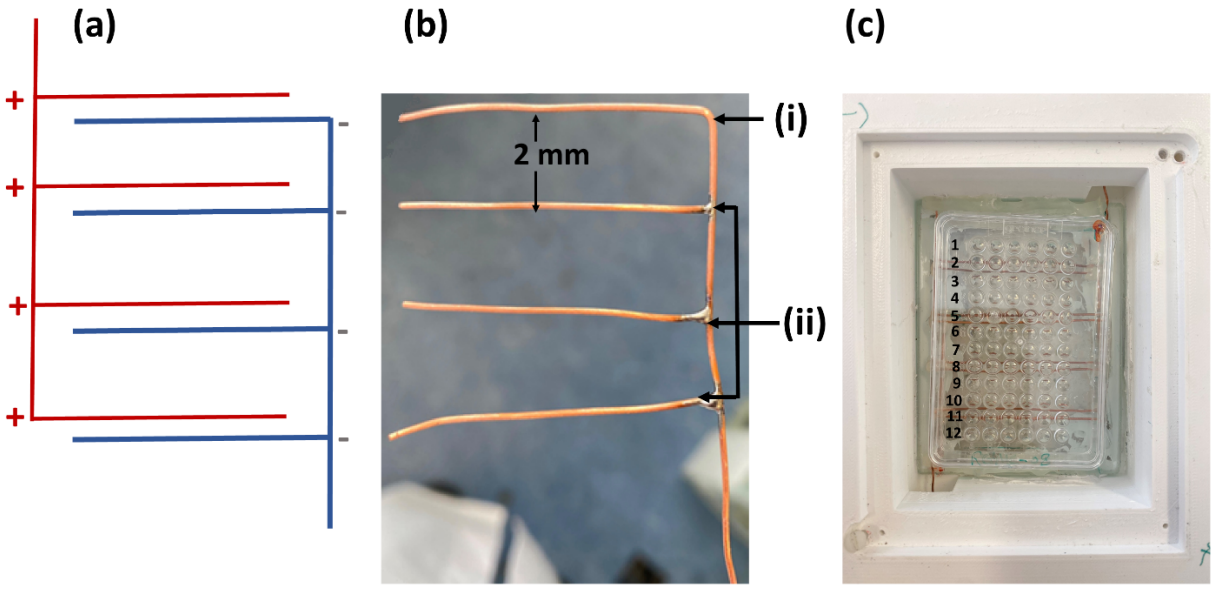

Figure 2.2. The configuration of the copper electrode arrays used in the microbatch under-oil setup. (a) A schematic diagram of the electrode arrays constituting four pairs of electrodes. (b) The negative copper electrode array was made using the soldering technique. The copper wire was bent at point (i) and soldered with smaller pieces of copper wire at positions marked (ii). (c) Each well in rows 2, 5, 8, and 11 in the crystallisation tray falls between two electrodes.

The electrodes were connected to high-voltage cables using spade connectors. The cables were then connected to a safe high voltage (SHV 5 kV) power cable via banana plugs and covered by three layers of Kapton tape for insulation. The other end of the cable was connected to the power source via a BNC connector. The power source was connected to the earth through a ground cable that was plugged into the power supply's earth inlet.

2.2.3.4. Safety measures

As the electric-field-assisted crystallisation experiments involve the use of high voltage, an electrically insulating polymer material (PLA) was used as the main compartment. In addition to PLA, and due to its high dielectric strength and resistivity, glass was used to allow continuous visualization of the plate. Glass was securely fixed in the setup to prevent electrical shock. All the connections and cable ends were secured with three layers of Kapton tape for enhanced protection, and high voltage cables were inserted into flexible silicone tubes for additional insulation.

2.3. Results

2.3.1. Microbatch under-oil crystallisation screening of HEWL

The effect of the electric field on the crystallisation of HEWL was studied using the microbatch technique in Setup I. Prior to the application of the electric field, HEWL crystallisation screening was performed at various conditions. The purpose of the screening experiments was to understand the phase behaviour of HEWL and decide on the conditions to be used to study the influence of electric field.

HEWL was screened at concentrations (10, 15, 20 mg mL^{-1}) and sodium chloride (precipitant) concentrations ranging from 0.6 to 1.6 M. The pH was varied in the range of 4.0 - 4.9. The data was collected weekly after mixing. The experimental results show that under these conditions, HEWL tends to form microcrystals at high salt concentrations (1.4 and 1.6 M) and doesn't crystallise at low salt concentrations (0.6, 0.8 M). In addition, decreasing the concentration of HEWL leads to undersaturation, and hence the crystallisation occurs at fewer

conditions. In addition, the number of crystals decreases, and larger crystals are formed when the pH is increased from 4.0 to 4.9 at higher salt concentrations.

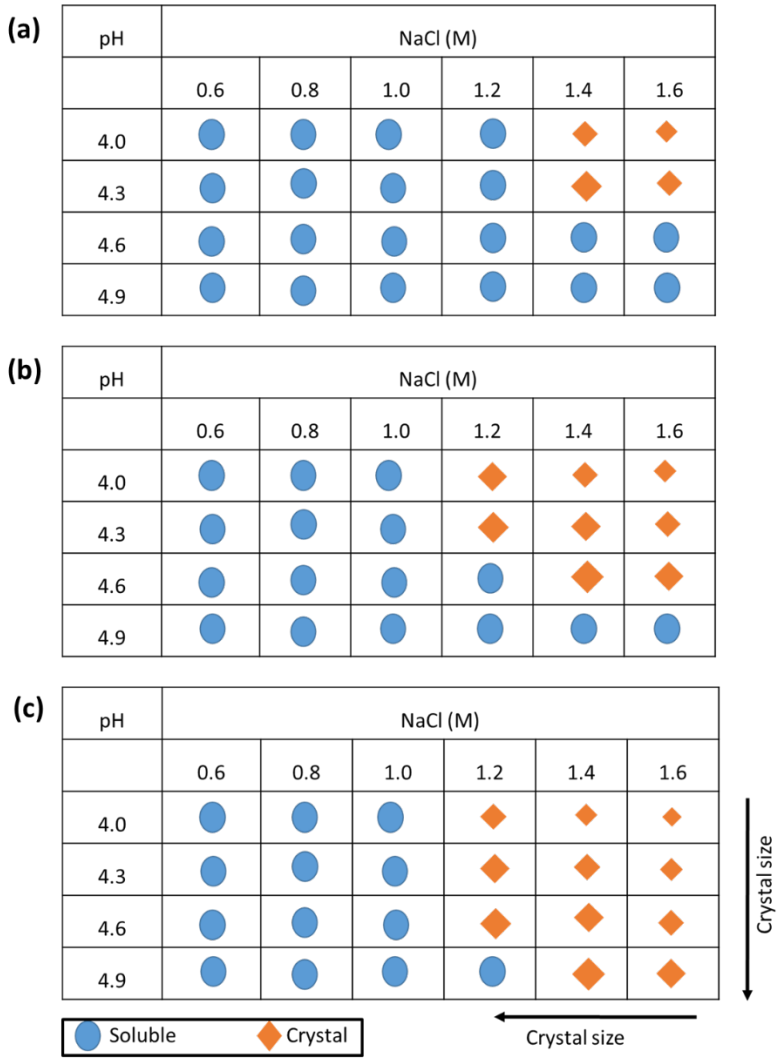

Figure 2.3. HEWL phase behaviour at various experimental conditions with HEWL concentration (a) 10 mg mL^{-1} in, (b) 15 mg mL^{-1}, and (c) 20 mg mL^{-1} in. Microcrystals form at higher salt concentrations. In addition, at a HEWL concentration of 20 mg mL^{-1}, the size of crystals increases with increasing the pH and decreasing salt concentration.

The oil used in the microbatch under-oil experiments plays an essential role in the crystallisation process. Three types of oil were used in the microbatch under-oil crystallisation experiments, namely: paraffin or mineral oil, silicone oil, and Al's oil (a 1:1 mixture of paraffin and silicone oils). These oils are used due to their inert nature and their ability to seal the crystallisation trials allowing no or minimal evaporation of the droplets [80]. Paraffin oil has a low penetration rate of water molecules, silicone allows more penetration of the water

molecules, and the mixture of both oils at different ratios can be used to control the penetration [80].

To validate this effect, HEWL was crystallised using the three types of oil. When silicone oil was used to seal the HEWL crystallisation droplets, the crystallisation drop dried out within a few hours. As paraffin oil allows slower diffusion of water from the crystallisation droplet, it resulted in slower nucleation, and larger crystals were formed compared with Al's oil, which resulted in faster nucleation and microcrystal formation (Fig. 2.4.). Paraffin oil was used as the crystallisation oil in further experiments.

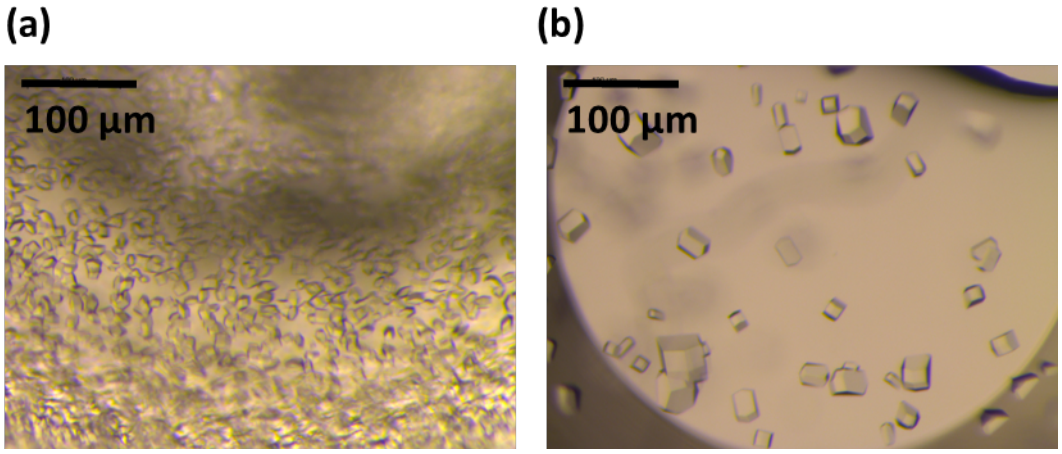

Figure 2.4. The effect of the type of oil on HEWL crystallisation (20 mg mL^{-1}, 1.4 M NaCl, 0.1 M NaOAc, pH 4.6). (a) HEWL crystals under Al's oil (1:1 silicone oil and paraffin oil mixture). (b) HEWL crystals under paraffin oil. Larger and fewer crystals are formed when paraffin oil is used.

It has been reported in the literature that an electric field can decrease the number of the resulting crystals [36, 37, 51, 58, 60, 82]. In addition, electric field was found to increase the nucleation rate [63, 65, 100]. To observe the effects of the electric field, HEWL was crystallised under paraffin oil at a concentration of 20 mg mL^{-1} and salt concentrations of 1.2-1.4 M at pH 4.6 and 4.9. At these concentrations, HEWL crystallises within a few days, and a range of crystal sizes and numbers are produced.

2.3.2. Electric-field-assisted microbatch under-oil crystallisation of HEWL.

To date, several studies have investigated the effect of electric field on lysozyme crystallisation using the microbatch under-oil technique. Al-Haq and colleagues [60] crystallised HEWL) under the effect of DC electric field (270 V) using the microbatch method, which resulted in a lower mean number of crystals [60]. Koizumi et al. were able to control the nucleation rate of lysozyme using AC electric field in a containerless microbatch setting [63]. In addition, they studied the effect of various precipitants' ionic strength on lysozyme nucleation rate under the effect of AC electric field [99]. The quality of Lysozyme crystals was found to improve with the application of AC electric field [74, 83, 97].

In this research, HEWL is crystallised under the effect of direct current (DC) external electric field using the microbatch-under oil technique in Setup I. In addition, to study the effect of the polarity of the high voltage on the crystallisation outcomes, the electric field was applied using a negative and a positive voltage output power sources simultaneously. Due to the stochastic nature of the crystallisation process, the experiments were repeated at least three times for validation and statistical analysis. The experiments were monitored weekly by optical microscopy, and the crystals were counted manually using ImageJ software.

2.3.3. Effect of electric field on HEWL nucleation

The effect of electric field on nucleation was studied by observing the number of crystals over time (Fig. 2.5). The crystals obtained from three experimental trials were counted, and the averages were plotted against time (Fig. 2.6). In contrast to the control experiment, the number of crystals growing with time was higher when electric field was applied regardless of the voltage polarity, with a larger extent observed when the negative voltage was applied.

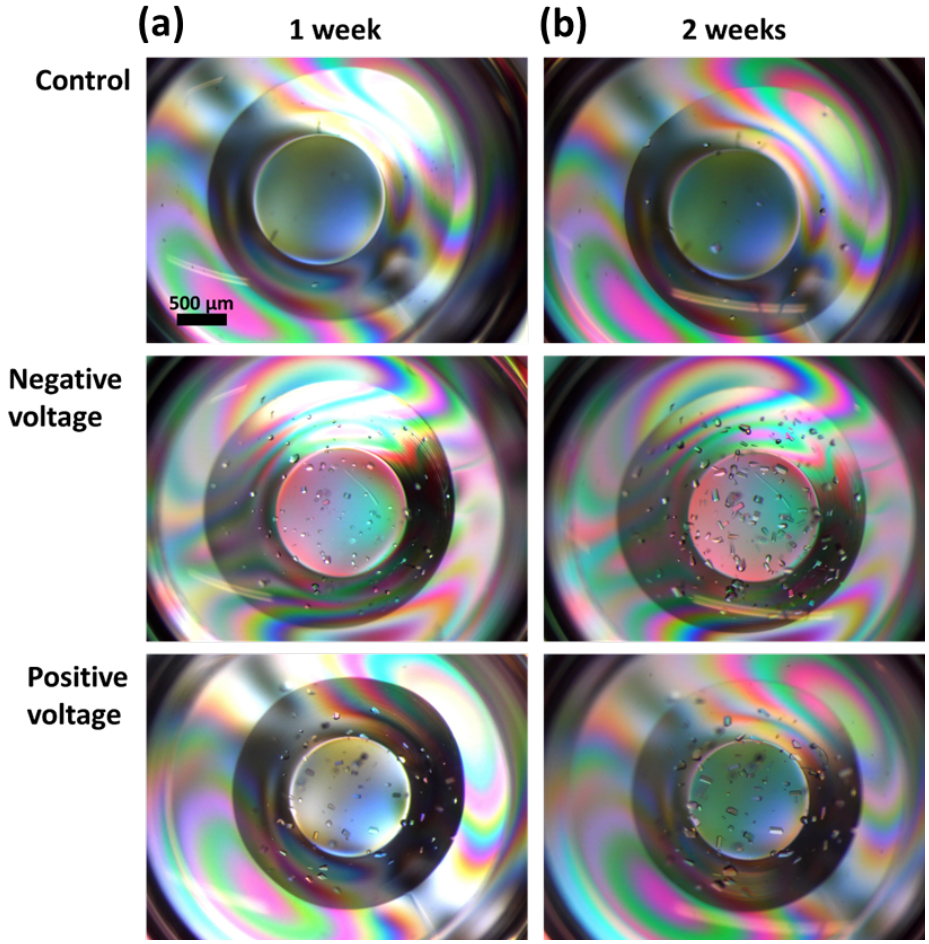

Figure 2.5. Micrographs illustrating the difference in the number of crystals of HEWL (20 mg mL^{-1}, 0.1 M NaOAc, 1.4 M NaCl, pH 4.6) with and without electric field after (a) one week and (b) two weeks of mixing the drops.

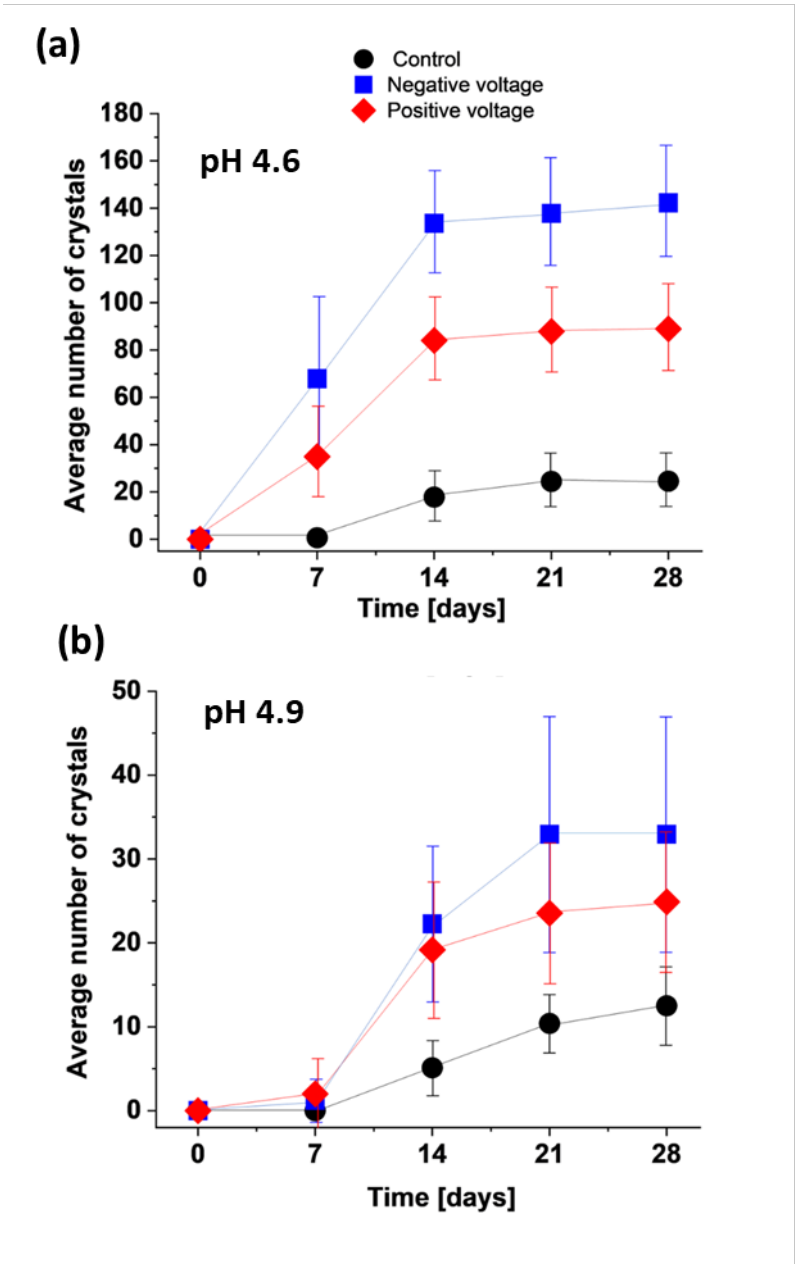

Figure 2.6. The average number of HEWL crystals with time (20 mg mL^{-1}, 0.1 M NaOAc, 1.4 M NaCl) at (a) pH 4.6 and (b) pH 4.9.

The nucleation rate during the crystallisation process in each condition can be obtained by fitting the data to a straight line and calculating the slope (Fig. 2.7). At pH 4.6, the nucleation started in the first week after mixing the crystallisation drop.

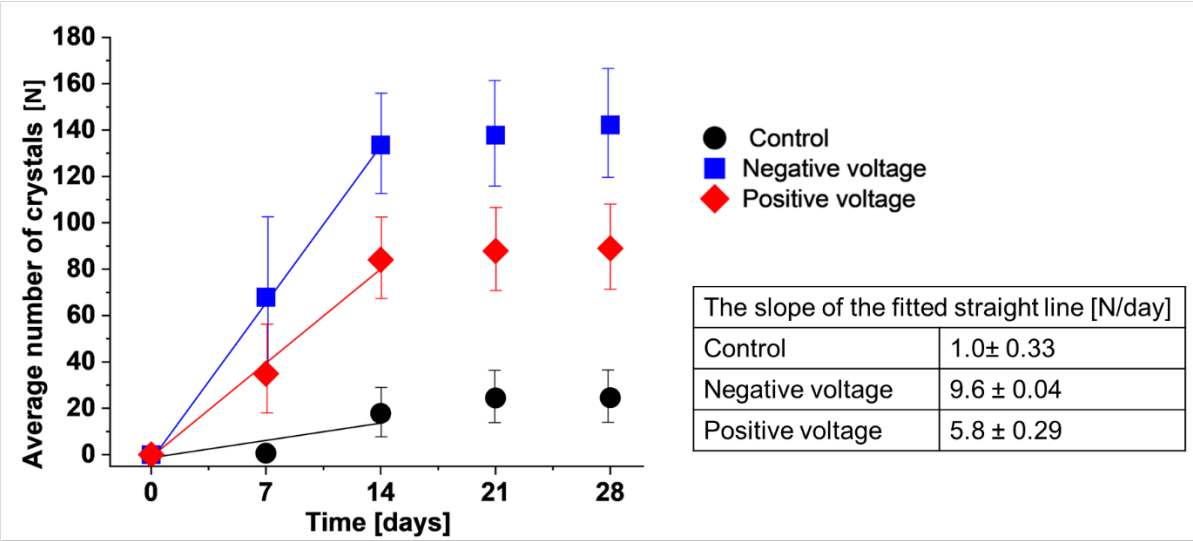

The slope of the fitted straight line [N/day]	
Control	1.0± 0.33
Negative voltage	9.6 ± 0.04
Positive voltage	5.8 ± 0.29

Figure 2.7. Linear fitting of the average number of HEWL crystals with time in the first two weeks of nucleation (20 mg mL^{-1}, 0.1 M NaOAc, 1.4 M NaCl, pH 4.6). The slope of the straight line is considered as the nucleation rate. Higher nucleation rates are observed when an electric field is applied.

At pH 4.9, the nucleation started in the second week of the experiment, and the number of crystals obtained was less than that of pH 4.6. Similarly, the nucleation rate, in general, is higher when an electric field is applied (Fig. 2.8).

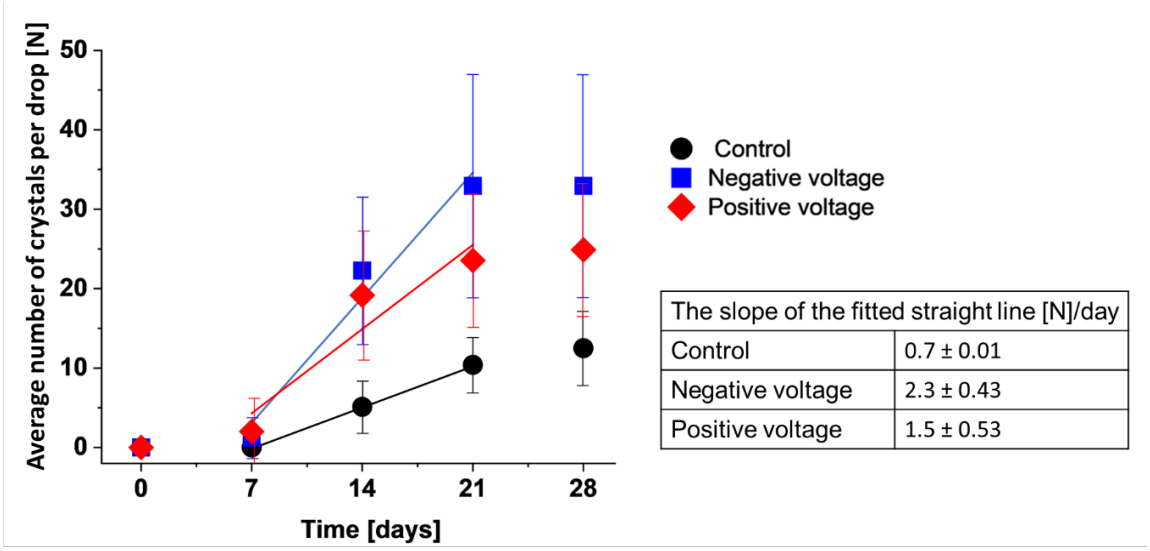

The slope of the fitted straight line [N]/day	
Control	0.7 ± 0.01
Negative voltage	2.3 ± 0.43
Positive voltage	1.5 ± 0.53

Figure 2.8. Linear fitting of the average number of HEWL crystals per drop within the first two weeks of nucleation (20 mg mL^{-1}, 0.1 M NaOAc, 1.4 M NaCl, pH 4.9). The slope of the straight line is considered as the nucleation rate. Higher nucleation rates are observed when the electric field is applied.

2.3.4. Effect of electric field on number of HEWL crystals

The effect of electric field on the number of crystals was studied by counting the number of crystals in a drop after four weeks of the experiment, where no more nucleation was observed. The numbers of crystals were plotted to compare the effect of electric field in comparison to the control experiments (Fig. 2.9).

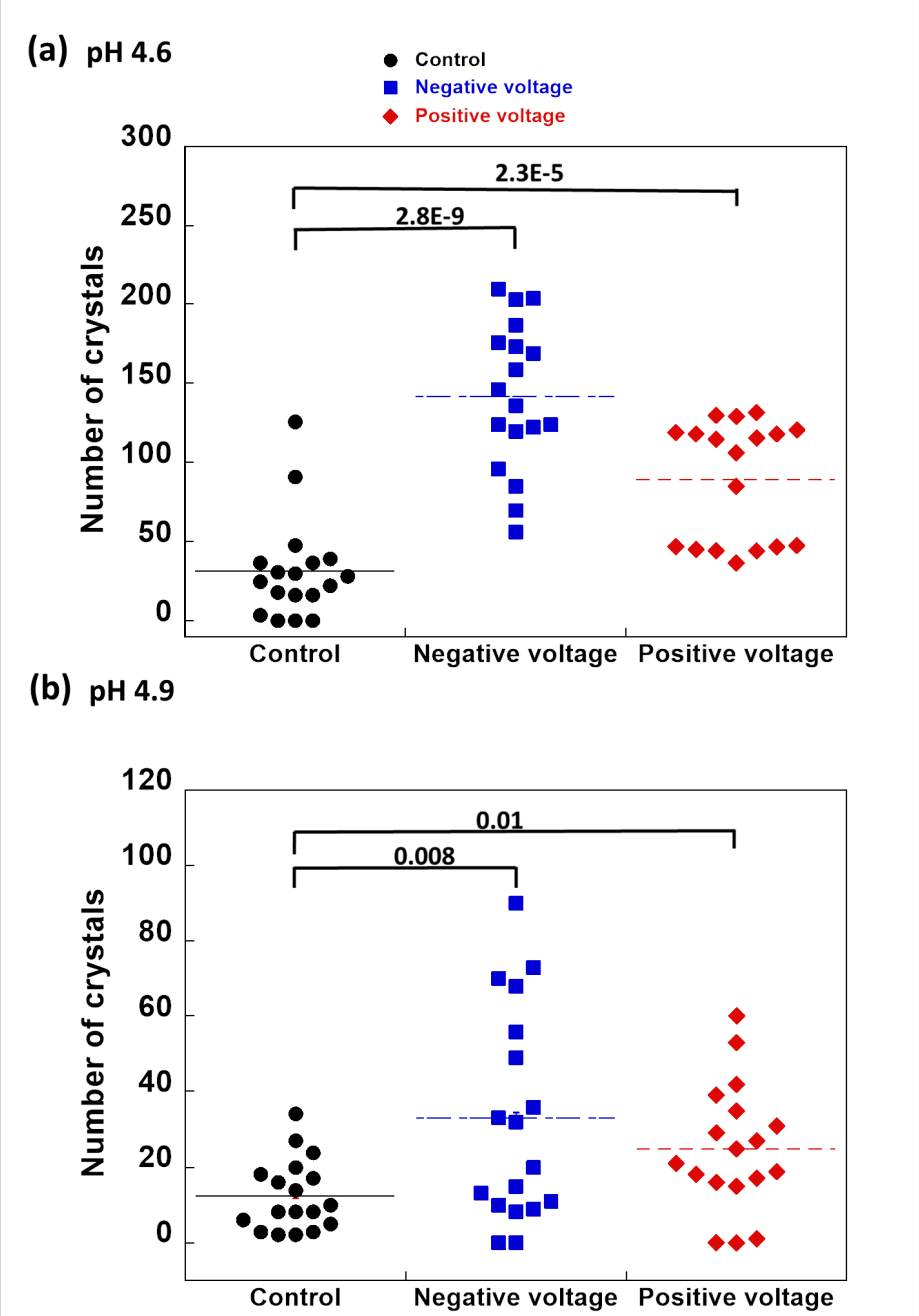

Figure 2.9. The effect of direct current electric field (2 x 10^5 V m^{-1}) on the number of HEWL crystals (20 mg mL^{-1}, 0.1 M NaOAc, 1.4 M NaCl) at (a) pH 4.6 and (b) pH 4.9. A higher number of crystals is produced when electric field is applied. P-values are illustrated, showing significant differences between datasets (p-value < 0.05).

Both negative and positive voltage resulted in a noticeable increase in the number of HEWL crystals; however, a higher effect was observed when negative voltage was used (Table 2.1). In addition, the effect of electric field on the number of crystals is higher at pH 4.6 compared

to pH 4.9. The mean number of crystals produced is higher when the electric field is applied. Kurtosis values indicate if the data are heavy-tailed or light-tailed relative to a normal distribution, where positive kurtosis denotes heavier tails and a higher-peaked distribution, whereas negative kurtosis denotes lighter tails and a flatter distribution. Electric field resulted in narrower distribution at both pH values. Skewness is a measure of symmetry in the normal distribution, where positive skewness suggests a longer tail on the distribution's right side, whereas negative skewness indicates a longer tail on the distribution's left side. At both pH values, smaller values of skewness are observed when electric field is applied, which indicates the longer tail on the left side of the distribution (i.e. smaller crystals).

Table 2.1. Statistical analysis of the crystal count data

	pH 4.6			pH 4.9		
	Control	Negative voltage	Positive voltage	Control	Negative voltage	Positive voltage
Mean number of crystals	31.56	142.22	88.94	12.5	32.94	24.89
Standard Error	7.54	10.98	8.92	2.21	6.65	3.97
Median	26.50	141	110.5	9	26	23
Standard Deviation	31.10	46.58	37.84	9.37	28.20	16.84
Sample Variance	1023.67	2169.24	1432.06	87.79	795.47	283.63
Kurtosis	4.054	-0.860	-1.920	-0.058	-0.856	-0.071
Skewness	1.882	-0.250	-0.315	0.821	0.652	0.380
Range	126	154	95	32	90	60
Minimum	0	56	37	2	0	0
Maximum	126	210	132	34	90	60
Sum	568	2560	1601	225	593	448

2.3.5. **Effect of electric field on HEWL crystal size and size distribution**

The electric field can also affect the size of the resulting crystals, where smaller sizes are observed when an electric field is applied (Fig. 2.10). Both negative and positive voltage resulted in the production of smaller crystals; however, the crystals grown under the negative voltage were smaller than those grown under positive voltage and the control experiment at pH 4.6. At pH 4.9. The size of the crystals was reduced to a similar extent when positive and negative voltage was applied.

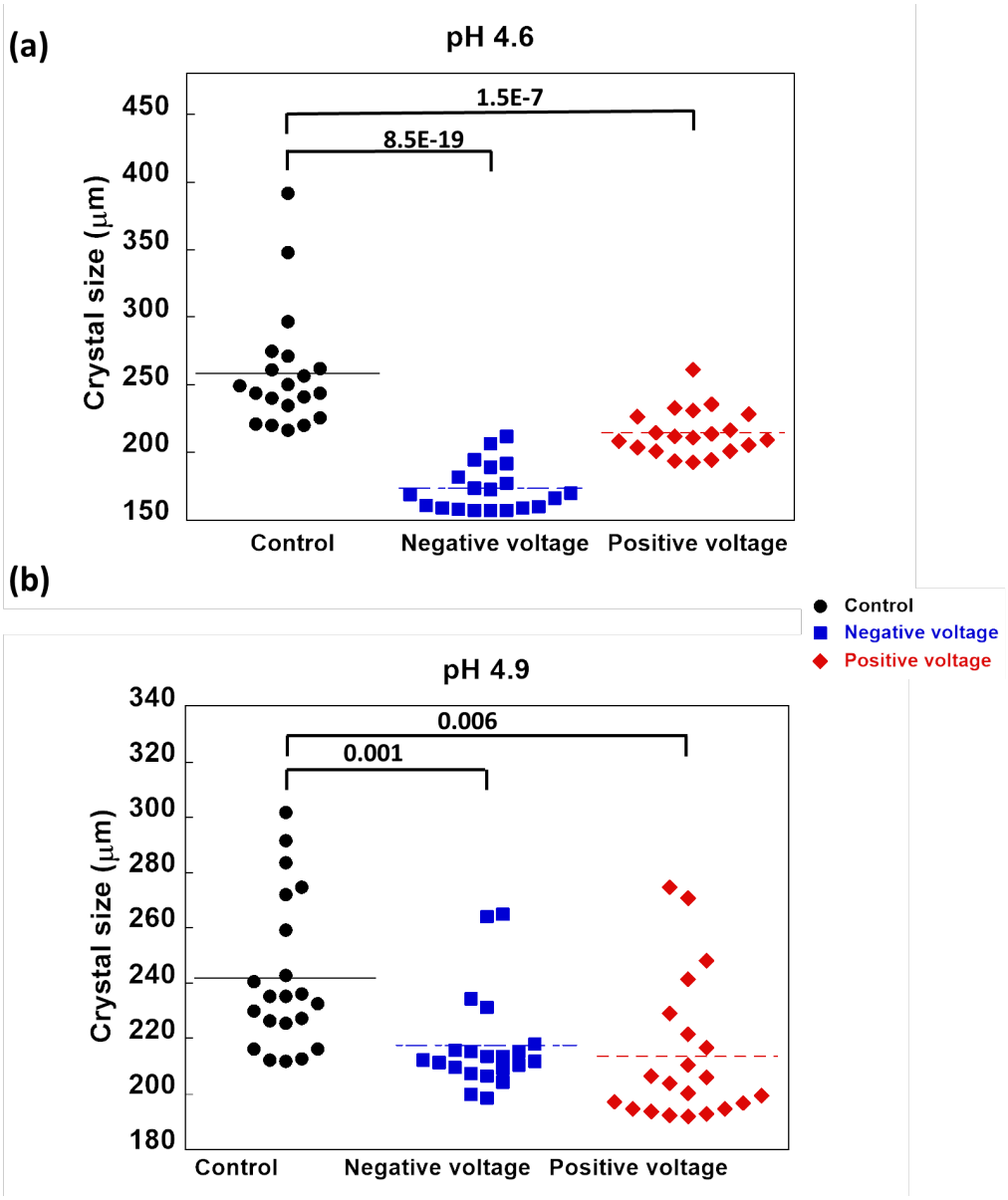

Figure 2.10. The effect of direct current electric field (2 x 10^5 V m^{-1}) on the size of HEWL crystals (20 mg mL^{-1}, 0.1 M NaOAc, 1.4 M NaCl) (a) at pH 4.6, (b) at pH 4.9. Smaller crystals are produced when electric field is applied. P-values are illustrated, showing significant differences between datasets (p-value < 0.05).

Table 2.2 shows the descriptive statistical analysis of the experimental data. Both negative and positive voltage resulted in a noticeable decrease in the crystal size; however, smaller crystals were observed when negative voltage was used. In addition, the effect of electric field

on the size of crystals is higher at pH 4.6 compared to pH 4.9. The mean size of crystals produced is lower when the electric field is applied.

Table 2.2. Statistical analysis of the crystal size data

	pH 4.6			pH 4.9		
	Control	Negative voltage	Positive voltage	Control	Negative voltage	Positive voltage
Mean	101.10	81.82	89.22041	114.11	101.76	103.07
Standard Error	2.03	0.63	0.972799	3.35	1.79	2.22
Median	94.66	80.85	84.082	106.86	98.18	100.09
Standard Deviation	51.94	30.85	39.13021	57.54	44.67698	50.77
Sample Variance	2698.13	951.60	1531.174	3310.31	1996.032	2577.80
Kurtosis	2.421	-0.147	0.444	0.268	0.356	-0.424
Skewness	1.065	0.310	0.683	0.632	0.570	0.339
Range	380.53	212.14	251.52	287.87	252.25	264.69
Minimum	11.45	0	9.821	13.89	12.577	9.82
Maximum	391.98	212.137	261.336	301.76	264.823	274.51
Sum	66424.25	193836	144358.6	33664.14	63700.51	53697.6

The crystals were further subjected to size distribution measurements, where the apparent longest axis of the crystals is measured. The results are illustrated in Figure 2.11. The control experiment shows a wider distribution of crystal sizes around the mean than those grown under electric field, as indicated by the higher standard deviation. At pH 4.6, the negative electric field results in narrowing the crystal size distribution compared to the control and the positive electric field experiment.

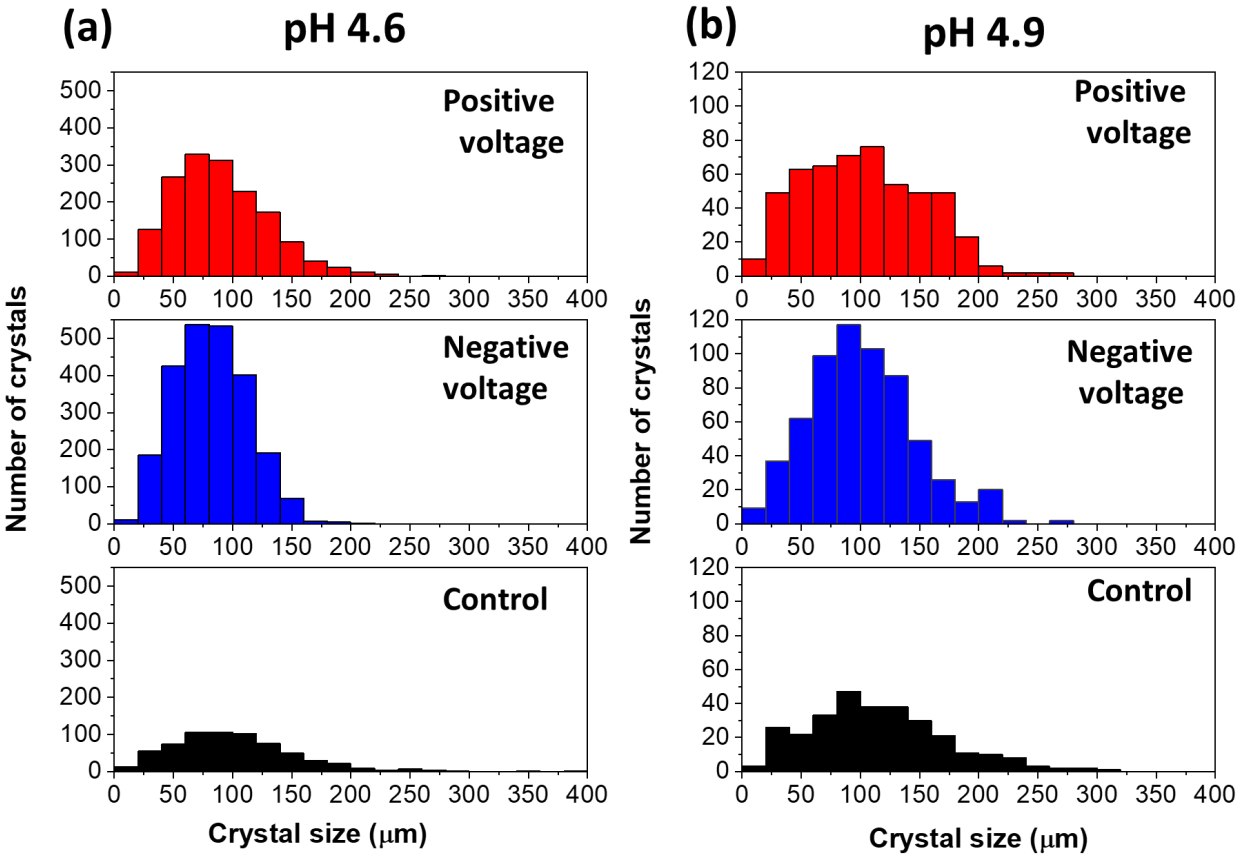

Figure 2.11. Crystal size distribution of HEWL (20 mg mL^{-1}, 0.1 M NaOAc, 1.4 M NaCl) at (a) pH 4.6 and (b) pH 4.9. Crystal size is represented by the length of the longest apparent axes.

2.3.6. **Effect of electric field on HEWL crystals growth**

The growth rate of HEWL tetragonal crystals was monitored by measuring the length (l) of the 001 face (Fig. 2.12) [101]. The growth rate was measured by the change in the length of the l axes over time.

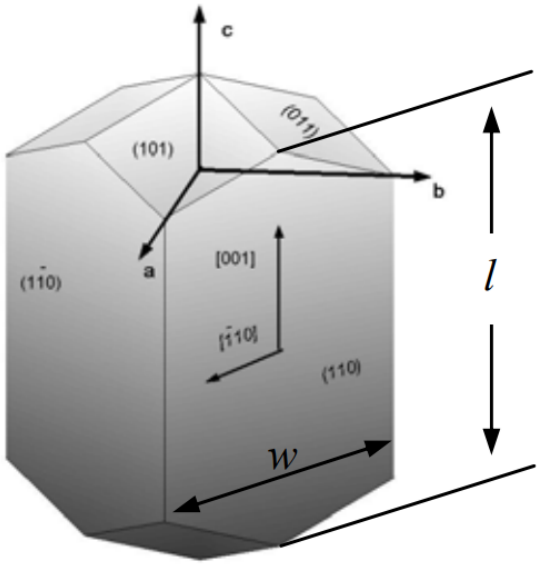

Figure 2.12. Tetragonal HEWL morphology, showing crystallographic axes and faces. The growth of the crystals was monitored by measuring the length (l) with time (copied from reference [101]).

The size of HEWL crystals grown with and without electric field against time is illustrated in Figure 2.13. In the first week, at pH 4.6, HEWL crystals grown under the effect of electric field grow at faster rates and reach their maximum size within approximately two weeks, whereas the growth stops at around three weeks in the control experiment, with slower growth in the beginning compared to the electric field experiments. At pH 4.9, the growth started in the second week of the experiment, with a relatively faster growth throughout the experiment when the electric field was applied.

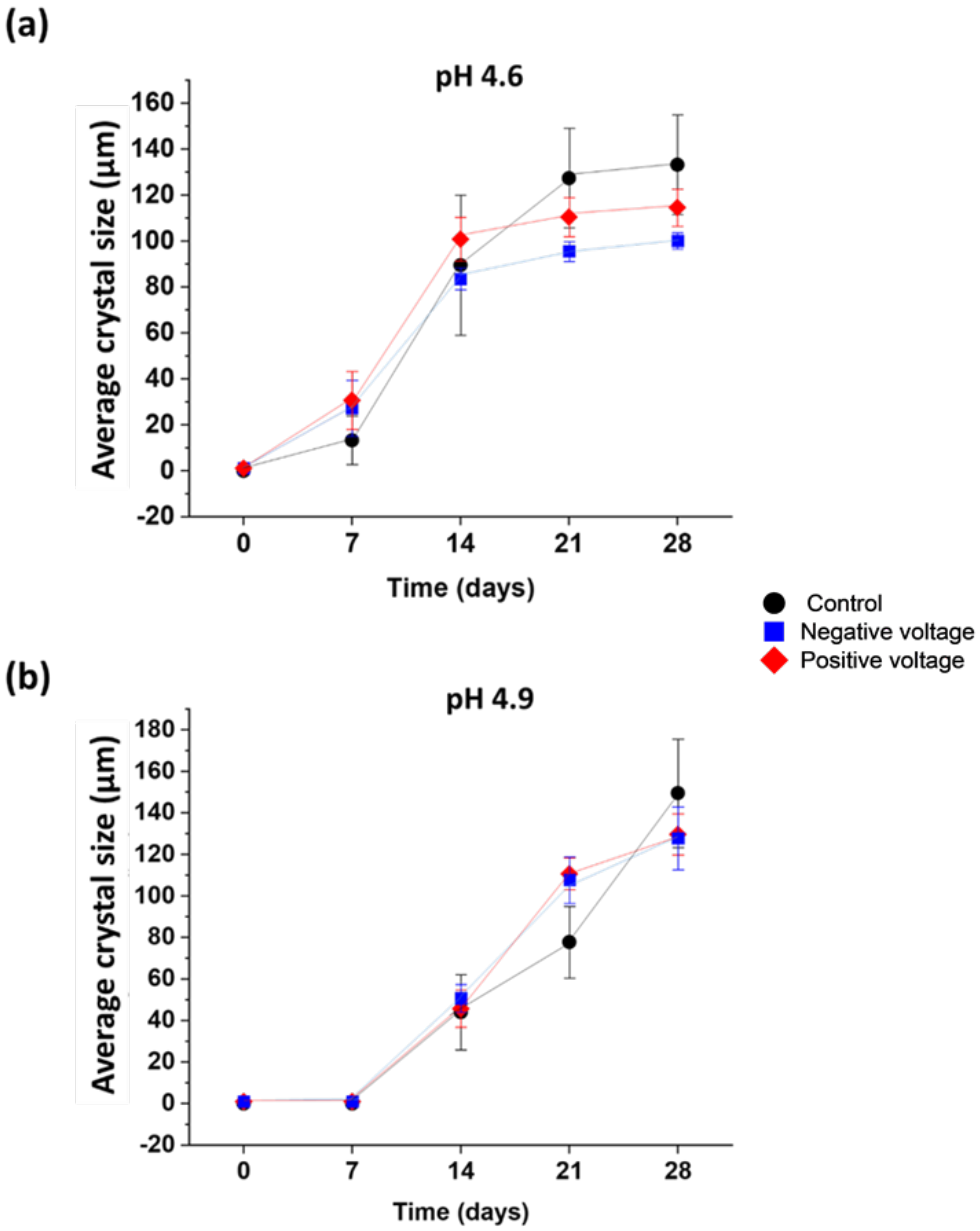

Figure 2.13. The average growth of HEWL tetragonal crystal (20 mg mL^{-1}, 0.1 M NaOAc, 1.4 M NaCl) with time at (a) pH 4.6 and (b) pH 4.9. Crystals grow relatively faster when electric field is applied compared to the control experiment.

2.3.7. Microbatch under-oil crystallisation screening of REMC1

The REMC1 screening experiments resulted in crystallisation of REMC1 at 50, 37.5 and 31.25 mg mL^{-1} within 24 hrs, whereas no crystallisation occurs at lower protein concentrations. Figure 2.14 shows the resulting crystals after 24 hours. The crystals forming at higher protein

concentrations grew faster and exhibited structural irregularities, with the majority of the crystals in a cubic-like shape.

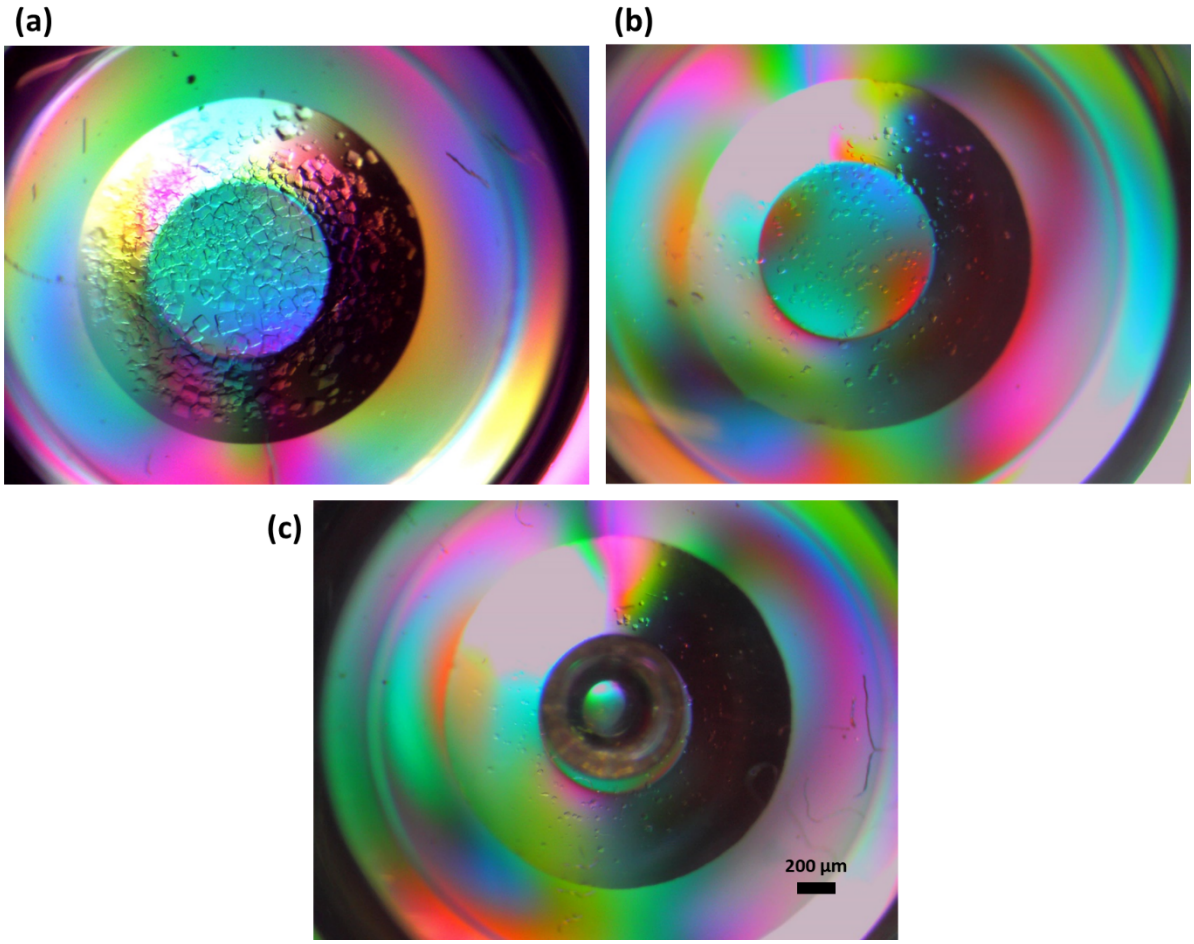

Figure 2.14. The crystallisation outcomes of REMC1 in in 50 mM Tris pH 8, 250 mM NaCl after 24 hrs at protein concentration without the application of electric field (a) 50 mg mL^{-1}, (b) 37.5 mg mL^{-1} and (c) 31.25 mg mL^{-1}. Larger and irregular structures are formed at higher concentration.

2.3.8. Electric-field assisted microbatch under-oil crystallisation of REMC1

In further experiments, the protein was crystallised under the effect of the electric field at a concentration of 37.5 mg mL^{-1} using both positive and negative polarity voltage. The preliminary results from this study showed larger crystals were formed with the electric field (Fig. 2.15).

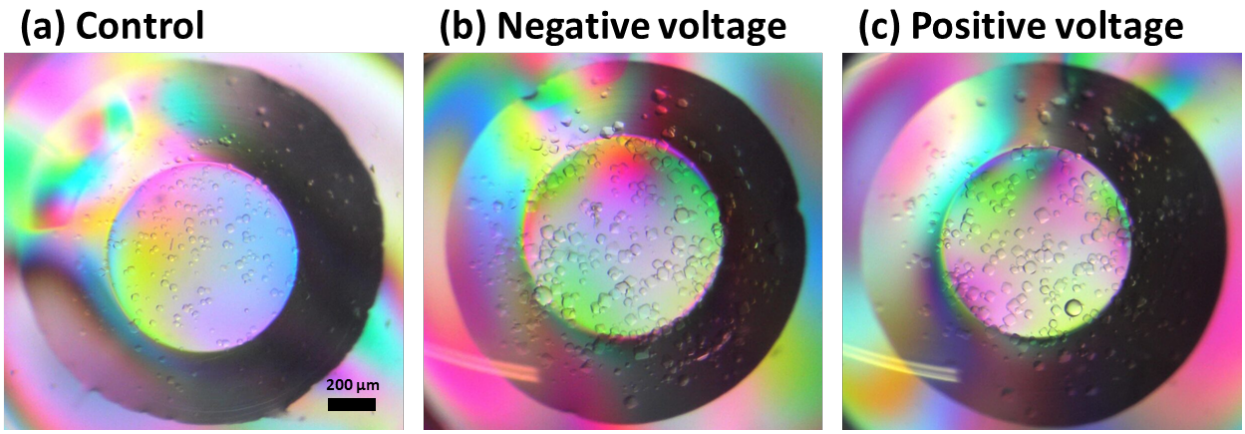

Figure 2.15. The crystallisation outcomes of REMC1 (37.5 mg mL^{-1} in 50 mM Tris pH 8, 250 mM NaCl) after 48 hrs (a) control experiment, (b) under negative voltage (800 V, 2 x 10^5 V m^{-1}, 48 hrs), and (c) under positive voltage (800 V, 2 x 10^5 V m^{-1}, 48 hrs). Larger crystals are formed when electric field is applied.

Crystals obtained with and without the electric field were harvested and cryoprotected using a 30% glycol solution before flash cooling. The crystals were subjected to single-crystal XRD analysis using a synchrotron beamline. All the crystals exhibited no or poor diffraction. No useful data were collected at this point.

2.4. Discussion

2.4.1. Electric-field assisted microbatch under-oil crystallisation of HEWL

The results indicate a noticeable effect of the electric field on the crystallisation of HEWL, mainly on the nucleation and growth of the resulting crystals. To explain the mechanism, one can refer to the effect of the electric field on the equilibrium state of the crystallisation process.

Electric field is known to add extra energy to the chemical potentials of the solid and the liquid phases [65] (Section 1.6.1). It affects and modifies the chemical potentials of the two phases, and hence it affects the equilibrium state, which also depends on the field strength [73].

In 2000, Kashchiev demonstrated the factors affecting nucleation, including the effect of external electric field [102]. They stated that the nucleation can be stimulated when the electrical permittivity of the crystals (cluster) is greater than that of the solution or (medium) [102]. A uniform electric field can stimulate nucleation at effective supersaturation [102]. At pH 4.6, the supersaturation of the crystallisation droplet is higher than that at 4.9. The results are consistent with Kashchiev's finding, as the nucleation is stimulated with electric field, leading to more crystals forming compared to the control experiments.

The nucleation rate can also be related to the phase transition of the protein molecules from the liquid to the solid phase, as illustrated in Figure 2.16 [103]. In batch experiments, the process starts in the high supersaturation zone, which leads to the nucleation, and eventually the growth of the crystals. In the presence of an electric field, the nucleation zone is expanded, which allows more nucleation compared to crystallisation without an electric field [103].

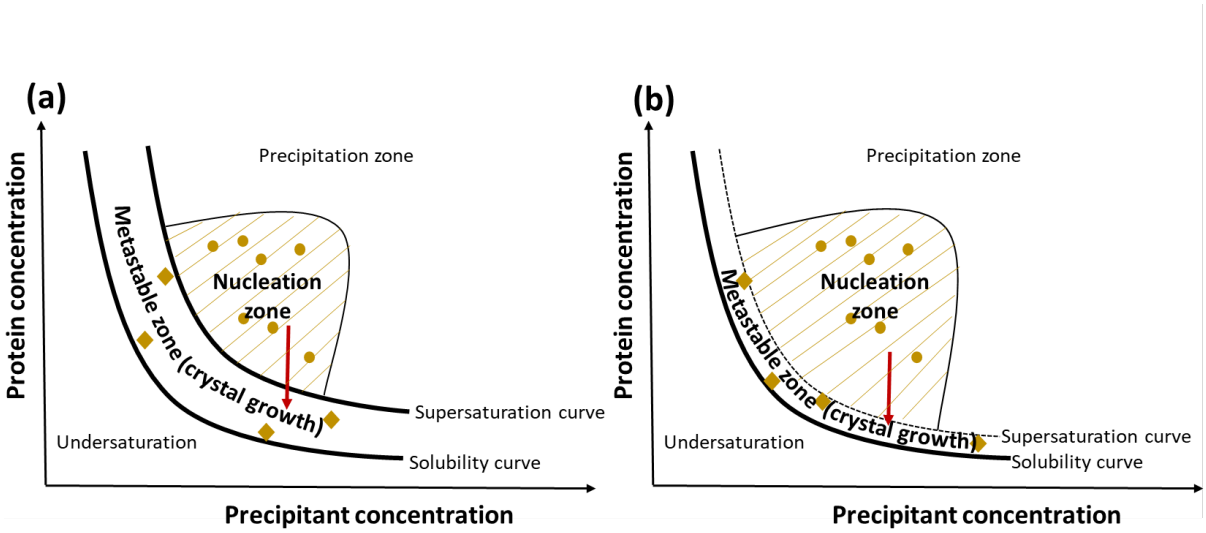

Figure 2.16. Phase diagram of protein crystallisation (a) with and (b) without electric field. Microbatch crystallisation is initiated at the nucleation zone. Electric field have potentially

expanded the nucleation and supersaturation zones allowing more nucleation at relatively lower supersaturation with supressed growth.

The electric field enhances the electromigration of both the protein and the salt ions by the potential difference, which stimulates the local supersaturation in the crystallisation drop hence the nucleation [49, 104]. In addition, the electric field was found to decrease the viscosity of paraffin oil [105, 106]. Faster nucleation was reported when decreasing the viscosity of the oil used in microbatch crystallisation [107], which can lead to the increase in the number of nucleation centres, as observed in the screening experiments. This can be explained by the increase in the rate of penetration of water molecules through the oil, leading to higher supersaturation in the medium.

Looking at the results obtained in this research, the nucleation rates of HEWL under the effect of electric field are higher than that of the control experiment. The rates are calculated by plotting the number of crystals against time and fitting the plots to a linear equation. The slope of the fitted line (S) is considered as the nucleation rate.

At pH 4.6, the nucleation starts within the first week of the experiment, whereas, at pH 4.9, the nucleation occurs in the second week. In both conditions, higher nucleation rates are observed with the application of external electric field. It has been reported that pH variation has a substantial effect on lysozyme nucleation [108]. Judge et al. explained the variation by the sensitivity of molecular charge distribution to the solution conditions, which affects changes in the charge at localized locations on the protein molecule's surface [108]. When considering the effect of the electric field on the nucleation rates at different pH values, one can add the extra energy added to the chemical potential of the solution [65], in addition to the effect of the electromigration of charged ions.

It is worth noting that higher nucleation rates are observed when negative voltage is applied compared to positive voltage and the control, which is reported for the first time.

To verify the effect of electric field on the number and size of crystals, hypothesis testing (t-test) of the data was performed assuming non-equal variance. The null hypothesis (H_0) assumes equal means for the two data sets (with and without electric field), whereas the alternative hypothesis (H_a) assumes non-equal means.

$H_0 = X_{negative\ voltage} - X_{control} = 0$

$H_a = X_{negative\ voltage} - X_{control} \neq 0$

When the two datasets are statistically equivalent, the null hypothesis is true, and when there is no statistical difference in the mean responses of these two datasets.

The results show that there is a significant difference between the two data sets, which verifies the effect of the electric field on the number and size of crystals. A probability value (p-value) for significance is calculated to test these hypotheses. If the p-value is less than the chosen level of significance (alpha =0.05), the probability that the null hypothesis is correct is low. As a result, the null hypothesis should be rejected, and the alternative hypothesis should be accepted [109]. The same is applicable to the number and size of crystals produced under positive voltage compared to the control.

Electric field has been reported to decrease the crystallisation yield (number of crystals) in many cases [51, 65, 69, 82]. However, a few studies reported the opposing observation, where a larger number of crystals were produced when an electric field was applied. Li et al. reported an increase in the number of crystals when HEWL is crystallised in a continuous flow microfluidic device under the effect of electric field [67]. Also, Pareja-Rivera et al. observed a higher number of crystals are produced with increasing the frequency of AC electric field, compared to a control experiment [37]. Saban et al. found that the number of crystals increases when electric field strength is $\geq 0.5 \times 10^6$ V m^{-1} [54].

It is worth considering that the intensity of the electric field reaching the crystallisation drop may not be equal to the electric field applied due to the presence of dielectric media between the copper electrodes and the droplet (i.e., air and plastic plate)[51], which can attribute to the reduced actual intensity. Penkova et al. found that depending on the strength of the electric field, the nucleation of proteins could be enhanced or suppressed. Their experimental results showed a suppression of the nucleation of ferritin and apoferritin at a low field strength, whereas the opposite is true when a strong fields were applied [110].

The faster nucleation of HEWL under an electric field resulted in a substantial decrease in the size of the resulting crystals at both the negative and the positive high voltage polarities. While larger crystals are desired for protein structural analysis using X-ray crystallography, higher spatial resolution can be obtained with micro electron diffraction (MicroED) using small crystals [15, 89]. For X-ray diffraction, the limitation of the large crystal size is due to the radiation damage, which becomes more significant as the size of the crystals decreases [89]. In contrast, crystals 10^6 times smaller than those used for X-ray diffraction can be analyzed using MicroED [21]. Smaller crystals have many advantages, such as the ability to improve data quality in the case of crystal disorders. In addition, crystal treatments such as perturbations of small crystals are more rapid and uniform compared to larger crystals [21, 89]. MicroED can diffract and extract high-resolution structural data from samples that don't readily form big crystals while consuming a lot less material [15]. Whilst nanocrystals (smaller than ~500 nm), are ideal for MicroED, thicker crystals can also be used.

2.4.2. Microbatch under-oil crystallisation of REMC1

The crystallisation screening of REMC1 protein have resulted in spontaneous crystallisation at higher protein concentrations and forming cube-like structures. The fast nucleation at higher concentration (50 mg mL^{-1}) resulted in structural irregularities, which is a result of rapid nucleation and a high supersaturation (Fig. 2.14).

However, the shape and number of crystals formed at intermediate concentration (37.5 mg mL^{-1}) resulted in more uniform-shaped crystals. These conditions were suitable for further testing the electric field effect on the crystallisation outcomes. Using this protein concentration, the preliminary results of application of electric field showed an increase in REMC1 crystal size. REMC1 crystals have been analysed by XRD previously by the research group, which resulted in poor diffraction properties. To assess the effect of electric field on the quality of the crystals, over 20 crystals grown under electric field were harvested and subjected to XRD analysis. However, these crystals showed no diffraction, indicating the absent effect of electric field on improving crystal quality.

The main purpose of crystallising REMC1 under electric field was to improve its crystal properties and solve its molecular structure. To try improving the crystals properties, a change in the type and setting of the experiment was performed. A new devise for electric field assisted vapour diffusion crystallisation for in situ XRD analysis was designed (Chapter 3).

2.5. Conclusions

Electric-field-assisted crystallisation of HEWL was investigated using the setup I at varying pH and high voltage polarity. The results show an increase in nucleation rate and the number of HEWL crystals when the electric field is applied, regardless of the voltage polarity. However, the result is observed to a greater extent when the negative voltage is applied. Smaller size crystals are produced when the electric field is applied than in the control experiment. These effects are a result of the energy added to the process by the electric field, which enhances the electromigration of the protein and precipitant ions, resulting in enhanced nucleation. REMC1 crystallisation under electric field, on the other hand, resulted in changes in the size of crystals but not crystal diffraction properties.

Although the setup provides an effective tool to study the effect of electric field on the crystallisation of proteins using the microbatch under-oil method, it can be further improved to enhance its efficiency. As the setup is designed for external electric field, the multiple dielectric media between the electrodes and the drop reduces the strength of electric field reaching the drop. In addition, the effect of the electric field is also influenced by the configuration of electrodes, resulting in a non-uniform electric field reaching the droplet.

Electric-field-assisted vapour diffusion crystallisation setup

3.1. Introduction

Vapour diffusion is considered the most commonly used crystallisation method [40, 43] of protein for screening and structural analysis due to its simplicity [91, 111], requirement of small protein volumes, and compatibility with automation [33].

In this technique, a droplet containing a mixture of protein and precipitant solutions is encapsulated in a sealed chamber containing a larger volume of precipitant solution [91]. Due to the lower concentration of precipitant in the droplet, the water vapour diffuses from the droplet to the precipitant, causing the protein to concentrate until an equilibrium is reached and the protein reaches its supersaturation zone [112, 113].

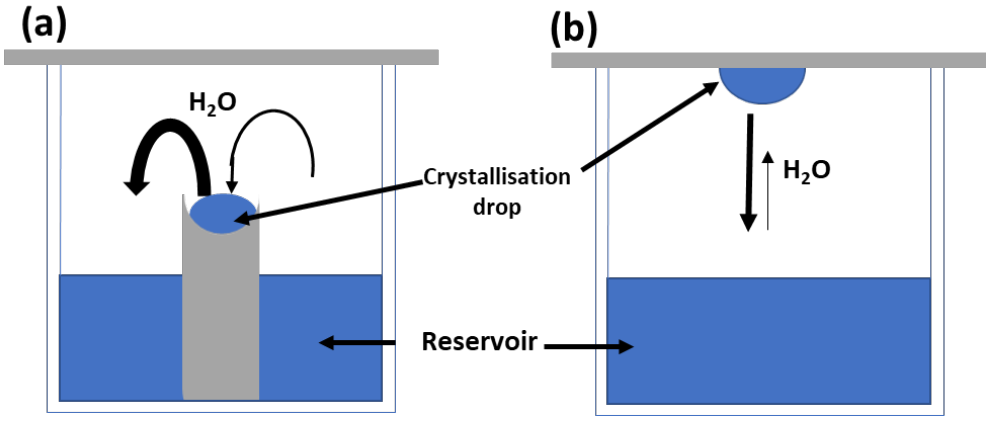

Figure 3.1. An illustration of Vapour diffusion crystallisation techniques. (a) Sitting drop vapour diffusion and (b) hanging drop vapour diffusion.

There are two main types of vapour diffusion crystallisation techniques: the hanging drop and the sitting drop settings. [91, 114]. In this chapter, all experiments are conducted in a sitting drop setting, where the protein droplet is placed on a substrate above the reservoir level. The well is sealed, and the crystallisation process occurs when the equilibrium between the droplet and the solution is reached.

Several studies have been conducted to investigate the effect of electric fields on the crystallisation of proteins using the vapour diffusion method. In 1999, Taleb et al. developed two devices to study the effect of an external DC electric field on the crystallisation of hen egg white Lysozyme (HEWL) by introducing metal electrodes at the sides of the crystallisation drop [51]. Both setups resulted in noticeable electric field effects on the size and quality of the resulting HEWL crystals. An alternative system used quasi-two-dimensional all-glass cells placed between two metal plate electrodes to study the effect of electric field on the crystallisation of HEWL, which resulted in a preferred orientation of the crystals along the c-axis [53, 55]. The advantages of these cells are the high visibility of the drops under a light microscope, the rapid cool down, and the suitability for electric-field application [55].

Flores-Hernández and colleagues designed an alternative vapour diffusion device for internal DC electric-field-assisted crystallisation, consisting of two parallel ITO-coated glass plates parallel to each other. A rubber material is shaped to contain two reservoirs and is sandwiched between the two glass plates connected to the power source [82]. This device is relatively easy to set up and use. A similar setup was used by Pareja and coworkers [37] to study DC and AC electric fields effects on crystallisation.

Despite the different approaches used to study the effect of electric fields on the crystallisation of proteins, most setups involve the design of new crystallisation plates/chambers or the alteration of commercially available plates. The setups also limit the study to a single condition per trial, which requires further validation due to the stochasticity

of the crystallisation process. Moreover, the monitoring process and post-crystallisation analysis techniques, such as X-ray crystallography, need to be considered. In this chapter, a novel low-cost crystallisation device was designed to study the effect of strong electric fields on vapour diffusion crystallisation. The setup allows the study of multiple conditions concurrently and can be developed further to utilise a full crystallisation plate.

3.2. Materials and methods

3.2.1. Materials

A 20 mg mL^{-1} working solution of HEWL was prepared as in section 2.2.1. The working solution is further diluted to 10 mg mL^{-1} by adding an equivalent volume of buffer. The precipitant solution (NaOAc, 1 M) was prepared as described in section 2.2.1. Sodium chloride stock solution (5M) was prepared by dissolving 29.2 g Sodium Chloride (Sigma Aldrich) in 100 mL Milli-Q water and filtering with a 0.22 μm syringe filter.

All vapour diffusion experiments were performed in 24-well Chryschem sitting drop crystallisation plates (Hampton Research, UK). To study the effect of the electric field on the nucleation of HEWL at varying protein concentrations and following crystallisation screening, all further experiments were conducted at pH 4.6 using 1.4 M NaCl concentration and 10 and 20 mg mL^{-1} protein concentration. 500 μL of the precipitant solution was pipetted into the crystallisation reservoir, and a droplet of 2 μL of HEWL and 2 μL of precipitant was pipetted into the crystallisation well. The plate was sealed with ultra-clear sealing tape (Shurtape, USA) and monitored at room temperature. The electric field (10,000 V, 5 x 10^6 V m^{-1}) was applied using a positive DC power supply for 48 hrs. In each experiment, a control experiment was conducted to compare the outcomes, and due to the stochastic character of the experiments, each experiment was repeated 4-5 times for statistical data collection.

3.2.2. Methods

3.2.2.1. The experimental setup

A novel low-cost experimental setup was designed and fabricated to study the effect of electric field on the crystallisation of proteins using the sitting drop vapour diffusion technique. The setup was designed using CAD design software (Solid Edge, 2019) and consists of two 3D-printed parts, two sets of copper plate electrodes, and a set of glass visualization plates. The 3D printed parts are printed with polylactic acid (PLA) filament material (2.85 mm, RS Pro, UK) using an Ultimaker3 3D printer. The visualization plates are made of clear annealed glass (3 mm thick, Viewforth Glazing, UK).

The electrodes were made of pure copper sheets (0.51 mm thick, Chudeng, China), which are connected to the high-voltage power source via high voltage cables (22 AWG, 40 kV, 4.76 mm diameter, China). High voltage DC power supply (HV350REG(+), Information Unlimited, Amherst, USA) was used to apply the electric field. Positive polarity voltage was used in all experiments. The experiments were monitored in real-time using an optical microscope (M5A, Wild Heerbrugg, Switzerland), equipped with a USB digital eyepiece microscope camera (MD500, Amscope, USA) and operated by a computer using imaging software provided by the manufacturer (Amscope v4.11.21462, Amscope, USA).

3.2.2.2. Image analysis

The experiments were initially monitored in real-time for 4 days, where time-lapse images were taken every 15 minutes. After that, all crystallisation wells were monitored once a week for up to 5 weeks. Images of the crystallisation drops were collected at different focal lengths and analysed using image analysis software. Amscope (v4.11.21462, Amscope, USA) was used to merge images of different depths into one image using the extended depth of focus (EDF)

feature. Crystal counting, size measurements, and other analyses were performed manually, using Fiji-ImageJ software (v.1.53, National Institutes of Health, Bethesda, USA).

3.2.3. Design and fabrication of the vapour diffusion electric-field-assisted crystallisation setup

3.2.3.1. The design

The overall design of the setup is illustrated in Figure 3.1. It consists of a 3D-printed part designed to hold the crystallisation plate and the electrodes. It is featured with two sets of inter-well panels equipped with two sets of parallel copper plate electrodes. The panels are first printed separately with dimensions (95 * 25 * 3 mm). The electrodes are then fixed along the panels using an epoxy adhesive (Araldite, Huntsman Advanced Materials, UK) before the panels are glued to the 3D-printed base unit. The two sets of electrodes are designed so that each well in columns number 2 and 5 in the crystallisation well falls between the panels, making the electrodes positioned on both sides of the crystallisation wells. This means that each well in columns 2 and 5 in the crystallisation plate falls between two parallel electrodes. The distance between each set of electrodes is 20 mm.

The second part of the setup consists of a PLA 3D-printed frame-like structure with a glass plate fixed at the top. The part serves as an insulator protecting the user from the high voltage, in addition to aiding the visualization and monitoring of the crystallisation process. The outer dimensions of the setup are 190 × 140 × 30 mm.

The setup is placed under an optical microscope to monitor the crystallisation process in real time. The camera is set to take time laps of one well every 15 minutes for four days. This allows the observation of induction time and nucleation and growth rate of the crystallisation trials. The wells are then imaged weekly to collect data on the numbers and size of the crystals.

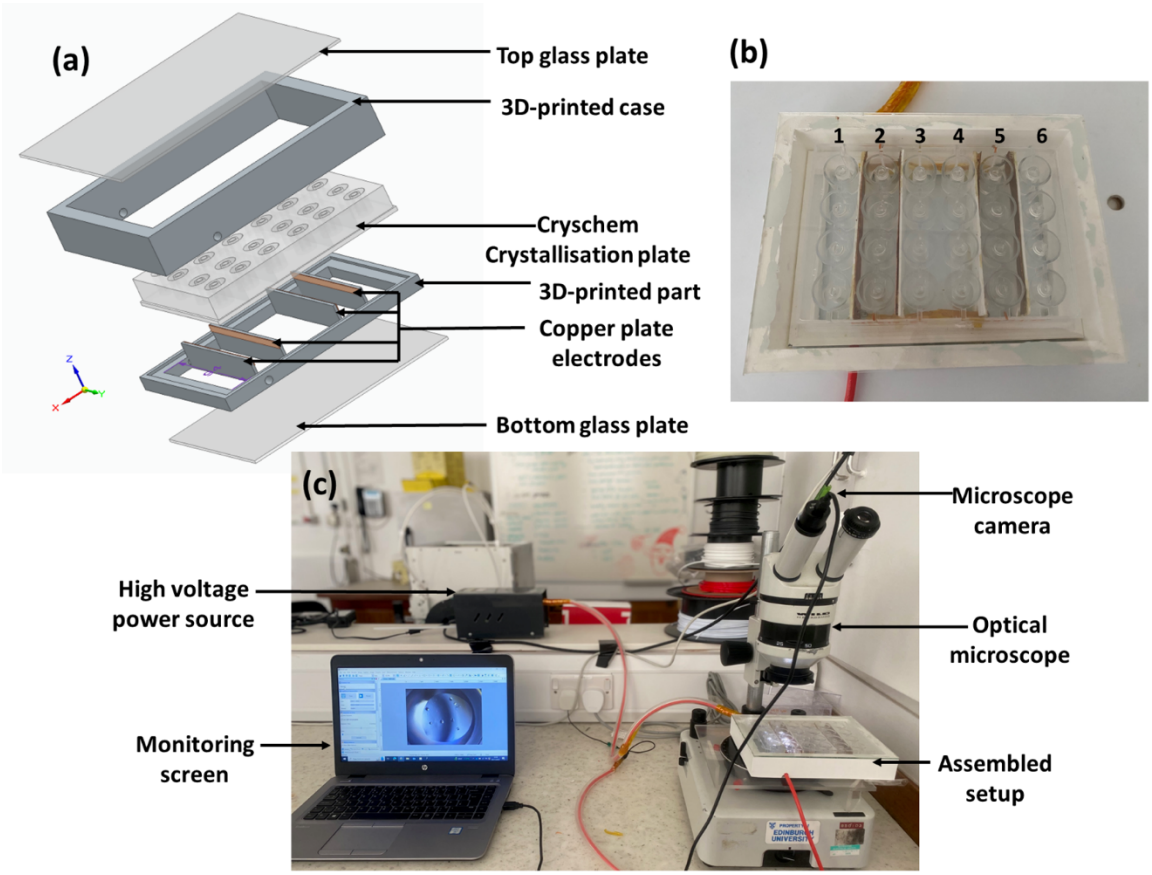

Figure 3.2. The CAD model and the corresponding photograph of the electric-field-assisted vapour diffusion crystallisation setup (Setup II). (a) The CAD model of the crystallisation setup, (b) a photograph of the 3D-printed casing equipped with the electrode connections and the crystallisation plate, and (c) a photograph of the whole setup connected to the high-voltage power source and placed under the microscope for continuous monitoring via the monitoring screen.

3.2.3.2. 3D printing

Ultimaker3 (Ultimaker, the Netherlands) 3D printer was used to print the main parts. The stl. files from Solid Edge software are converted to GCODE file format using Ultimaker Cura (4.13.1). The parameters used for printing are shown in Table S1.

3.2.3.3. High-voltage electrodes and connection

The electrodes in Setup II are designed to create a uniform electric field across the active crystallisation wells. In a 24-well Cryschem sitting drop crystallisation well, the active wells used in this setup are those in columns 2 and 5. The setup is designed so that each of the active wells falls between two parallel plate electrodes.

The electrodes are prepared by cutting four pieces of copper sheet to the desired dimensions (90* 9 mm) and introducing a perforation on the side of each sheet for the purpose of electrical connection (Fig. 3.2). Each electrode is connected to a safe, high voltage (SHV 5 kV) power cable (22 AWG, 40 kV, 4.76 mm diameter, China) through the perforation and fixed in place using the soldering technique. The electrodes are then fixed to the top part of the 3D-printed panels using an epoxy adhesive (Araldite, Huntsman Advanced Materials, UK) and left to dry for 48 hours. The right-side electrodes in each set are connected to a high-voltage power source via a banana plug, whereas the left-side electrodes are connected to ground. The distance between each set of electrodes is 20 mm. The power source is connected to the earth through a ground cable plugged into the power supply's earth inlet.

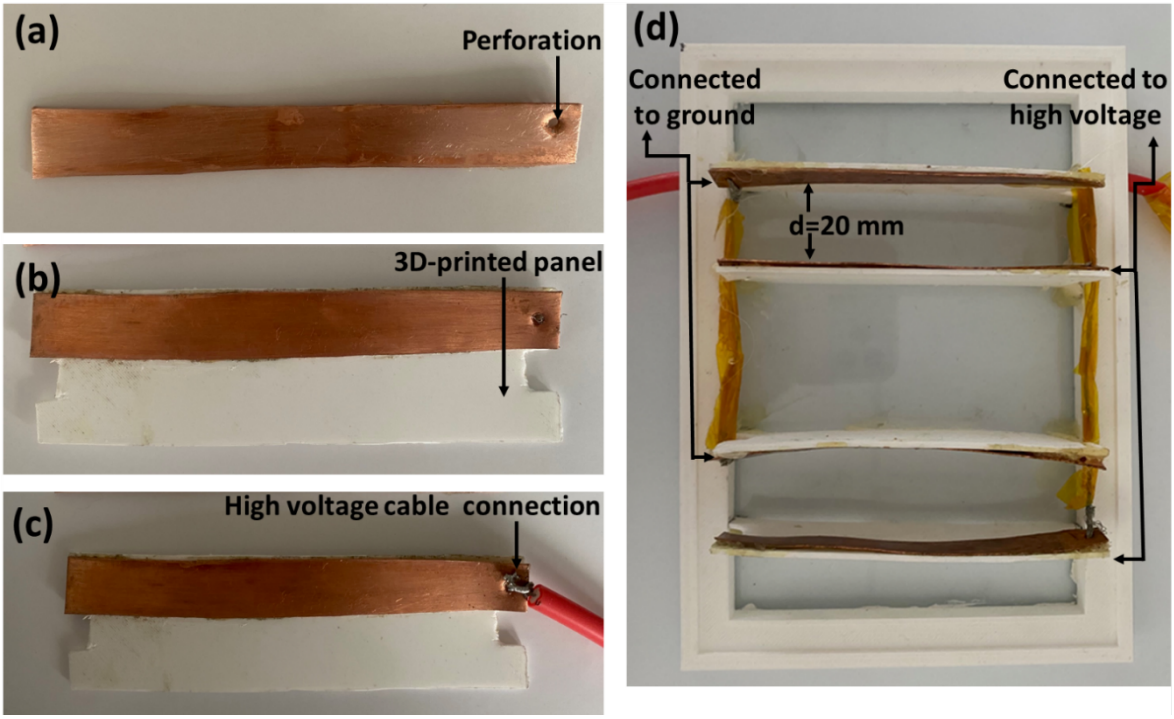

Figure 3.3. The configuration of the copper electrode plates used in the vapour diffusion setup. (a) A photograph of an electrode plate with a perforation, (b) the electrode fixed on the panel, (c) the electrode connected to the high-voltage cable, and (d) the setup with the two sets of electrodes.

3.2.3.4. Safety measures

As the electric-field-assisted crystallisation experiments involve the use of high voltage (10 kV), an electrically insulating polymer material (PLA) was used as the main compartment. In addition to PLA, and due to its high dielectric strength and resistivity, glass was used to allow continuous visualization of the plate. Glass was securely fixed in the setup to prevent electric shock. All the connections and cable ends were secured with three layers of Kapton tape for enhanced protection, and high voltage cables were inserted into flexible silicone tubes for additional insulation. The experiments are regularly monitored to maintain the safety.

3.3. Results

3.3.1. Effect of electric field on nucleation of HEWL

The effect of the electric field on the nucleation of HEWL at varying protein concentrations was studied by monitoring the change in the number of crystals with time compared to a control experiment. The statistical data were collected from three experiments, and the average number of crystals plotted against time.

The experimental results show enhanced nucleation of HEWL by the application of electric field at both protein concentrations. At a lower protein concentration (10 mg mL^{-1}), the HEWL crystals in the control experiment took about two weeks to nucleate fully, whereas when an electric field was applied, the full nucleation of HEWL crystals took about one week. The same effect was observed at higher protein concentrations (20 mg mL^{-1}) (Fig. 3.3).

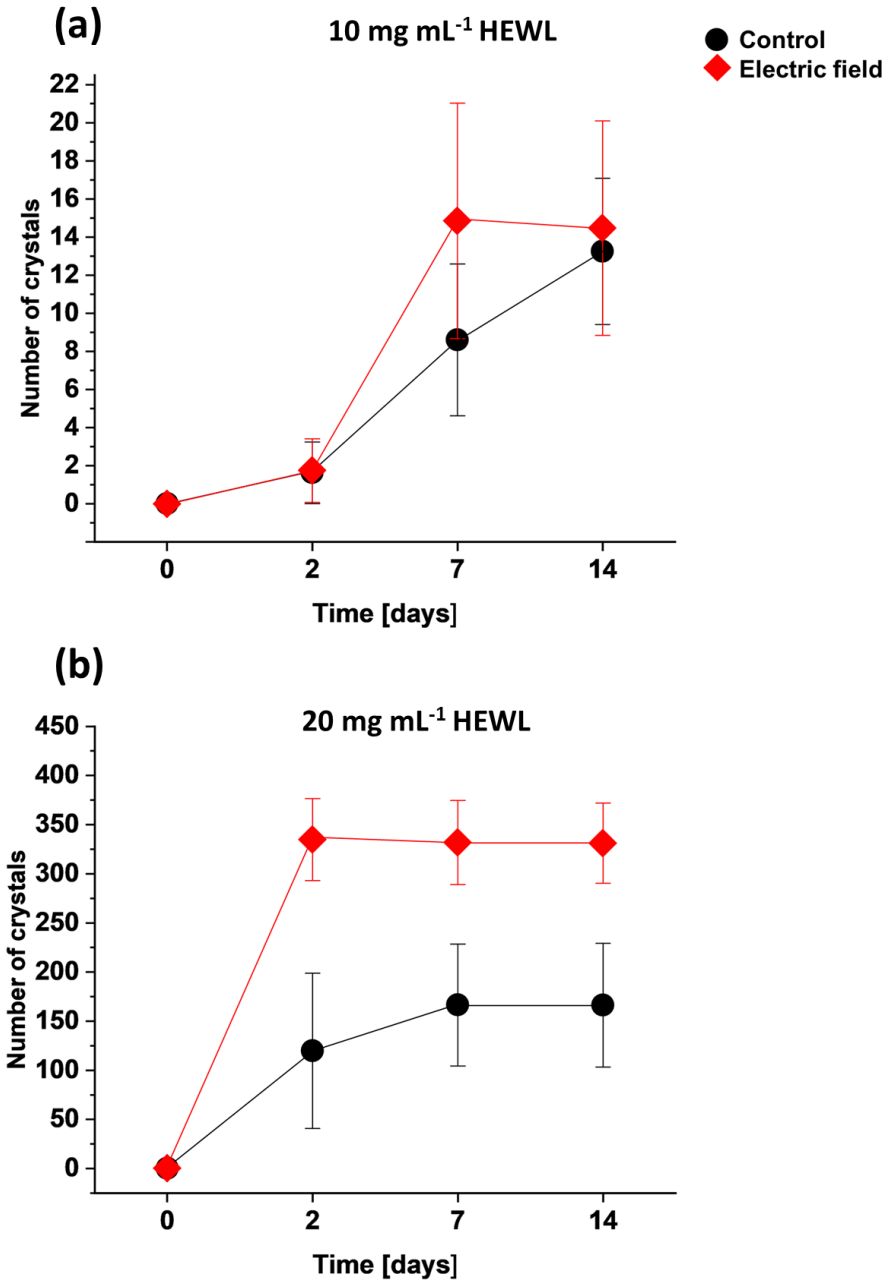

Figure 3.4. The effect of direct current positive electric field (5 x 10^6 V m^{-1}) on the number of HEWL crystals with time (pH 4.6, 0.1 M NaOAc, 1.4 M NaCl) at HEWL concentration (a) 10 mg mL^{-1} and (b) 20 mg mL^{-1}. A faster nucleation is observed at both HEWL concentrations when electric field is applied.

Whilst the control experiment shows random HEWL nucleation through the droplet volume, the majority of crystals appeared within the centre of the droplet when electric field is applied (Fig. 4.4).

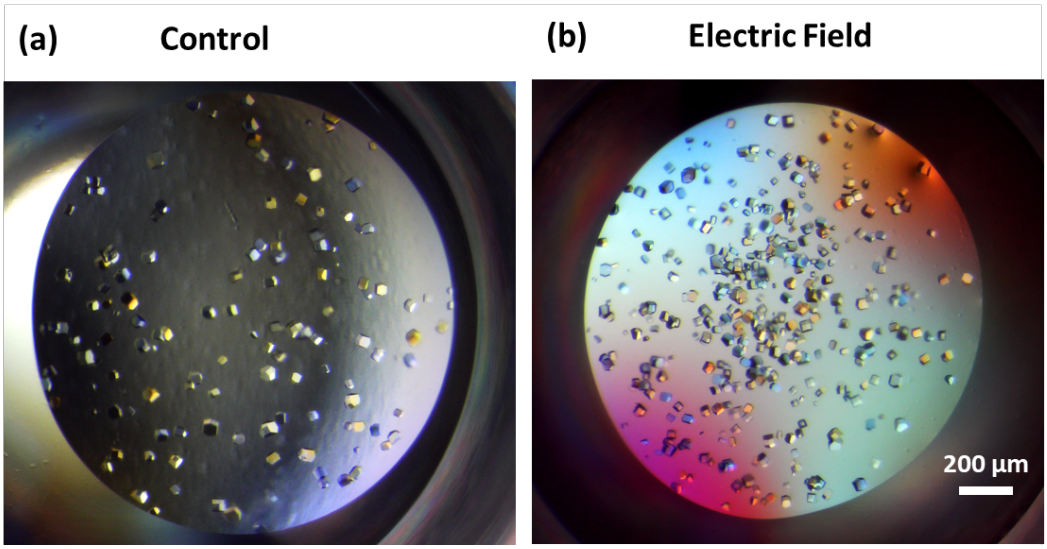

Figure 3.5. Micrographs showing the distribution of HEWL (20 mg mL^{-1}, pH 4.6, 0.1 M NaOAc, 1.4 M NaCl) crystals throughout the droplet volume after 14 days of the experiment conducted (a) without electric field and (b) with electric field.

3.3.2. Effect of electric field on the number of HEWL crystals

The effect of the electric field on the number of crystals was studied by counting the number of crystals in a drop after two weeks of the experiment, when no more nucleation was observed. The number of crystals was plotted to compare the effect of the electric field in contrast to the control experiments (Fig. 3.5).

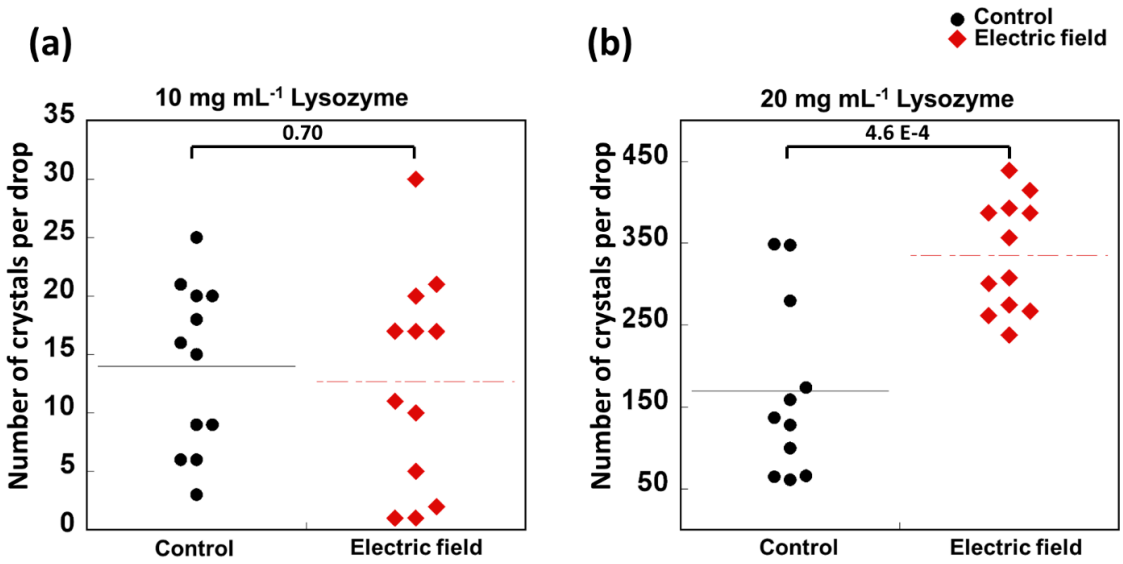

Figure 3.6. The effect of direct current electric field (5 x 10^6 V m^{-1}) on the number of HEWL crystals per drop (pH 4.6, 0.1 M NaOAc, 1.4 M NaCl) at (a) 10 mg mL^{-1} and (b) 20 mg mL^{-1}. A higher number of crystals is produced when electric field is applied. P-values are illustrated, showing a non-significant difference between datasets at 10 mg mL^{-1} (p-value > 0.05), whereas a significant difference is observed at 20 mg mL^{-1} (p-value < 0.05).

Table 3.1 shows the descriptive statistical analysis of the experimental data. At a protein concentration of 10 mg mL^{-1}, the number of crystals obtained when an electric field is applied exhibits no difference compared to the control experiment. On the other hand, a considerable effect of the electric field is observed at 20 mg mL^{-1}. The mean number of crystals produced with an electric field is slightly lower than the control at lower HEWL concentration, whereas at higher HEWL concentration, a higher mean number of crystals is observed with the electric field.

Table 3.1. Statistical analysis of the crystal count data. Main parameters affected by electric field are highlighted in bold.

	10 mg mL^{-1} HEWL		20 mg mL^{-1} HEWL	
	Control	Electric field (Positive voltage)	Control	Electric field
Mean	14	12.67	**217.75**	**335.75**
Standard Error	2.06	2.66	56.53	19.72
Median	15.5	14	148	332.5
Standard Deviation	7.15	9.22	**195.83**	**68.30**
Sample Variance	51.09	84.97	38350.21	4664.75
Kurtosis	-1.33	-0.90	**2.43**	**-1.47**
Skewness	-0.11	0.19	**1.75**	**0.03**
Range	22	29	685	201
Minimum	3	1	61	238
Maximum	25	30	746	439
Sum	168	152	2613	4029

Electric field resulted in narrower distribution at 20 mg mL^{-1} HEWL concentration. In addition, a smaller value of skewness is observed when electric field is applied, which indicates the longer tail on the left side of the distribution.

3.3.3. Effect of electric field on HEWL crystal size and size distribution

The effect of electric field on the crystal size and size distribution is obtained by measuring the longest apparent axis of the crystals. The application of electric field was found to affect the size of the resulting crystals, where smaller sizes are observed when electric field is applied. This effect is greater at 20 mg mL^{-1} HEWL concentration (Fig. 3.6).

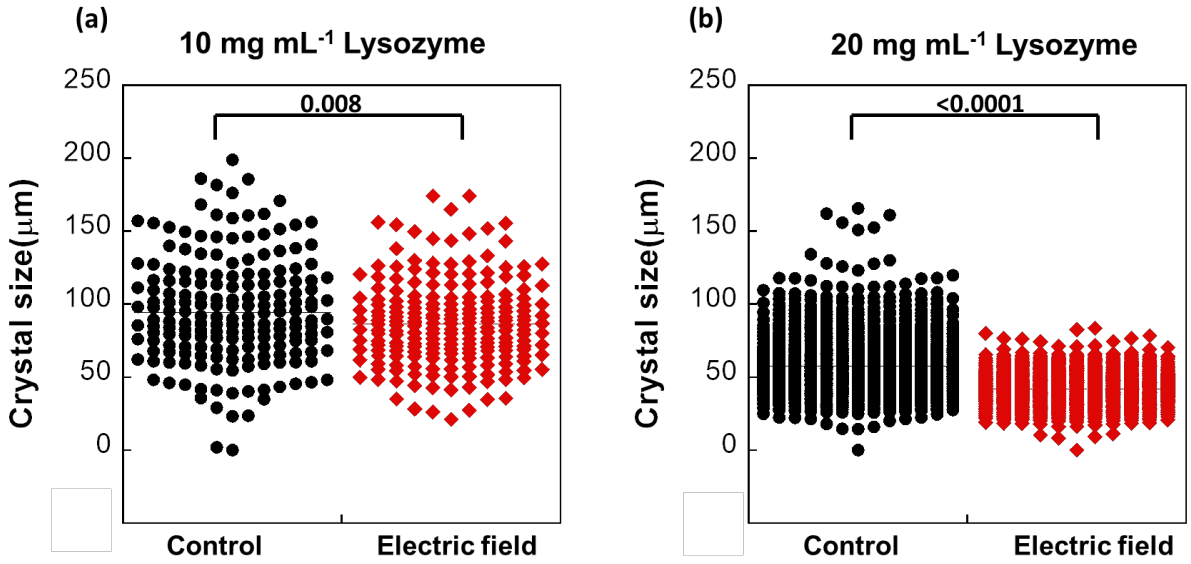

Figure 3.7. The effect of direct current electric field (5 x 10^6 V m^{-1}) on the size of HEWL crystals (0.1 M NaOAc, 1.4 M NaCl, pH 4.6) at (a) HEWL concentration 10 mg mL^{-1}, and (b) HEWL concentration 20 mg mL^{-1}. Smaller crystals are produced when electric field is applied. P-values are illustrated, showing significant differences between datasets at 20 mg mL^{-1} HEWL concentration (p-value < 0.05).

HEWL crystals are subjected to size distribution analysis by plotting crystal size ranges versus the frequency of each crystal size at varying protein concentration (10 and 20 mg mL^{-1}). The results are illustrated in Figure 3.7.

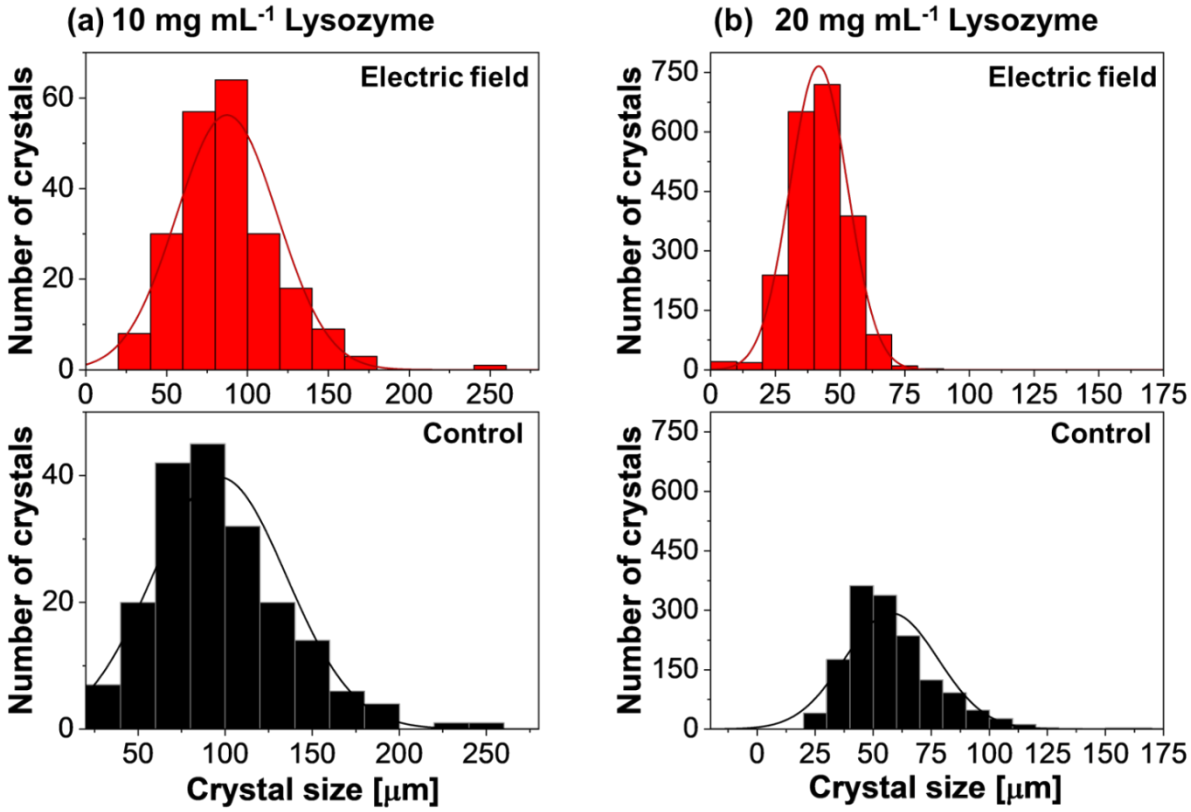

Figure 3.8. Crystal size distribution of HEWL (0.1 M NaOAc, 1.4 M NaCl, pH 4.6) at (a) 10 mg mL^{-1} and (b) 20 mg mL^{-1}. A narrower size distribution is observed when electric field is applied at a higher HEWL concentration.

The size distribution data show a noticeable decrease in the crystal size at both protein concentrations; however, smaller crystals were observed when the electric field was applied. In addition, the effect of the electric field on the size of crystals is greater at 20 mg mL^{-1} HEWL concentration compared to 10 mg mL^{-1}. The mean size of crystals produced is lower when the electric field is applied. The normal distribution of the crystals at 20 mg mL^{-1} HEWL concentration shows lower kurtosis and skewness than the control, which indicates a narrower size distribution. Table 3.2 shows the descriptive statistical analysis of the experimental data.

Table 3.2. Statistical analysis of the HEWL crystal size data at two protein concentrations (10 and 20 mg mL^{-1}). Main parameters affected by electric field are highlighted in bold.

	10 mg mL^{-1} HEWL		20 mg mL^{-1} HEWL	
	Control	Electric field (Positive voltage)	Control	Electric field
Mean	95.18	86.48	**57.73**	**42.14**
Standard Error	2.59	1.96	0.51	0.23
Median	89.02	85.01	54.00	42.10
Standard Deviation	35.75	29.01	**19.68**	**10.46**
Sample Variance	1278.32	841.78	387.13	109.51
Kurtosis	-0.12	0.29	**2.84**	**0.09**
Skewness	0.49	0.48	**1.23**	**0.18**
Range	175.99	153.00	151.23	75.48
Minimum	23.02	21.10	14.42	8.06
Maximum	199.01	174.09	165.65	83.55
Sum	18084.86	18939.61	85088.18	89331.37

3.3.4. Effect of electric field on HEWL crystal growth rate

The crystal growth rate data were collected by monitoring a crystallisation drop for four days and collecting time lapse images every 15 minutes. The images were then analysed, and the length of face 001 of the tetragonal HEWL crystals measured using ImageJ software and plotted against time (Fig. 3.12). Due to the limitation of the camera resolution, the smallest length measured was 7-9 µm. The growth rate was calculated by plotting the size of the crystal in the first 15 hours of growth against time and measuring the slope. The analysis was conducted at one experimental condition (HEWL concentration 20 mg mL^{-1}) due to the limitation of equipment and the slower growth at lower HEWL concentration (Fig. 3.8).

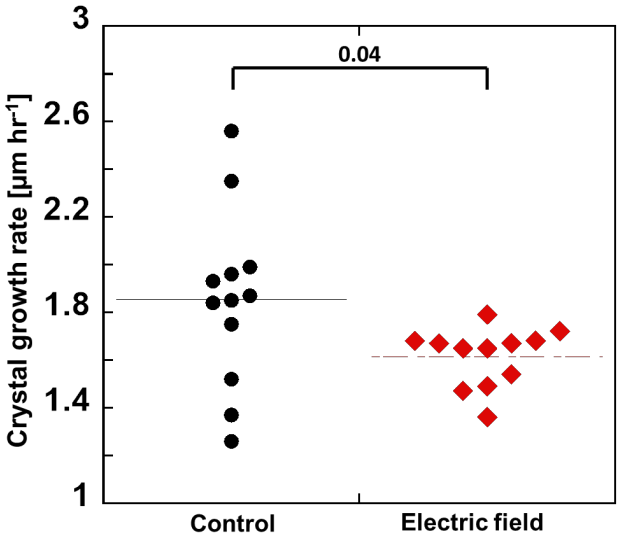

Figure 3.9. The effect of direct current electric field (5 x 10^6 V m^{-1}) on HEWL crystal growth rate (20 mg mL^{-1}, 0.1 M NaOAc, 1.4 M NaCl, pH 4.6). A slower growth rate is observed when electric field is applied. P-values are illustrated, showing a significant difference between the control and experimental results (p-value < 0.05).

3.4. Discussion

The experimental results of HEWL crystallisation under the effect of positive electric field at varying protein concentrations demonstrate a noticeable effect on the crystallisation process. The effect is more obvious at higher concentrations in the nucleation, size, number, and growth of the resulting HEWL crystals.

In Chapter 1 (section 1.6.1), the theoretical aspects of the effect of electric field on the crystallisation system are explained. It has been illustrated that electric field modifies the chemical potential of the solid and liquid phases, which results in the modification of the equilibrium states of these phases [49]. The difference in the chemical potential between the protein solid and liquid phases, the driving force for nucleation [1, 115], is enhanced when an electric field is applied [1, 103].

Electric field was found to enhance the nucleation of HEWL, which is demonstrated by higher number of crystals growing with time when electric field was applied compared to the control, in addition to the reduction of the time required for the nucleation to complete (Fig. 3.3). According to the two-step nucleation theory, protein molecules come together to form a dense liquid phase, which is considered the intermediate phase before crystal growth. The process of forming the dense phase or the nuclei can be thought of as a transition in both the concentration and the structure of the solution phase [116]. The concentration transition is governed by supersaturation, while the structural transition can be explained by the accumulation of structural fluctuations, such as the orientation of protein molecules in a crystal-like manner [116]. The electric field may have promoted the structural transition, leading to the formation of more nuclei.

Given that protein crystallisation is a stochastic process, and due to the sensitivity of proteins to minor changes in experimental conditions, the electric field and its parameters (strength, polarity, configuration… etc.) can be considered as extra variables that require further effort in testing and optimisation. In addition, the effect of electric field is also found to be dependent on the strength of the electric field [73, 97].

As the electric field modifies the equilibrium state of the crystallisation process, the result of this modification may appear in different ways depending on the experimental conditions. When nucleation occurs, numerous crystals grow almost simultaneously [116]. Promoted nucleation refers to forming more nuclei, which could result in the formation of smaller crystals with a larger surface area. As more crystals form, the simultaneous growth of these crystals results in a faster depletion of protein molecules from the solution [116, 117] leading to the subsequent reduction in crystal size (Fig.Fig. 3.6). In contrast, if nucleation is slow and fewer crystals nucleate at a time, the supersaturation in the solution gradually lowers, the nucleation of new crystals continues, and a population of crystals of diverse sizes emerges [116].

Whilst numerous studies resulted in a decrease in the number of crystals when an electric field is applied [36, 37, 51, 58, 60, 82], this effect was not observed with the conditions used in this study. At lower concentration (10 mg mL^{-1}), the effect of electric field on the number of crystals appeared to be absent or minimal as indicated by the high probability value ($p = 0.7$), which is much higher than the significance level ($p \leq 0.05$). However, a considerable increase in the number of crystals was observed at higher protein concentration (20 mg mL^{-1}) indicated by the lower probability ($p \leq 0.05$). This indicates the enhanced nucleation induced by the application of electric field and its dependence on the experimental conditions (Fig. 3.5).

The electric field is known to add extra energy to the crystallisation system, and due to the ionic nature of the system, electromigration plays a major role in the displacement of the protein and the salt ions by the potential difference, which stimulates the local supersaturation in the crystallisation drop, hence the nucleation [49, 104]. In addition, electric-driven convection within the crystallisation drop may be created by the high strength of the electric field, which may have resulted in enhanced HEWL nucleation. A similar effect was observed by Pencova et al. when investigating the sitting drop crystallisation of HEWL [110].

In many cases, the experimental results suggest that electric field can affect the location of the resulting crystals (Fig. 3.4). This was demonstrated by the appearance of the crystals close to (~300 µm) the center of the droplet. This can be explained by the induced rotational flow in the crystallisation drop by electric field [118]. These results are consistent with the findings of Pencova et al., who investigated the effect of electric field ranging from 2 to 6 x 10^5 V m^{-1}, on the nucleation of HEWL. Their results show enhanced HEWL nucleation and that the crystals are nucleated at a specific radius of the droplet (~100 µm) when electric field is applied. In contrast, in the absence of an electric field, the crystals were distributed randomly within the volume of the solution.

3.5. Limitations of the study

3.5.1. The experimental setup

The experimental setup presented in this chapter was designed to study the effect of electric field on crystallisation of proteins using a different technique and electrode configuration than those used in chapter 2. Due to the time constraints and the challenges associated with data analysis, the setup allows the investigation to be carried out at two experimental conditions considering the need for replicates (2 active columns, 8 wells). Nevertheless, extra electrodes could be added to cover the whole plate (6 columns) for a wider range of conditions.

Another factor to consider is the magnitude of the electric field that reaches the droplets during the crystallisation process. As mentioned in earlier chapters, the existence of dielectric media between the electrodes and the wells could have diminished the actual intensity that reached the crystallisation drops [9]. In Setup II, attempts were made to reduce the decrease in electric field strength by placing the electrodes on the sides of the reservoirs and applying a higher voltage to create a more uniform electric field across the wells. The shape and geometry of the crystallisation plate also influenced the control of this process, as the goal was to avoid altering the plate itself.

3.5.2. Data collection and processing

The measurements of induction and growth rates of the crystallisation process require high-resolution optical microscopic imaging for both control and experimental trials. The lack of identical equipment for data collection may have affected the accuracy of the data. In

addition, automated data processing was not possible due to the setting of the crystallisation well and the various orientations of the resulting crystals.

3.6. Conclusion

An experimental setup for electric-field-assisted crystallisation of proteins using the sitting drop vapour diffusion technique was designed and fabricated. The setup provides a low-cost, handy tool to investigate the effect of electric field at a wide range of conditions, while monitoring the process in real time. HEWL was used as a model protein to test the setup and validate the effect of electric field on protein crystallisation. The experimental results show an enhancement of HEWL nucleation and an increase in the number of crystals when the electric field is applied. However, the result is observed to a greater extent at higher protein concentration. In addition, smaller size crystals are produced when the electric field is applied than in the control experiment at HEWL concentration of 20 mg mL^{-1}. These effects may result from the enhancement of the chemical potential difference between the solid and liquid state of the medium, which is the driving force of nucleation. In addition, electromigration and electric-driven convection within the crystallisation drop resulted in enhanced nucleation. Although the setup resulted in higher nucleation, and since protein crystallisation is a stochastic process, further studies on HEWL and other proteins at various experimental conditions and field strength can aid in an improved understanding of the electric field effect.

Electric-field-assisted crystallisation setup for in situ vapour diffusion

4.1. Introduction

The most significant outcome of the crystallisation of proteins is the structure determination, which requires high-quality, well-ordered crystals for XRD studies. Protein crystals consist of molecular units packed into defined, orderly lattice space groups. The crystalline form is widely known to be a more energetically favorable state, with an estimated 3-6 kcal/mol higher stability than solution [119]. Only 65 space groups are feasible for protein crystals out of the 230 potential crystal unit symmetries [6, 120, 121]. This is because protein crystal structures are enantiomerically pure, where all the molecules are chiral and contain the same chirality. The space group of a chiral crystal structure only consist of first-kind symmetry operations such as translations, pure rotations, and screw rotations [6]. These groups are called Sohncke groups (a.k.a. non-enantiogenic space groups) and are listed in Table 4.1 [122].

Table 4.1. The 65 non-enantiogenic protein space groups [123].

Crystal system	Space Groups (65)
Triclinic	P1
Monoclinic	P 121, P 12_11, C 121
Orthorhombic	P222, P222_1, P2_12_12, P$2_12_12_1$, C222_1, C222, F222, I222, I$2_12_12_1$
Tetragonal	P4, P4_1, P4_2, P4_3, I4, I4_1, P422, P42_12, P4_122, P4_12_12, P4_222, P4_22_12, P4_322, P4_32_12, I422, I4_122
Trigonal	P3, P3_1, P3_2, R3, P312, P321, P3_112, P3_121, P3_212, P3_221, R32
Hexagonal	P6, P6_1, P6_5, P6_2, P6_4, P6_3, P622, P6_122, P6_522, P6_222, P6_422, P6_322
Cubic	P23, F23, I23, P2_13, I2_13, P4_32, P4_232, F432, F4_132, I432, P4_332, P4_132, I4_132

The most commonly detected space group in protein crystals is *P*2_12_12, an orthorhombic space group[120]. However, HEWL crystallises with multiple space groups. At pH 4.7, HEWL crystals exhibit a tetragonal space group (*P*4_32_12) with unit cell parameters of a = b = 79.1 and c = 37.9 Å [124, 125]. In addition, HEWL has been crystallised in monoclinic and orthorhombic space groups [126, 127]. It has been established that the alteration in the crystal environment initially impacts the intermolecular solvent molecules, resulting in subsequent modifications to the arrangement of the crystal [128].

To identify a protein's molecular structure and space group, usually a single protein crystal is subjected to XRD analysis. The quality of the crystals is crucial for successful structural data analysis. Therefore, improving the quality of protein crystals enhances the resolution and completeness of diffraction data, which are necessary for the quality of electron density maps rebuilt [129]. Crystal quality can be evaluated using different parameters, mainly the crystal resolution limit and mosaicity [34, 35]. In addition, the Wilson B factor or the molecular displacement factor can be used to measure crystal quality as it assesses the degree of order in the crystal [34, 130].

XRD investigations involve subjecting the samples to substantial radiation doses, producing photoelectrons and free radicals, which can impact the crystal lattice by radiation damage,

leading to a deterioration in diffraction quality [28]. Protein crystals are more fragile than nonbiologic crystals due to the high content of solvent molecules [10] and the weak intermolecular interactions; generally, hydrophobic interactions, H-bonds, and salt bridges between/within the proteins maintain the structure of protein crystals [119, 131, 132].

To minimise crystal degradation by radiation damage, handling them with care and avoiding distortion is crucial. The conventional procedure, which involves physically manipulating individual crystals, immersing them in cryoprotectants, and subjecting them to cryocooling, can potentially cause disintegration, cracking, or splitting of the crystals [28, 133]. In situ crystallisation eliminates the need to harvest the crystals and subject them to cryocooling [27]. This technique allows data collection for multiple crystals at room temperature by focusing the X-ray beam directly into the crystallisation plate.

The versatile Macromolecular Xtallography *in-situ* (VMXi) beamline at the Diamond Light Source facility is dedicated to gathering data from macromolecular crystals at room temperature fully automatedly. In situ diffraction is conducted without manipulating individual crystals, hence maintaining their integrity and protecting them from dehydration, physical handling, cold shock, and the effects of cryoprotectants [29, 30].

The data collected by the beamline can be of an exceptional quality comparable to that obtained using the MX cryo-beamlines. This is because the data could be collected from crystals in the same well are automatically processed together, potentially yielding complete datasets. Combining information from multiple crystals allows routine determination of high-quality room temperature structures [29]. For instance, Xia2.DIALS program allows the user to process multi-crystal diffraction data sets via indexing, integrating, and scaling the individual datasets [29, 134].

In this chapter, two experimental setups were designed and fabricated to investigate the effect of electric field on the quality of protein crystals. The setups allow the application of electric field in the in situ crystallisation plate format and the carrying out of in situ diffraction studies. The investigation was carried out using HEWL as a model protein. In addition, the effect of EF on the quality of REMC1 crystals was investigated.

4.2. Materials and methods

4.2.1. Materials

A 20 mg mL^{-1} working solution of HEWL was prepared as in section 2.2.1. The working solution is further diluted to 10 mg mL^{-1} by adding an equivalent volume of buffer. The protein was then centrifuged for 15 minutes at 16000 rpm, and aliquots of 50 µL were flash-frozen in liquid nitrogen. The precipitant solution (NaOAc, 1 M) was prepared as described in section 2.2.1. Sodium chloride stock solution (5M) was prepared by dissolving 29.2 g Sodium Chloride (Sigma Aldrich) in 100 mL Milli-Q water and filtering with a 0.22 µm syringe filter. The 5 M NaCl solution was used for subsequent dilutions.

Based on previous screening, HEWL was crystallised at varying pH (4.6 and 4.9), HEWL concentration (10 and 20 mg mL^{-1}), and salt concentration (1.0 and 1.2 M). The droplet size was 3 µL (1.5 + 1.5 µL), and the electric field (1000V, 2x 10^5 V m^{-1}) was applied using a negative voltage power source for 48 hrs. The experiment was repeated 3-5 times, and the plates were delivered to the Diamond Light Source synchrotron facility for diffraction analysis.

$REMC1_{100\text{-}525}$ (clone number: MRO 029) working solution and precipitant solution were prepared as described in section 2.2.1. REMC1 has been crystallised previously using vapour diffusion and microbatch methods at concentration 30-50 mg mL^{-1} yielding cubic-shaped crystals within 24 hrs. In Setup III, electric field (1,000 V, 2x 10^5 V m^{-1}) was applied using a negative voltage power source for 48 hrs. Since RMC1 nucleation takes around 24 hrs, the

duration of applying electric field in Setup IV was reduced from 48 hrs to 24 hrs (10,000 V, 2x 10^5 V m^{-1}).

All the in situ experiments were conducted in Greiner CrystalQuick^{TM}X Plates (MiTeGen, Ithaca, NY, USA). The plates feature two flat, square-shaped crystallisation wells per reservoir, which allows relatively small droplets to be used. The volumes used for the crystallisation drop ranged from 0.5-3 µL, and the reservoir solution volume was 40 µL. The plates are compatible with automated systems; however, manual pipetting was used in all experiments. A crystal-clear sealing tape (ClearSeal Film, Hampton Research, UK) was used to seal the plates, and they were monitored in real-time at room temperature. A triplicate of each condition was prepared in each experiment, and a control experiment was run to compare the outcomes. Each experiment was repeated 3-5 times for statistical data collection.

4.2.2. Methods

4.2.2.1. The experimental setups

Two experimental setups were designed and fabricated for the electric-field-assisted crystallisation and in situ diffraction studies. Both setups were designed using CAD design software (Solid Edge, 2019) and consist of two 3D-printed parts, copper electrodes, and glass visualisation plates. The 3D printed parts are printed with polylactic acid (PLA) material (2.85 mm, RS Pro, UK) using an Ultimaker3 3D printer (Ultimaker, the Netherlands). The visualization plates are clear annealed glass plates (3 mm thick, Viewforth Glazing, UK).

The electrodes were made of single copper wire (0.2 mm diameter, Genvolt Ltd, UK) in the first setup (Setup III), and copper sheets (0.51 thick, Chudeng, China) in the second setup (Setup IV). High voltage was connected to the setups using high voltage cables (22 AWG, 40 kV, 4.76 mm diameter, China). High-voltage power was applied using USB, a negative

polarity DC power source (CAEN, DT5470P, +5 kV/200 µA, 1 W max, CANBERRA UK Limited and Mirion Technologies) and a positive polarity DC power source (HV350REG(+), Information Unlimited, Amherst, USA). The experiments were monitored in real-time using two optical microscopes (M5A, Wild Heerbrugg, Switzerland, and Olympus CK2; Olympus, NZ), equipped with USB digital eyepiece microscope cameras (MD500, Amscope, USA) and operated by a computer using imaging software provided by the manufacturer (Amscope v4.11.21462, Amscope, USA).

4.2.2.2. Image analyses

The experiments were monitored in real time. Images of the crystallisation drops were collected and analysed using image analysis software. Crystal counting, size measurements, and other analysis were performed manually, using Fiji-ImageJ software (v.1.53, National Institutes of Health, Bethesda, USA).

4.2.2.3. X-ray diffraction (XRD) studies

All X-ray diffraction analyses were conducted at the VMXi beamline at the Diamond Light Source (DLS) synchrotron facility (Didcot, UK). The in situ plates were delivered in person to DLS, where they were registered, scanned, and stored before the data were collected. The web interface allows the user to set the data collection parameters, select and centre the crystals to be analysed, and collect the data remotely. Centring the crystals involves aligning the horizontal and vertical axes by double-clicking the crystal image. Criteria used to select the crystals included their size, location and degree of hindrance, where preference is given to crystals that are spatially distinct to reduce interference. Multiple crystals were selected from each drop before the automated data collection was initiated.

Data collection requests were formulated and submitted through the web interface, and all requested beamline actions were completely automated. The data underwent automated processing using multiple approaches and programs. Data were processed using the xia2.DIALS program and analysed to compare the outcomes. The datasets were cut off at the highest resolution shell where the signal-to-noise ratio (I/σ(I)) is >1, and data with 60% completeness was processed. The parameters used for data collection are illustrated in Table 4.2.

Table 4.2. Parameters used in diffraction data collection.

Parameter	Definition	Value
Flux	The flux in photons per second	> 5x 10^{13} ph/s
Ω Start:	The starting omega angle for the data collection	-30.0°
Ω Osc:	The number of degrees of oscillation taken during an image	0.10°
Ω Overlap	Ω delta - Ω Osc: Used when taking screening images, separated by a Ω delta	0°
No. Images	The number of images collected	600
Resolution	The obtainable resolution given the placement of the detector.	1.95 Å
Wavelength	The wavelength at which data was collected	0.7749 Å
Exposure	The exposure time per image/frame that was used	0.0018s
Transmission	The relative transmission used on the beamline, compared to the maximum on the beamline.	5.00%
Beam size	The beam size horizontal by vertical	10 x 10 µm
Type	An inferred or supplied experiment type, this often does not represent the experiment undertaken and is being reviewed	single anomalous dispersion (SAD)

4.2.3. Design and fabrication of experimental setups

4.2.3.1. Electric-field-assisted vapour diffusion crystallisation setup for in situ diffraction studies, Setup III

The overall design of the setup is illustrated in Figure 4.1. It consists of two 3D-printed parts and a glass plate equipped with a pair of copper wire electrode arrays. The bottom part of the setup is designed to hold a CrystalQuickX crystallisation plate. In contrast, the top part is designed to hold the electrodes and the visualisation plate (Fig. 4.1a). The two parts are fixed together using plastic screws for insulation. The copper wires are fixed on the bottom side of the glass plate (i.e. facing the crystallisation plate) using hot glue, making each active well in the crystallisation plate fall between two electrodes. In this setup, the active wells are those located in rows C, E, and G, which allow a wide range of conditions to be examined (Figure 4.1b).

The setup is placed under an optical microscope (M5A, Wild Heerbrugg, Switzerland) equipped with a USB digital eyepiece microscope camera (MD500, Amscope, USA) to monitor the crystallisation process in real-time (Figure.1c).

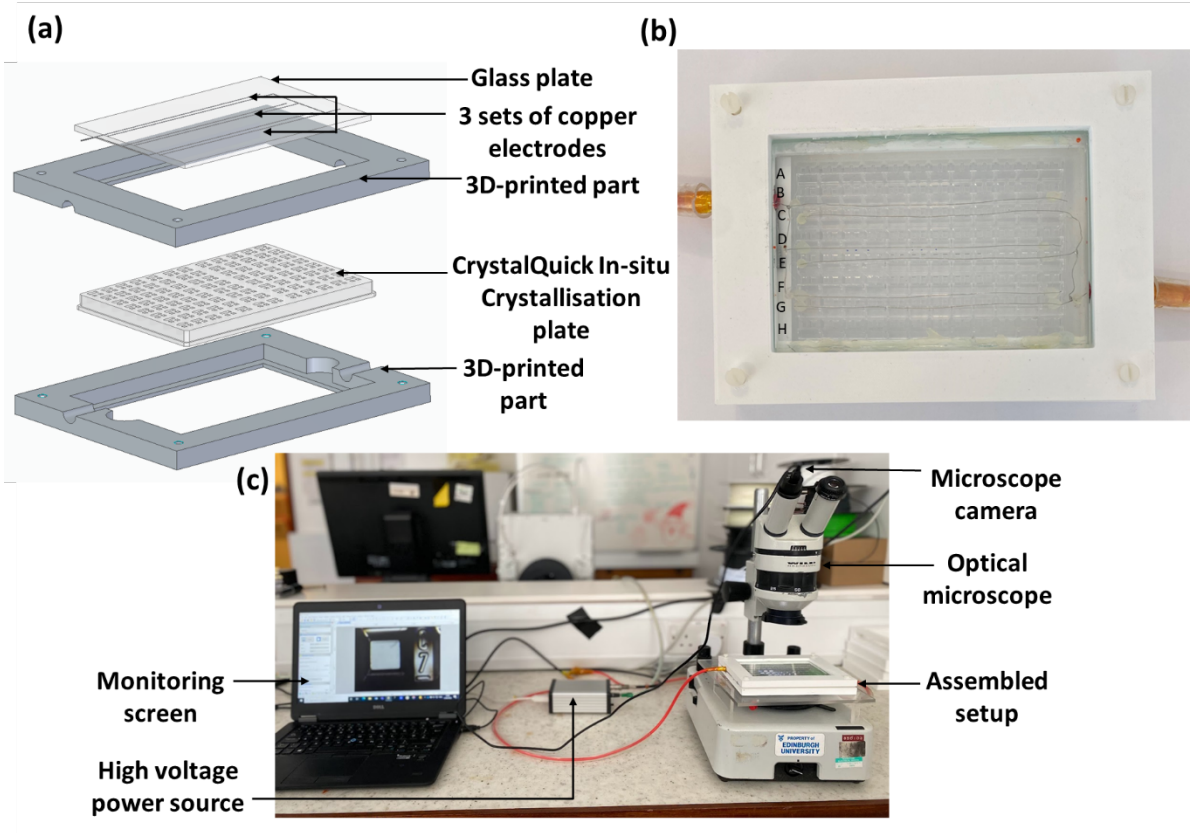

Figure 4.1. The CAD model and the corresponding photograph of the electric-field-assisted in situ crystallisation setup (Setup III). (a) The CAD model of the crystallisation setup, (b) a photograph of the 3D-printed casing equipped with the electrode connections and the crystallisation plate, and (c) a photograph of the whole setup connected to the high voltage

power source and placed under the microscope for continuous monitoring via the monitoring screen.

The electrodes are prepared by cutting a copper wire into eight pieces 11 cm long and using the soldering technique to fix them together and make two arrays. The arrays are then fixed on the glass plate and connected to high voltage cable using spade connectors (Fig. 4.2). The upper electrode array in each set is connected to a high voltage power source via a spade plug, whereas the lower electrode array is connected to the ground. The distance between each set of electrodes is 5 mm. The power source is connected to the earth through a ground cable plugged into the power supply's earth inlet. High-voltage power was applied to the setup using a USB high-voltage power supply (CAEN, DT5470P, -3 kV/200 µA, 1 W max, Mirion Technologies CANBERRA UK Limited).

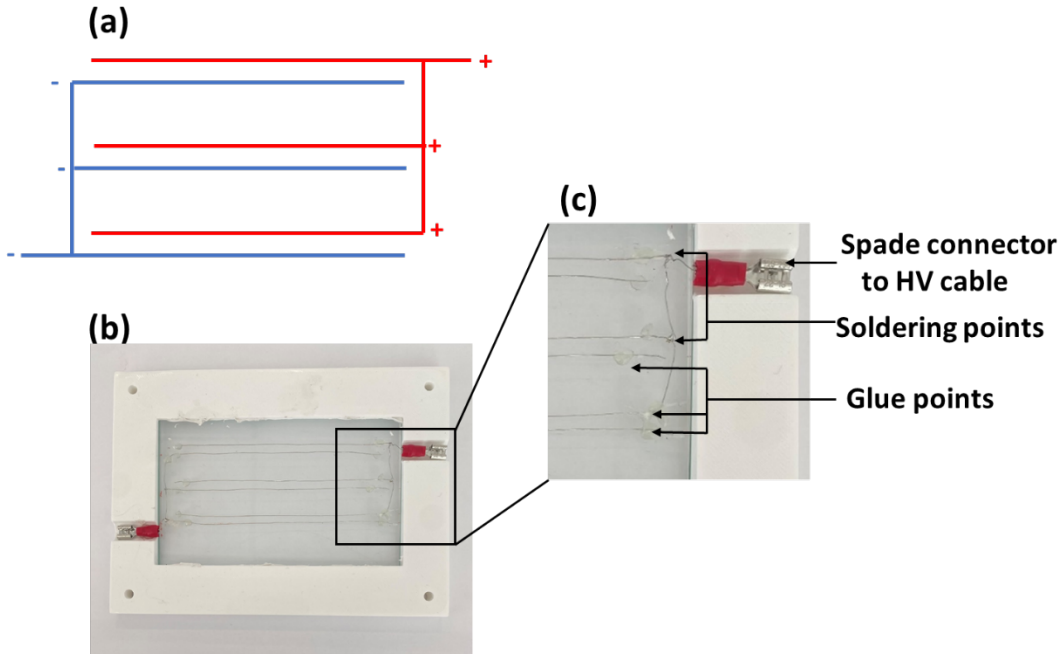

Figure 4.2. The configuration of the copper electrode arrays used in the in situ crystallisation setup. (a) A schematic diagram of the electrode arrays constituting three pairs of electrodes. (b) a photograph showing the electrode array fixed in the glass plate. (c) a section of the electrodes configuration showing the soldering, gluing and HV connection points.

4.2.3.2. Electric-field-assisted vapour diffusion crystallisation setup for in situ diffraction studies, Setup IV

To create a uniform electric field throughout the crystallisation plate, the previous setup (Setup III) was modified. The copper wire electrodes were replaced with copper plate electrodes fixed at the sides of the setup (Figure 4.3).

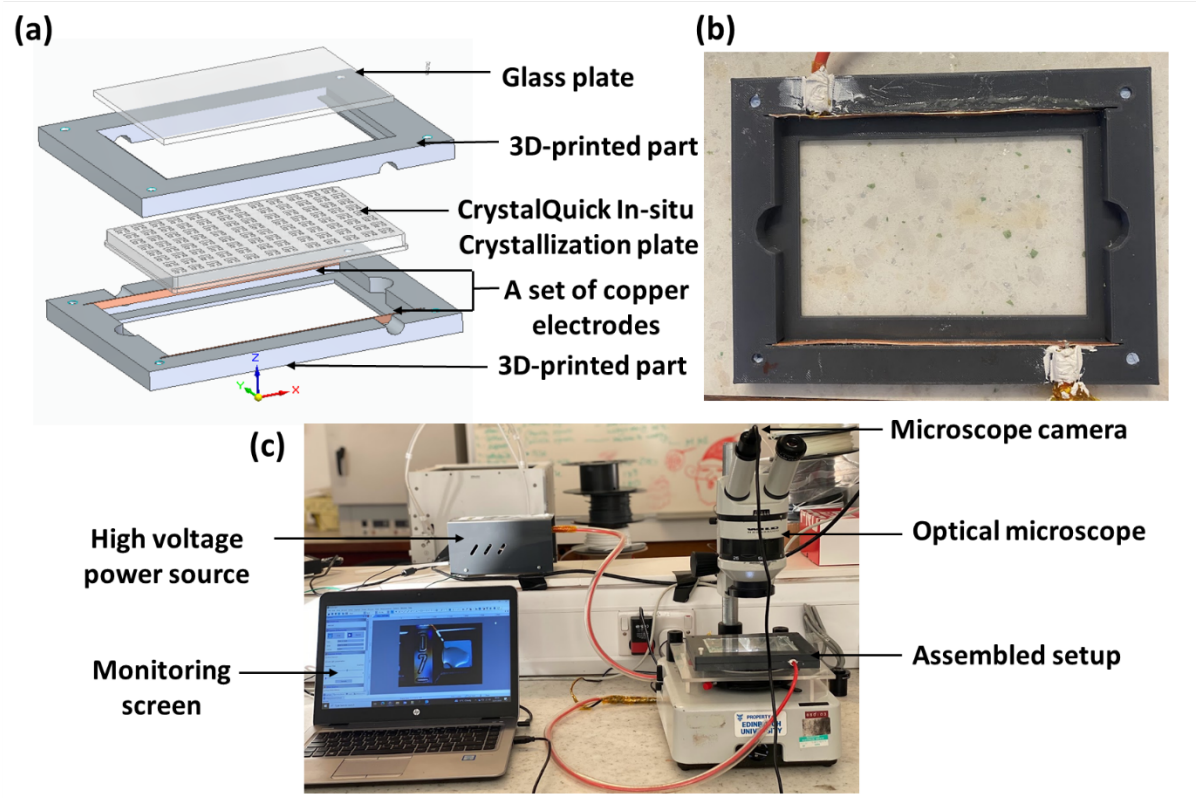

Figure 4.3. The CAD model and the corresponding photograph of the electric-field-assisted in situ crystallisation setup with plate electrodes (Setup IV). (a) The CAD model of the crystallisation setup, (b) a photograph of the 3D-printed casing equipped with the electrode connections and the crystallisation plate, and (c) a photograph of the whole setup connected to the high voltage power source and placed under the microscope for continuous monitoring via the monitoring screen.

A pair of copper electrodes is fixed at the inner walls of the plate holder to create a uniform field through the plate (Fig. 4.3). The electrodes are made by cutting a copper sheet (0.51 mm thick, Chudeng, China) to the dimensions (12.7 cm x 2 cm), introducing a plate perforation, and connecting the high voltage cable by the soldering technique (Figure 4.4).

The plates are then fixed inside the setup using an epoxy adhesive (Araldite, Huntsman Advanced Materials, UK). The distance between the electrodes is about 10 cm.

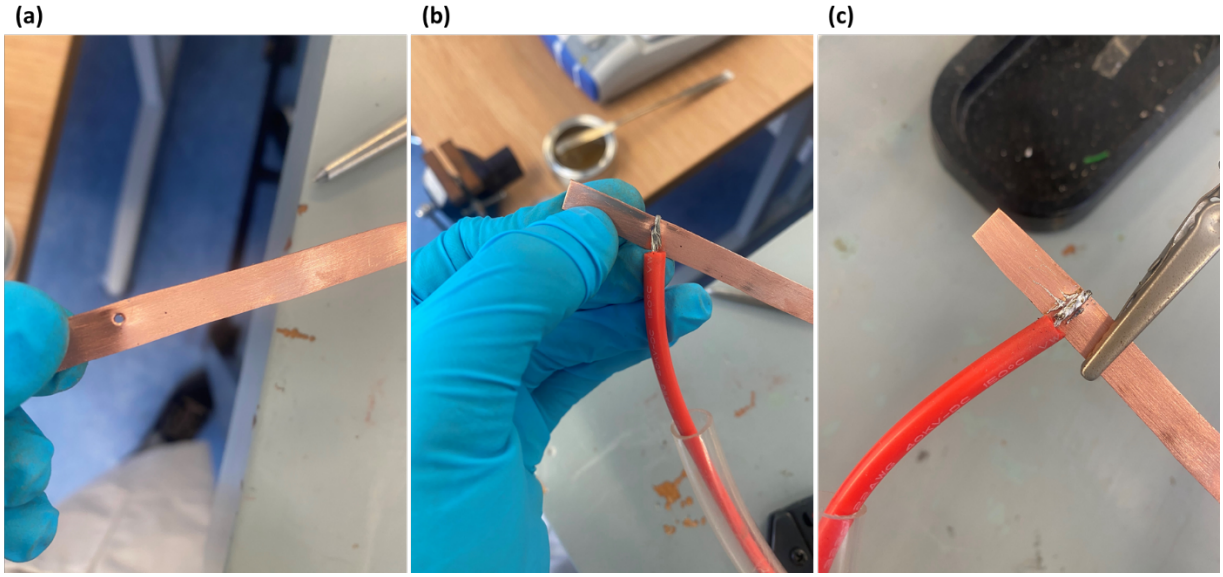

Figure 4.4. Photographs showing the process of connecting a plate electrode to the high voltage cable. (a) a perforation is introduced in the copper plate, (b) the cable is connected through the perforation, and (c) the HV cable is soldered to the copper electrode plate.

4.2.3.3. 3D printing

Ultimaker3 (Ultimaker, the Netherlands) 3D printer was used to print the main parts. The stl files from Solid Edge software are converted to GCODE file format using Ultimaker Cura (4.13.1). The parameters used for printing are shown in Table S1.

4.2.3.4. Safety measures

As the electric-field-assisted crystallisation experiments involve the use of high voltage, an electrically insulating polymer material (PLA) was used as the main compartment in both setups. In addition to PLA, and due to its high dielectric strength and resistivity, glass was used

to allow continuous visualization of the plate. Glass was securely fixed in the setup to prevent electrical shock. All the connections and cable ends were secured with three layers of Kapton tape for enhanced protection, high-voltage cables were inserted into flexible silicone tubes for additional insulation.

4.3. Results

4.3.1. Electric-field assisted in situ crystallisation of HEWL, Setup III

HEWL crystallisation was carried out in Setup III to study the effect of electric field on the quality of crystals using in situ diffraction studies. The results of HEWL crystallisation presented no considerable apparent change in the number and size of crystals produced (Fig. 4.5).

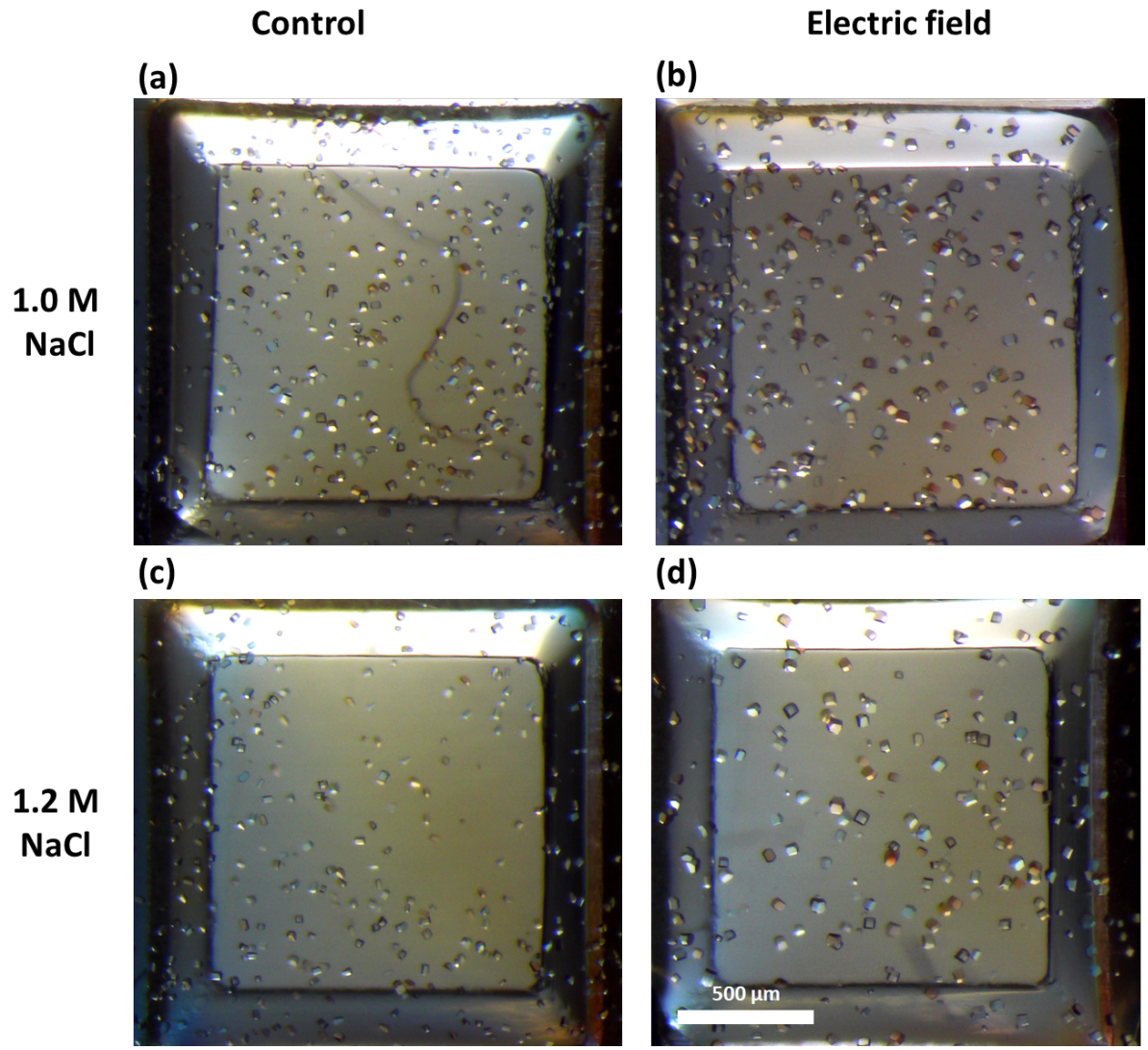

Figure 4.5. Micrographs showing HEWL (20 mg mL^{-1}, pH 4.6) crystals grown with and without the application of a negative electric field (Control). The droplet volume is 1.5+1.5 µL, and the electric field strength is 2 x 10^5 V m^{-1} (48 hrs). (a) HEWL crystals grown without electric field (1.0 M NaCl), (b) HEWL crystals grown with electric field (1.0 M NaCl), (c) HEWL crystals grown without electric field (1.2 M NaCl), and (d) HEWL crystals grown with electric field (1.2 M NaCl).

4.3.2. **Data acquisition**

To assess the quality of HEWL crystals grown under EF, resolution, mosaic spread, and Wilson B-factor, data were extracted and compared with data from control crystals. Fewer crystals were produced at lower protein concentration (10 mg mL^{-1}) and lower salt content

(1.0 M NaCl); thus, no substantial data were collected. However, at higher protein concentration, a considerable amount of data was collected for both the control and EF experiments (Table 4.3). A representative summary dataset for HEWL crystal diffraction experiment is given by Fig 4.6.

Table 4.3. Experimental conditions at which HEWL crystals are used in the diffraction data collected for HEWL.

Protein (mg mL^{-1})	10		20	
NaCl (M)	1.0	1.2	1.0	1.2
pH 4.6	No substantial data	Data collected and auto-integrated	Data collected and auto-integrated	Data collected and auto-integrated
pH 4.9	No substantial data	No substantial data	Data collected and auto-integrated	Data collected and auto-integrated

(a)

Space Group	A	B	C	α	β	γ
P 4_1 2_1 2	78.58	78.58	37.70	90.00	90.00	90.00

	Overall	Low resolution	High resolution
Resolution (Å)	37.70 - 1.81	37.71 - 4.91	1.84 - 1.81
Observations	45724	2520	1338
Unique reflections	9921	545	427
Multiplicity	4.6	4.6	3.1
Completeness	88.27%	85.42%	79.07%
Mean I/σ(I)	10.3	38	0.7
R_{merge}	14%	4%	>100%
R_{meas}	15%	4%	>100%
R_{pim}	6%	2%	88%
$CC_{½}$	0.996	0.999	0.272

(b)

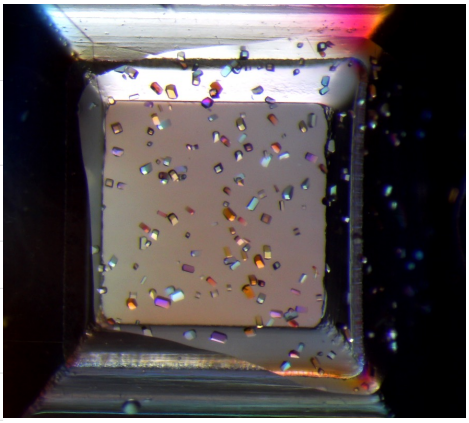

Figure 4.6. The diffraction data obtained from a single HEWL (20 mg mL^{-1}, pH 4.6) crystal and processed by the xia2.dials program. The crystal was grown under a negative electric field (10000 V, 1 x 10^5 V M^{-1}, 24 hrs). The datasets were cut off at signal-to-noise ratio (I/σ(I)) >1, and 60% completeness.

4.3.3. Effect of electric field on HEWL crystals at a varying protein concentration

The diffraction data collected from conditions with higher salt content (1.2 M NaCl), lower protein concentration (10 mg mL^{-1}), and pH 4.6 exhibited no considerable improvement in the resolution and mosaic spread was observed when electric field was applied; however, at higher protein concentration (20 mg mL^{-1}), a significant reduction the mosaic spread values was observed (Fig. 4.6).

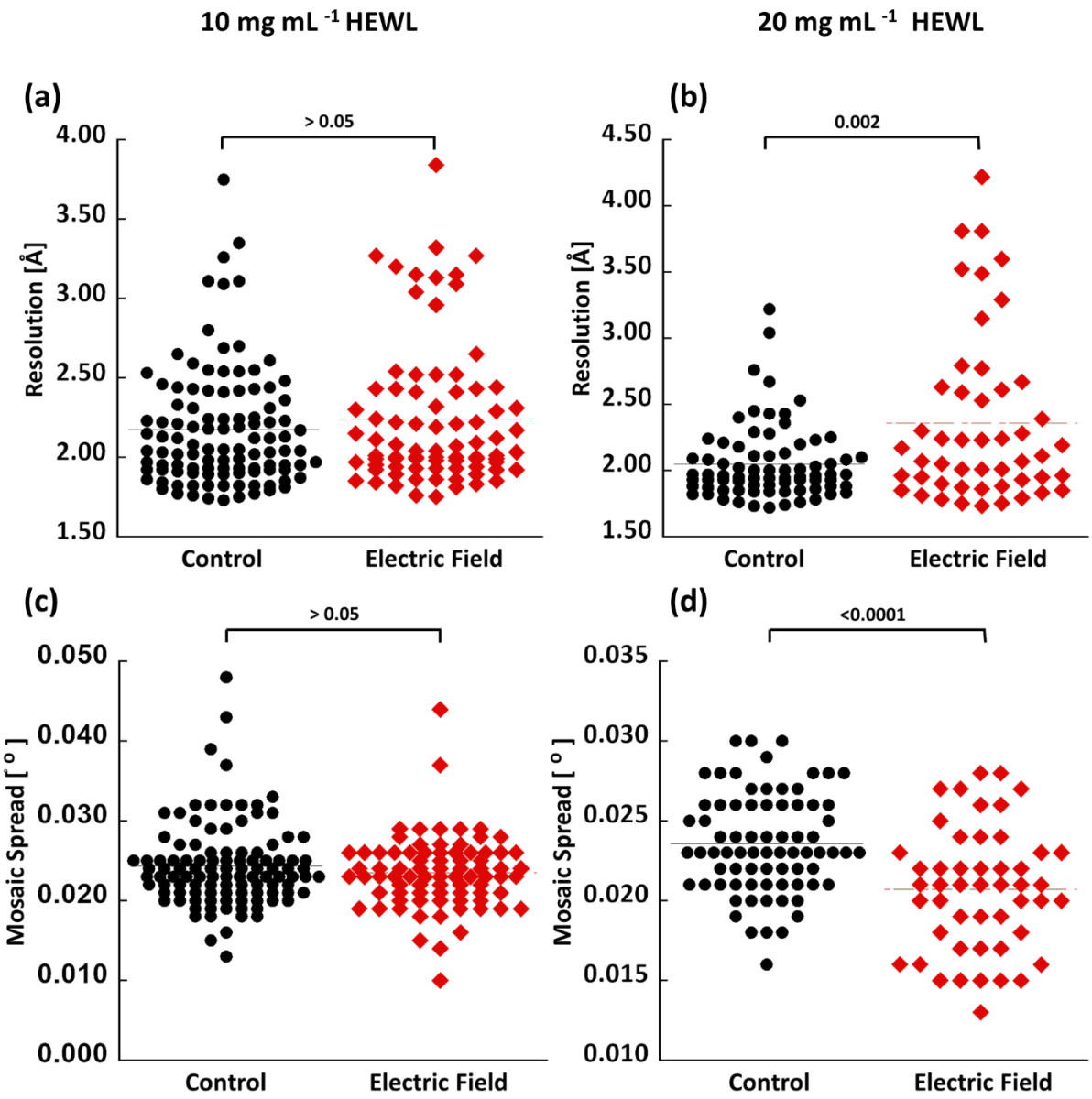

Figure 4.7. The diffraction parameters of crystals grown with and without the application of a negative electric field at a salt concentration of 1.2 M NaCl, pH 4.6, and varying HEWL concentration. (a) resolution of crystals grown at a lower protein concentration (10 mg mL^{-1}), (b) resolution of crystals grown at a higher protein concentration (20 mg mL^{-1}), (c) mosaic spread of crystals grown at a lower protein concentration (10 mg mL^{-1}) and (d) mosaic spread grown at a higher protein concentration (20 mg mL^{-1}).

4.3.4. **Effect of electric field on HEWL crystals at varying salt concentration**

When comparing the quality of crystals grown at higher protein concentration (20 mg mL^{-1}) and varying salt concentration, the results illustrated improved mosaicity and B-factor values at higher salt content (1.2 M NaCl) compared to lower salt content (1.0 M NaCl) when electric field is applied (Figure 4.7).

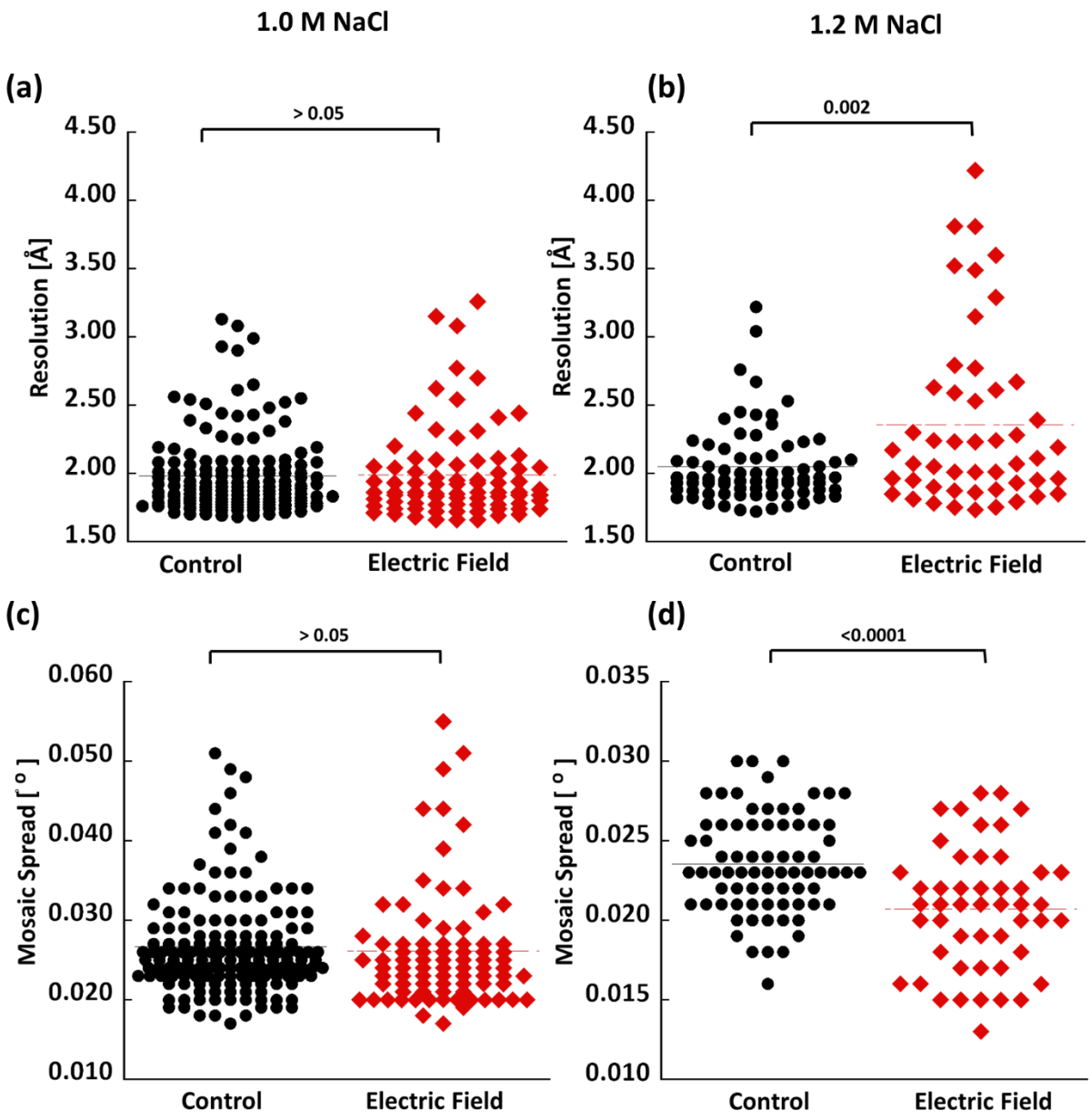

Figure 4.8. Resolution and mosaic spread of crystals grown with and without the application of a negative electric field at protein concentration (20 mg mL^{-1}), pH 4.6, and varying NaCl concentration. (a) resolution of crystals grown at the lower salt concentration (1.0 M NaCl), (b) resolution of crystals grown at a higher salt concentration (1.2 M NaCl), (c) mosaic spread of crystals grown at a lower salt concentration (1.0 M NaCl) and (d) mosaic spread grown at a higher salt concentration (1.2 M NaCl). The datasets were cut off at signal-to-noise ratio (I/σ(I)) >1, and 60% completeness.

4.3.5. **Effect of electric field on HEWL crystals at varying pH**

In addition to protein concentration and salt content, the diffraction properties of HEWL crystals were investigated at two pH levels. The results obtained from crystals grown at higher protein and salt concentrations (20 mg mL^{-1}, HEWL, 1.2 M NaCl) at pH 4.6 and 4.9 showed a noticeable improvement in the mosaic spread and B-factor at both pH values; however, the resolution ranges were reduced to a considerable extent at I/σ(I) >1 (Figure 4.8).

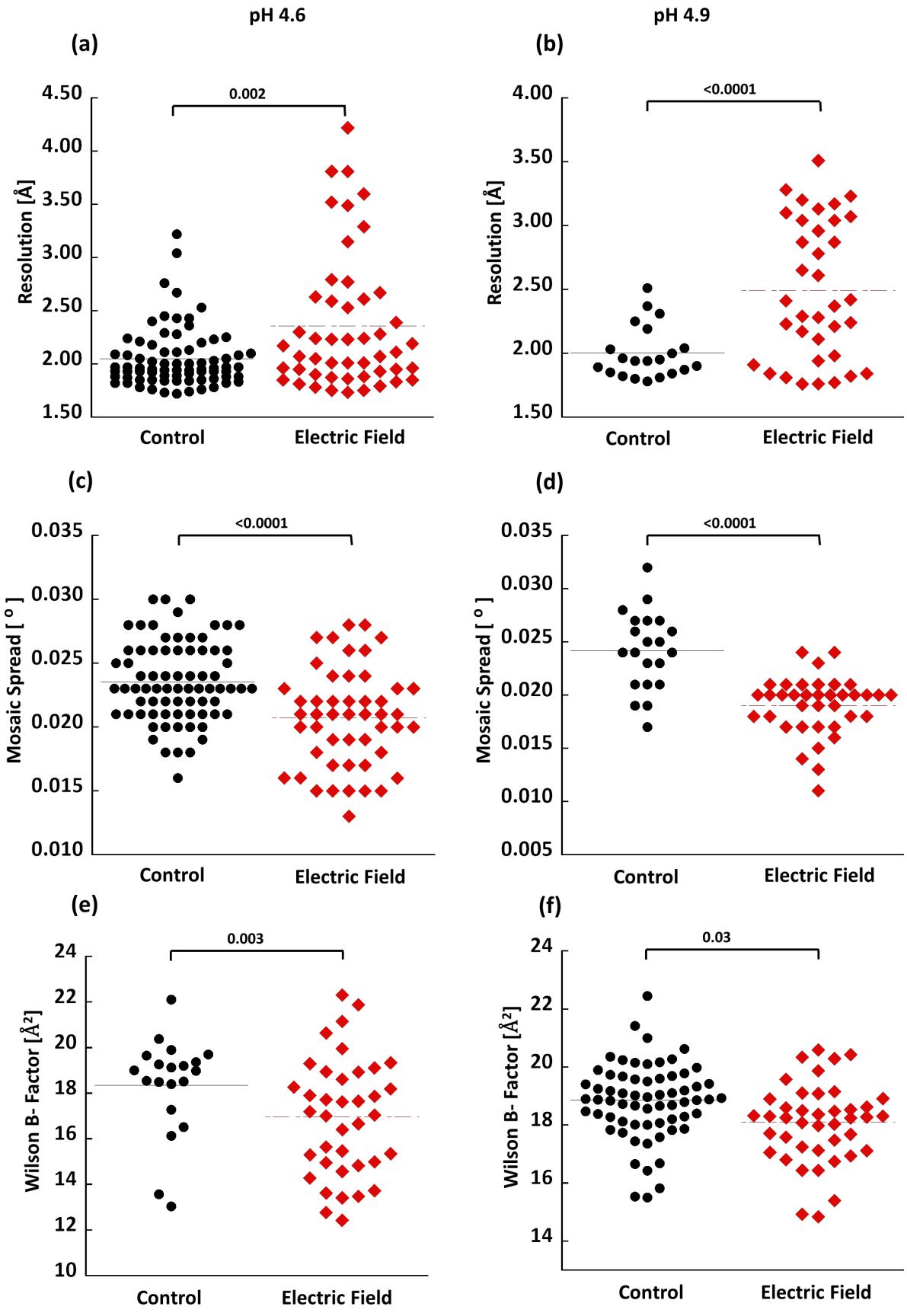
pH 4.6
pH 4.9
(a)
(b)
(c)
(d)
(e)
(f)
0.002
<0.0001
<0.0001
<0.0001
0.003
0.03
Resolution [Å]
Mosaic Spread [°]
Wilson B- Factor [Å²]
Control
Electric Field

Figure 4.9. The diffraction parameters of HEWL crystals grown with and without the application of a negative electric field at protein concentration (20 mg mL^{-1}), salt concentration (1.2 M NaCl), and varying pH (4.6 and 4.9). (a) and (b) represent the resolution of crystals grown at pH 4.6 and 4.9, respectively; (c) and (d) represent the mosaic spread of crystals grown at pH 4.6 and 4.9, respectively, and (e) and (f) represent Wilson B-factor of crystals grown at pH 4.6 and 4.9 respectively. The datasets were cut off at signal-to-noise ratio (I/σ(I)) >1, and 60% completeness.

4.3.6. Effect of electric field on HEWL crystals space group

The crystallographic data were automatically processed using xia2.DIALS program, which used the diffraction pattern and intensities to specify the space group of each crystal. Three types of space groups were detected for HEWL crystals at varying experimental conditions, namely, tetragonal, orthorhombic and monoclinic space group types. The effect of electric field on the percentage of space group types of HEWL crystals at varying experimental conditions is higher at higher protein and salt concentration. A summary of the percentages of space group types is illustrated in Table 4.4.

Table 4.4. The percentage of HEWL space group types

HEWL (mg mL^{-1})	pH	NaCl (M)	Tetragonal (%)		Orthorhombic (%)		Monoclinic (%)	
			Control	EF	Control	EF	Control	EF
10	4.6	1.2	82.4	88.9	8.3	4.9	9.3	6.2
20		1.2	82.4	88.9	8.3	4.9	9.3	6.2
		1.0	89.7	88.9	6.5	4.9	3.9	6.2
20	4.9	1.0	75.8	85.7	8.1	3.6	16.1	10.7
		1.2	71.4	81.1	4.8	8.1	23.8	10.8

Although the tetragonal space groups are found to predominate at all experimental conditions, the application of an electric field resulted in more crystals in an apparent tetragonal space group and a lower percentage of monoclinic space group crystals in most of

the experimental conditions used, with a more significant effect at higher pH. The percentages of space group types at pH 4.9 are illustrated in Figure 4.9.

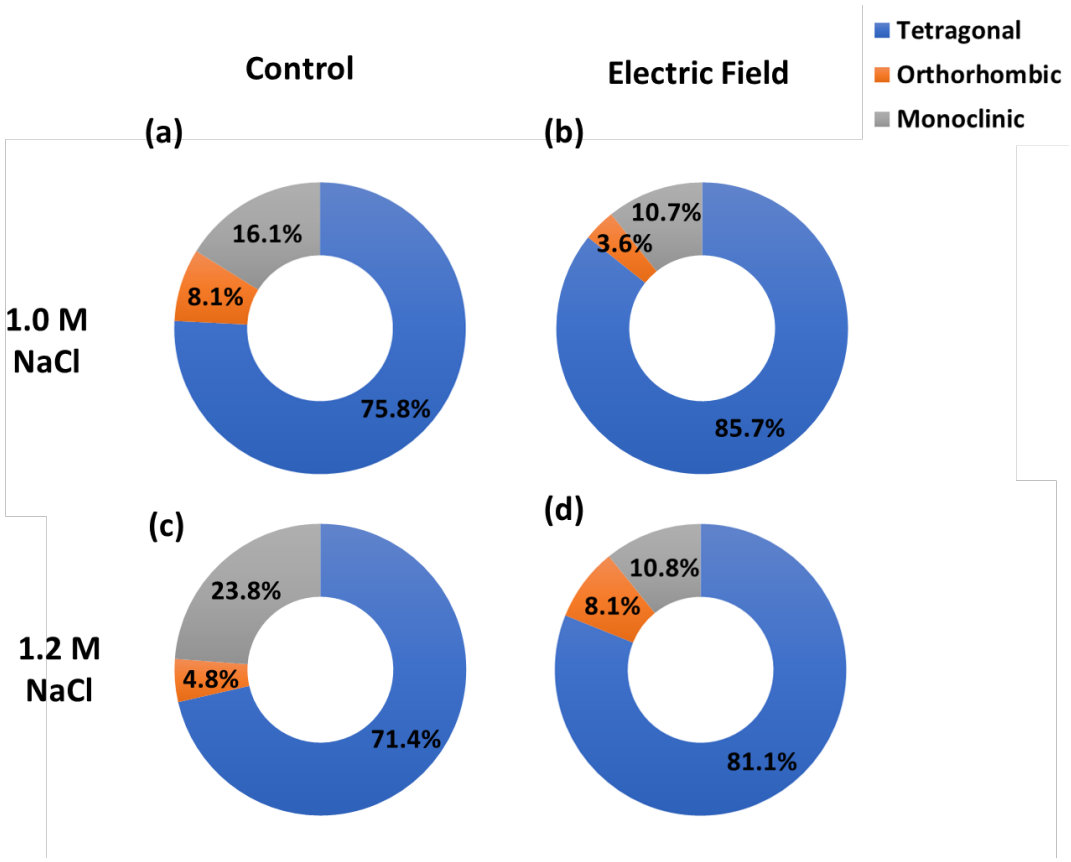

Figure 4.10. Percentages of space group types of HEWL (20 mg mL^{-1}) crystals grown with and without the application of a negative electric field at pH 4.9. (a) Space group percentages of crystals gown at 1.0 M NaCl without and with electric field application (b) Space group percentages of crystals gown at 1.2 M NaCl without and with electric field application.

4.3.7. Electric-field assisted in situ crystallisation of REMC1, Setup III

REMC1 has been crystallised previously, and the crystals were harvested and subjected to XRD analysis; however, weak diffraction was observed due to poor lattice properties. To enhance the quality of REMC1 crystals, the crystallisation was carried out under an electric field. In addition, in situ room temperature data collection was used to assess if the poor diffraction is an intrinsic property or an effect of the harvesting and cryo-cooling process.

REMC1 crystallisation in the in situ setup (Setup III) resulted in a preliminarily delayed induction time. In addition, larger crystals were observed when the electric field was applied (Fig. 4.10). The control experiment presented nucleation within 2-3 hrs, whereas electric field delayed nucleation up to 6-24 hrs. As the purpose of this study was diffraction studies, no further investigation of the effects of the electric field on the size and number of crystals was carried out.

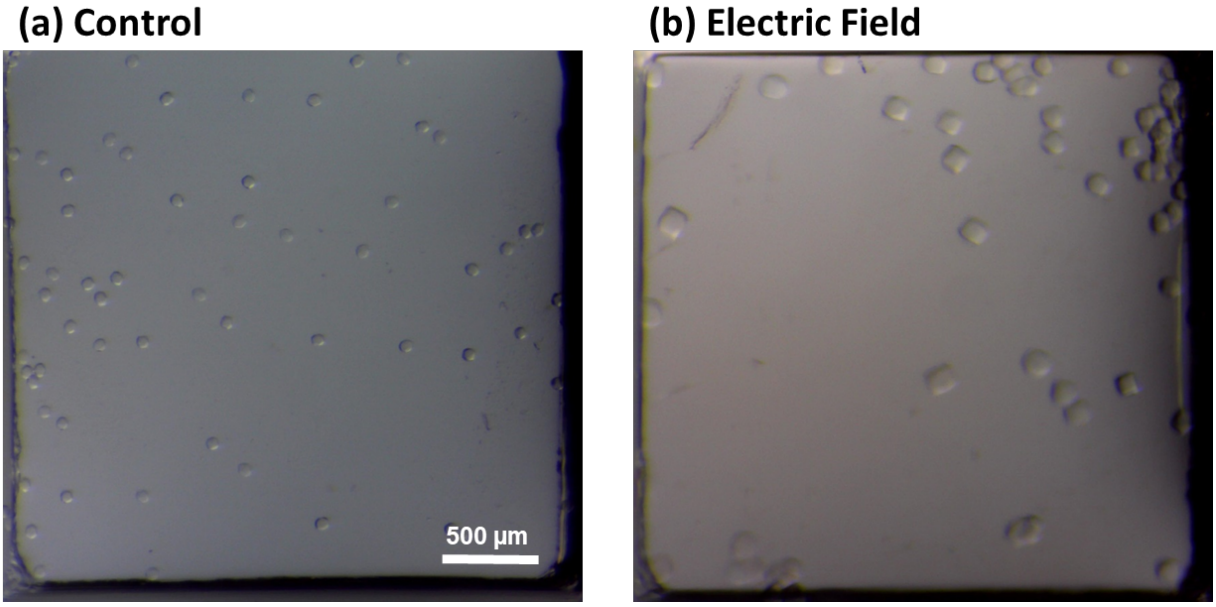

Figure 4.11. Micrographs showing REMC1 crystals (50 mg mL^{-1}, 900 mM $MgSO_4$, pH 8) (a) without and (b) with the application of a negative electric field (1000 V, 2 x 10^5 V m^{-1},48 hrs) after one week of the experiment. The droplet size used is (1+1 µL). Larger crystals appear when EF is applied.

REMC1 was crystallised at (50, 37.5 and 25 mg mL^{-1}) to assess any changes in the morphology of the crystals formed. The results show the formation of solid clusters at the edges of the drop at 50 and 37 mg ml^{-1} (Figure 4.11). At 25 mg mL^{-1}, no significant crystallisation occurred; hence, no data are presented. The crystallisation drops exhibit clustered crystal-like structures at the drop edges, which is more significant when electric field is applied. Also, cube-shaped crystals appeared in both conditions with and without electric field. The experiment was repeated at 37.5 mg mL^{-1} three times, and the plates were delivered to the DLS for diffraction studies.

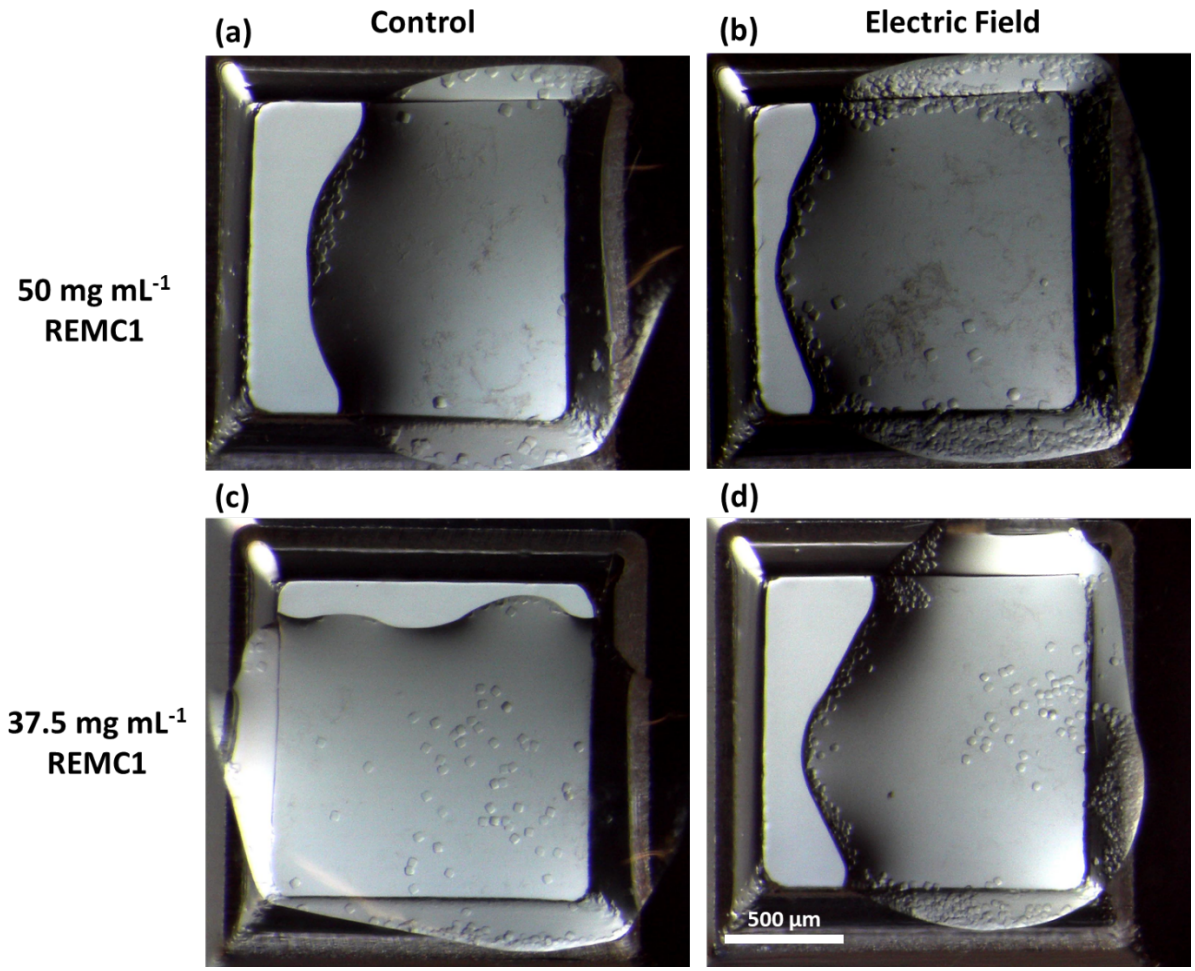

Figure 4.12. Micrographs showing REMC1 crystals grown with and without the application of a negative electric field application (Control). The droplet volume is 0.5+0.5 µL, and the precipitant is 900 mM $MgSO_4$, pH 8. (a) REMC1 (50 mg mL^{-1}) crystals grown without electric field, (b) REMC1 (50 mg mL^{-1}) crystals grown with electric field (2 x 10^5 V m^{-1}, 24 hrs). (c) REMC1 (37.5 mg mL^{-1}) crystals grown without electric field. (d) REMC1 (37.5 mg mL^{-1}) crystals grown with electric field (2 x 10^5 V m^{-1}, 24 hrs). The scale bar in the plate represents 500 µm.

The diffraction data were collected in the VMXi beamline and subjected to automatic data processing via xia.DIALS. Interestingly, the auto-processing revealed that only two crystals showed diffraction properties among 330 control and 359 crystals grown under an electric field However, the diffraction data are unreliable due to the low signal-to-noise value and the negative Wilson B factors, which suggest the inaccurate auto-processing of the data by xia2.DIALS due to the weak diffraction signals. Manual analysis of the data is required for validation.

The remaining crystals have no diffraction properties (Figure 4.12), and the automated processing failed to report any results. Examples of the diffraction images (no diffraction spots) for control and electric field crystals are demonstrated in Figure 4.7.

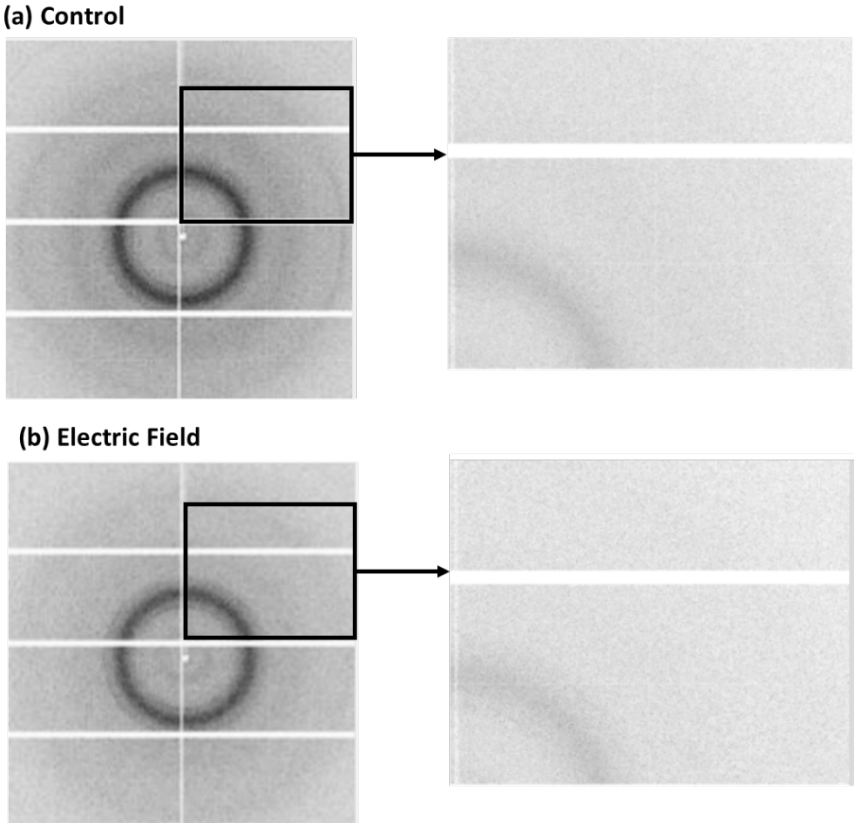

Figure 4.13. Diffraction images of REMC1 (37.5 mg mL^{-1}) crystals (precipitant: 900 mM $MgSO_4$, 100 mM Tris pH 8.0) (a) without electric field and (b) with electric field. No diffraction spots are observed due to poor lattice properties.

4.3.8. Electric-field assisted in situ crystallisation of REMC1, Setup IV

REMC1 was crystallised under the effect of electric field using Setup IV. REMC1 crystallised readily, resulting in two types of solid structures in each drop: cube-like structures inside the droplets and amorphous clusters at the droplet edges (Fig. 4.13).

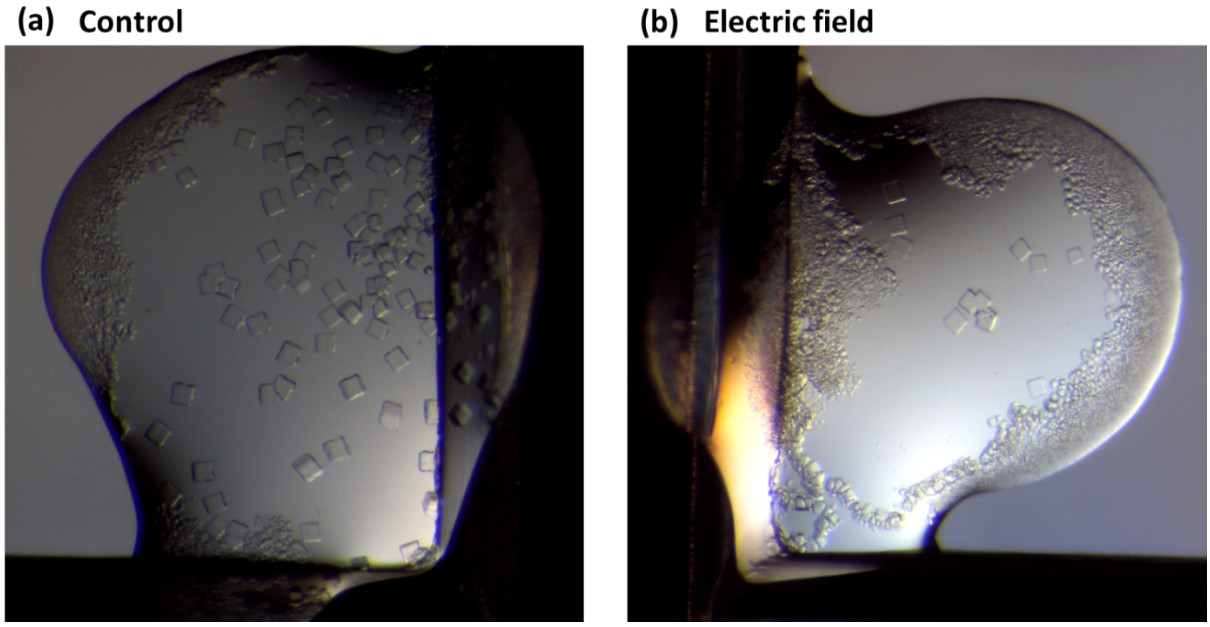

Figure 4.14. Micrographs showing REMC1 (11 mg mL^{-1}, 900 mM $MgSO_4$, pH 8.0) crystals grown (a) without and (b) with the application of a neagtive electric field. Distinct cubic-like crystals and amorphous clusters appear in both cases.

Although the REMC1 crystals appear cube-like, their growth seems to be mostly 2-dimensional rather than 3-dimensional. Most of the crystals were damaged when the plates were transported to the synchrotron, as observed by fissures in the crystals, resulting in poor diffraction properties (Fig. 4.12).

Although 104 crystals were exposed to the beam, only one crystal showed diffraction spots and was processed by Xia2.DIALS, indicating that almost none of them showed sufficient internal order to diffract. The dataset of the single crystal exhibited errors in data processing due to the incomplete data set and lack of internal order in the crystals.

4.4. Discussion

4.4.1. Electric-field-assisted crystallisation of HEWL

HEWL was crystallised under electric field using in situ crystallisation setups II. HEWL is used widely as a model protein. In this chapter, it was used to test the ability of electric field to enhance the quality of protein crystals using the designed experimental setup (Setup III). The resultant HEWL crystals were subjected to diffraction studies using the VMXi beamline to assess the effect of EF on crystal quality.

The diffraction data proved that high-quality properties of HEWL crystals can be grown with and without the application of an electric field. Although there was no apparent change in the shape and size of the crystals (Fig. 4.5), deep analysis of some diffraction parameters of HEWL crystals revealed a noticeable effect of electric field in the internal order of the crystals, which is more evident at higher protein and salt concentrations (Figs. 4.7 and 4.8).

To explain the effects of electric field on the internal order of the crystals, it is essential to revisit the mechanism of the HEWL crystallisation and its interaction with the electric field. The crystallisation process involves the presence of charged species (protein molecules, salt ions, and buffer molecules) of different strengths and quantities. These charged species interact with electric field in different ways, leading to the interruption/disturbance of the crystallisation process. HEWL has a high isoelectric point (pI = 11.1), which retains a net positive charge at low pH. To reduce the repulsion between the similarly charged protein molecules, NaCl was used to stabilise the protein in the solution by suppressing the ionic interactions and enhancing the hydrophobic interactions between protein molecules [135]. As the concentration of NaCl increases in the solution, it decreases the protein solubility and promotes crystallisation by the salting-out effect [136].

Due to the complex interactions between protein molecules, including van der Waals forces, hydrogen bonds, and electrostatic forces [103], it is important to find a way to regulate these forces and create high quality crystals. This approach has been implied by many researchers using electric fields [37, 51, 52, 85].

Several parameters have been used to assess the crystal quality. The main parameters that give a clear idea about the crystal quality are the resolution limit, the mosaic spread, and the Wilson B-factor [34, 36, 37]. Although the merging R factor (Rmerge) is commonly used to assess the agreement between the multiple measurements of the experimental crystallographic datasets, it is no longer considered a key quality indicator as it is not useful in determining low-resolution limits [137].

Mosaic spread is the most used parameter to study the changes in the internal order of protein crystals [56, 57, 131, 138-140]. In addition, Koizumi et al. used the full width of half-maximum (FWHM) on the rocking curves as a comparative measure [51, 65]. Moreover, a high signal-to-noise ratio at the highest resolution shell is considered as an indicator of high quality crystals [86].

The data obtained from the diffraction studies of HEWL indicate a considerable alteration of the crystals' internal order. However, these changes are only observed at higher protein and salt concentrations. At lower protein and salt concentrations (10 mg mL^{-1} HEWL, 1.0 M NaCl) concentration (1.0 mg mL^{-1}), there was no noticeable change in the diffraction parameters (resolution and mosaic spread) between control crystals and those grown under the application of electric field. However, at higher protein and salt concentrations (20 mg mL^{-1} HEWL, 1.2 M NaCl), there was a considerable decrease in the mosaic spread of the crystals, indicating a better crystal quality imposed by electric field than the control crystals. Salt ions facilitate crystallisation by preventing the intense electrostatic repulsion between the positively charged protein molecules. It stabilises the positive charges by counterions (Cl^-), located in the electric double layer surrounding the protein molecule and in the protein crystal lattice [55], contributing to the overall water content.

An external electric field induces an extra dipole in these charged proteins. However, this influence cannot dramatically affect the protein's charge distribution. Instead, it easily changes the location of Cl− ions in the electric double layer, resulting in enormous dipoles that encompass the layer itself [55]. The orientation within the dipole is governed by the

protein's highest positively charged region, which aligns the molecules much more effectively, resulting in a better internal order of the molecules inside the crystal lattice.

Although a lower resolution may indicate a higher disorder in the crystal lattice, conformational variations, or rotational disorders [131], the observed minor reduction in resolution limit may be attributed to the data collection method or the size of the crystals. (Fig. 4.6). Larger crystals have more unit cells, resulting in stronger diffraction compared to smaller crystals.

When comparing the effect of electric field on the quality of crystals grown at varying pH (4.6 and 4.9), both conditions presented a similar trend: a lower resolution and a lower mosaic spread. However, the crystals were also compared in terms of the Wilson B-factor, which indicated higher crystal quality by lower values when electric field is applied (Figure 4.8). The internal order of the crystals can be attributed to electric field-induced oriented dipole[85], resulting in a favoured molecular orientation [1, 47, 68, 141].

According to the Protein Data Bank (PDB), HEWL has been crystallised in various space groups, with the most occurring is the tetragonal space group ($P4_32_12$) with unit cell parameters of a = b = 79.1 and c = 37.9 Å [124, 125]. Other tetragonal space groups ($P4_1$, $P4_3$, $I4$, $P4_12_12$, $I422$) are also reported in addition to triclinic ($P1$), monoclinic ($P12_11$, $C121$), orthorhombic ($P2_12_12$, $P2_12_12_1$, $C222_1$, $C222$, $I222$) and trigonal ($P3_1$, $P3_221$), hexagonal ($P622$, $P6_122$, $P6_222$, $P6_422$) and cubic ($P2_13$, $F4_132$, $I432$) space groups.

The highest percentage of crystals processed by Xia2.DIALS retained the enantiomorphic space group $P4_12_12$ [142], with unit cell parameters analogous to the $P4_32_12$ space group. It has also retained other tetragonal space groups ($P4_122$, $P42_12$, $P422$), which have been reported previously in the PDB. Lower percentages of the crystals retained orthorhombic and monoclinic space groups. Although the majority of the space groups retained from the auto-

processing of the data showed previously reported space groups, it is important to consider that partial datasets were collected from multiple crystals with various settings and orientations. Automatic merging and processing may result in errors in indexing the space group, affecting the space group assignment.

To illustrate the effect of an electric field on changing the type of the crystal space group, the data were presented by the space group reported by xia2.DIALS (Figure 4.9). The experimental results revealed that electric field assisted in forming more tetragonal space group crystals than the monoclinic and the orthorhombic space groups. This effect is also higher at higher protein concentration. This can be correlated with the higher impact of electric field in orienting protein molecules at higher concentrations, thus promoting the growth of the most favourable space group for HEWL at the experimental conditions used in the in situ experiments [125].

4.4.2. Electric-field-assisted crystallisation of REMC1

REMC1 crystallisation spontaneously resulted in the formation of cube-shaped, non-diffracting crystals. However, attempts to improve the REMC1 crystal quality by applying EF and conducting in situ diffraction studies using Setup III were not promising. Only two crystals showed some diffraction spots (Table 4.5). Further optimisation of the crystallisation process, including the configuration and the intensity of the electric field, is required to validate any effect imposed by the electric field. In addition, the data could be investigated by other programs or handled manually for more accurate evaluation, as there were diffraction spots that are not correct, in addition to the negative Wilson B-factor values indicating an error in data processing. Also, the diffraction data from these two crystals can potentially complement existing data for REMC1 structural studies.

To improve the REMC1 crystallisation outcomes, the setup was modified by changing the configuration of the electrodes, which, in theory, creates a uniform electric field through the plate (Setup IV, Fig. 4.3). The strength of the electric field was maintained by using a higher voltage, and the conditions were not changed to observe the effect of electrode configuration on the electric field effect. Again, the effect of electric field on REMC1 crystallisation was negligible and only one crystal out of over 1500 data collection trials showed some diffraction (Fig. 4.14). The crystal was obtained under the electric field effect, however, the data could be re-processed for a more accurate idea about the quality of the crystals and their internal order.

4.5. The limitations of the study

4.5.1. Sample preparation and handling

In situ crystallisation is an effective technique for crystallographic studies due to its robustness and automation compatibility. However, due to the lack of automated systems such as crystallisation robots, the experiments were prepared manually, resulting in irregular droplet shapes and locations. This had effects on the surface tension parameters, and thus, it was not possible to perform kinetic studies on these experiments.

4.5.2. The Experimental Setup

Another consideration while explaining the results is the configuration of the electrodes and the shape of the resultant electric field. In Setup III, the electrodes are copper wires placed on top of the crystallisation wells. This configuration has two implications; firstly, it produces a non-uniform electric field due to the shape of the electrodes (Fig. 4.15). Secondly, the actual intensity of the electric field reaching the drop may be much less than the applied electric

field intensity due to the distance between the electrodes and the droplet. Also, dielectric media between the electrodes and the droplet may have reduced field strength throughout the crystallisation droplets [51]. This effect was addressed by Taleb et. al as the presence of dielectric media between the crystallisation and the droplet which has been eliminated later to strengthen the intensity of the electric field [51]. However, the relationship between the configuration of the electrodes and the intensity of electric field effect across the crystallisation droplet has not been studied adequately.

4.5.3. **Diffraction analysis**

The primary purpose of the in situ diffraction studies was to prevent crystal damage by eliminating the need for harvesting and cryo-cooling measures. Despite that, and due to the need to deliver the plates to the synchrotron facility in person, there has been significant crystal damage imposed by the vibration and temperature variations during transportation, which could have been avoided if the experiments had been carried out at the beamline. This led to the loss of many potential datasets that were not scanned. Figure 4.15 illustrates an example of crystal damage REMC1 crystals.

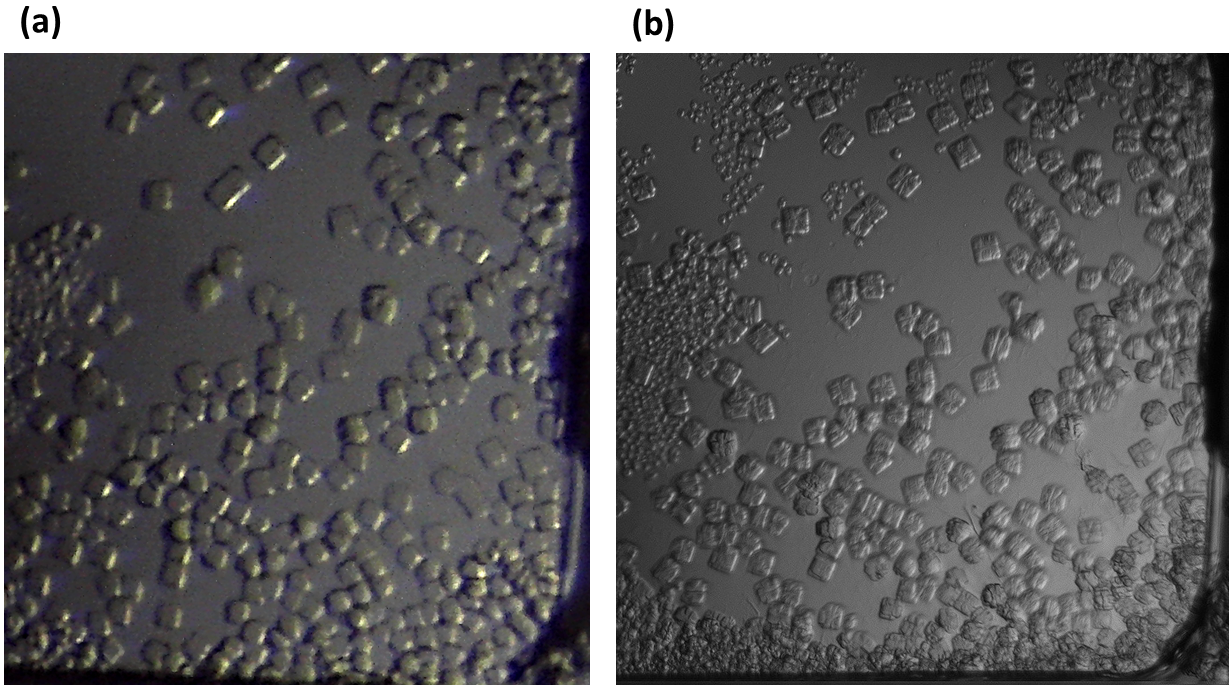

Figure 4.15. REMC1 (11 mg mL^{-1}, 600 mM $MgSO_4$, pH 8) crystals (a) before and (b) after transportation to DLS.

During diffraction studies, the first step was to screen the plates and mark the crystals to be analysed later in situ. However, during data collection, the crystals experienced some displacement from their marked locations due to movement in the droplet's volume as the plate was tilted. This issue resulted in missing potential datasets.

Additionally, it is noteworthy to mention that the crystals in the in situ plates are present in different locations and orientations. Although the robot is programmed to collect data from different orientations by tilting the in situ plate, there might be some false or incomplete data collection for some crystals. This might have implications in the data processing by the commonly used auto-processing programs such as Xia2.DIALS, resulting in inaccurate assigning of space groups for the HEWL crystals.

4.6. Conclusion

The effect of electric field on the quality of protein crystals was examined using two experimental setups. In the first experimental setup, wire electrodes are placed on top of the crystallisation plate, while in Setup III, plate electrodes are used. The results show improvements in the internal order of HEWL crystals when grown under the electric field effect at higher protein and salt concentrations than control crystals. This can be explained by the electric field aligning the dipole of the protein molecule. Preliminary findings from REMC1 crystallised under an electric field resulted in insufficient diffraction data, which may be a result of poor growth characteristics regardless of the experimental conditions. However, further optimisation of the experimental conditions may be required to confirm any effect on crystal quality. Also, the data obtained from diffracted crystals may complement existing data available for REMC1 structural studies.

General discussion

5.1. Overview of key findings

In the preceding chapters, various experimental setups were designed, fabricated, and used to investigate protein crystallisation under electric fields. Employing techniques like microbatch and vapour-diffusion, this research has deeply explored electric-field-assisted protein crystallisation. The setups have been used to crystallise HEWL under the effect of an external DC electric field at various experimental conditions. Microbatch crystallisation of HEWL under electric field enhanced nucleation and faster crystal growth so that lower numbers of smaller crystals were produced. The crystal size distribution was narrowed by the electric field exhibiting lower standard deviations, indicating improved crystal size homogeneity.

Similar results were obtained using the vapour diffusion crystallisation method, where an electric field enhanced nucleation, yielding a higher number and smaller size of crystals. Moreover, the in situ X-ray diffraction studies of HEWL crystals grown under the effect of an electric field exhibited improved crystal quality compared to the control crystals. Lower mosaic spread and Wilson B-factor indicated improved internal order in the crystal lattice.

Due to the stochasticity and sensitivity of the crystallisation process to the changes in experimental conditions, including the strength and configuration of the electric field, the results indicate a distinct pattern from most reported impacts of the electric field on protein crystallisation findings. For example, contrary to previous studies resulting in fewer larger crystals when the electric field was applied [1-6], a higher number of smaller crystals were produced when the newly designed experimental setups were used (setup I and Setup II).

Comprehensive analyses of the experimental results have yielded significant insights into how electric fields impact the crystallisation kinetics of these complex biological macromolecules. This chapter illuminates the underlying principles and emerging patterns in the electric field's influence on protein crystallisation.

5.2. Effect of electric field on protein crystallisation at different experimental conditions

The experimental results underline a significant influence of electric fields on protein crystallisation, a phenomenon verified by extensive research over the past three decades. Nonetheless, a comprehensive understanding of the mechanisms behind this effect remains critical. Unravelling how electric fields interact at a molecular level is essential for effectively controlling and optimising the crystallisation process for specific applications, paving the way for further advancements in the field.

The electric field effect on HEWL crystallisation was studied using microbatch under oil and vapour diffusion methods. HEWL has a globular structure [71, 143, 144] with both α-helices and β-sheets [68]. At acidic conditions, it holds a positive overall charge due to the presence of positively charged amino acid residues such as arginine (Arg), histidine (His) and lysine (Lys) [7, 11, 55, 145].

During the crystallisation process, electrostatic repulsion among the similarly charged protein molecules is mitigated by introducing counterions (Cl^-), stabilising the protein-protein interactions [61, 131, 146]. The influence of salt concentration (NaCl) on crystallisation is established through two contrasting mechanisms. Initially, at lower salt concentrations, NaCl assists in maintaining the solubility of protein molecules within the solution by providing additional ions for charge screening. However, as salt concentration increases (in vapour

diffusion) and the protein solution approaches supersaturation, salt molecules compete with the protein for water molecules. This competition reduces the solubility of the protein, effectively initiating the crystallisation process. Thus, higher salt concentrations tend to accelerate the nucleation of proteins compared to lower salt concentrations (Figure 2.3). Also, higher protein concentration resulted in faster nucleation and more crystals than in control experiments (Figures 3.3 and 3.5). Increased supersaturation (higher protein and salt concentrations) is known to result in faster nucleation, producing higher numbers of smaller crystals [147].

Lysozyme has been crystallised at different solution pH. However, because of its stability and solubility, crystallisation around pH 4.5 is usually preferred. As pH determines the net charge on protein molecules [38], it is considered the most sensitive variable in the crystallisation process. Judge et al. found that crystal numbers varied by two orders of magnitude between pH 4.0 and 5.2, indicating the significance of solution pH on the crystallisation process [147]. Iwai et al. reported that the metastable zone of lysozyme is narrowed as the pH decreases, resulting in the suppression of crystal growth of lysozyme [38]. This effect was evident as higher numbers of crystals were produced at pH 4.6 compared to pH 4.9 (Figure 2.3). The metastable zone is narrowed further upon applying an electric field, and the nucleation zone is expanded [21], leading to higher numbers and smaller crystals than in control trials (Figure 2.10).

It has been illustrated that the electric field introduces extra energy and modifies the chemical potentials of the solid and liquid phases in the crystallisation system, promoting the formation of a metastable phase and, subsequently, the nucleation of protein molecules. Intriguingly, the research findings raise questions about the observed preference for increased nucleation over crystal growth under present conditions, suggesting that in-depth research is needed to elucidate the underlying mechanisms of electric field influences in such settings.

The observed effect is most likely explained by an electric field's enhanced convective flow inside protein droplets. Pencova et al. observed that electric field strength correlates with the solution shear flow rate, which can either enhance or suppress nucleation [110]. This effect is mostly observed in the sitting drop vapour diffusion setting and translated into the appearance of crystals close to the centre of the droplet (Figure 3.4). According to Reguera et al., shear flow caused by external forces influences the nucleation process by modifying the diffusion coefficient of the clusters in the metastable phase [148].

To emphasise more in this effect, it is essential to revisit the crystal growth mechanism and its relationship to convection. According to the classical nucleation theory, when protein molecules in a crystallisation drop form a nucleus of critical size, its growth becomes thermodynamically favourable, prompting it to grow to a macroscopic scale. To accomplish this, the molecules need to be transported through the solution to the nucleus/crystal surface, where they can attach and become integrated. In the absence of convection, the molecules are carried through the solution via diffusion, which creates a concentration gradient by depleting the protein molecules from the solution surrounding the nucleus. Thus, only a few crystals form near growing crystals. The rate of mass transport/ growth (*J*) by diffusion is given by [146, 149]

$$J = \frac{D\ A\ (c^* - c)}{\delta} \qquad 5.1$$

Where *D* is the diffusion coefficient, *A* is the surface area, δ is the boundary layer thickness, and (c^*- *c*) is the difference in the equilibrium solution concentration and the solute concentration in the bulk solution [149]. The boundary layer thickness refers to the effective distance that a molecule needs to diffuse to travel from the bulk solution with concentration *c* to the surface of the crystal.

When diffusion is the sole means of transportation, the value of δ is approximately equal to the radius of the crystal. Larger crystals need to attract molecules from greater distances.

Hence, the rate of growth constrained by diffusion diminishes over time as the crystal expands. However, buoyant convective flows affect mass transport in most protein crystallisation techniques. When convection contribution is present in an environment, the concentration depletion zone narrows. It is challenging to embed new molecules in the lattice with the correct orientation, resulting in the formation of smaller crystals or the reduction of crystal quality. This effect was evident in microfluidic systems, where the solution flow produces more crystals [67]. To reduce convection in the crystallisation drops, reducing volumes, growing in gels [150], enhancing viscosity by adding polymers or glycerol [151], and crystallisation in microgravity [152] are commonly used techniques [146].

It has been demonstrated that electric fields play a crucial role in modifying the interactions and alignment of molecules, thereby impacting the process of crystal formation. The combined interplay between solution convection and the alignment of molecular dipoles under the influence of an electric field has yielded smaller homogenous crystals while concurrently enhancing their quality. This was translated into the crystals' improved mosaicity and B-factor values (Figure 4.8), offering unique material characteristics desired for good diffraction experiments.

5.3. Technical and methodological insights of electric-field-assisted crystallisation

In this thesis, experimental setups for electric-field-assisted crystallisation were designed and fabricated using CAD and 3D printing. 3D printing is an emerging technology offering low-cost solutions in various technical aspects with increasing applications in the protein crystallisation field. A significant benefit of 3D printing is its capacity to build and customise crystallisation platforms instantly. It offers the ability to design and fabricate plates and setups with complex shapes and characteristics that are challenging or unattainable using conventional techniques.

An example is the 3D-printed sitting drop bridge by Talapatra et al. that allows broader conditions per a crystallisation reservoir [153]. In addition, Mathew Tomas et al. 3D-printed an airlift crystalliser offering shorter desupersaturation profiles and producing larger, less agglomerated crystals with preserved biological activity [154]. A 3D-printed multichannel microfluidic cell (MFC) was designed recently by A. Marchenkova and his group to investigate the structure of complex solutions by small-angle X-ray scattering (SAXS) [155].

In this thesis, four experimental setups were designed. Consisting mainly of cost-effective 3D-printed parts, these setups offer simplicity and accessibility. Using polylactic acid (PLA) filament, a low-cost polymer primarily made from renewable resources, along with applying the provided CAD files and safety precautions in place, replicating them is straightforward. Designed to accommodate the commonly used commercially available crystallisation plates, researchers can easily subject their samples to different electric field conditions by placing them inside the setups and applying high voltage as needed. Applying an electric field during crystallisation screening is helpful as its effect varied with experimental conditions.

The experimental setups designed in this study allow application of high-magnitude electric fields. However, a notable challenge arises from using unmodified crystallisation plates, which inevitably introduces a dielectric medium between the electrodes and the crystallisation droplets. This issue is addressed by minimising the distance between the electrodes and employing higher voltage levels to ensure effective electric field penetration to the crystallisation drops. This approach guarantees that the electric field exerts its intended influence on the crystallisation process despite intervening dielectric media. In addition, these measures aid in applying a uniform electric field across the crystallisation drops.

Electric field applications can be via positive or negative high voltage polarity. The effect of changing the polarity of the high voltage on the crystallisation process was explored in Chapter 2. It has been demonstrated that in the current setting (Setup I), a similar effect was observed when positive and negative voltage was applied. However, a more substantial

impact (i.e., a higher number of crystals) was observed with the negative voltage, which was reported for the first time.

One needs to differentiate between the two conditions to understand the effect of high voltage polarity on the crystallisation process. Positive voltage refers to applying electric potential higher than a reference point (i.e., ground), whereas negative voltage refers to applying electric potential lower than the reference point (Figure 5.1).

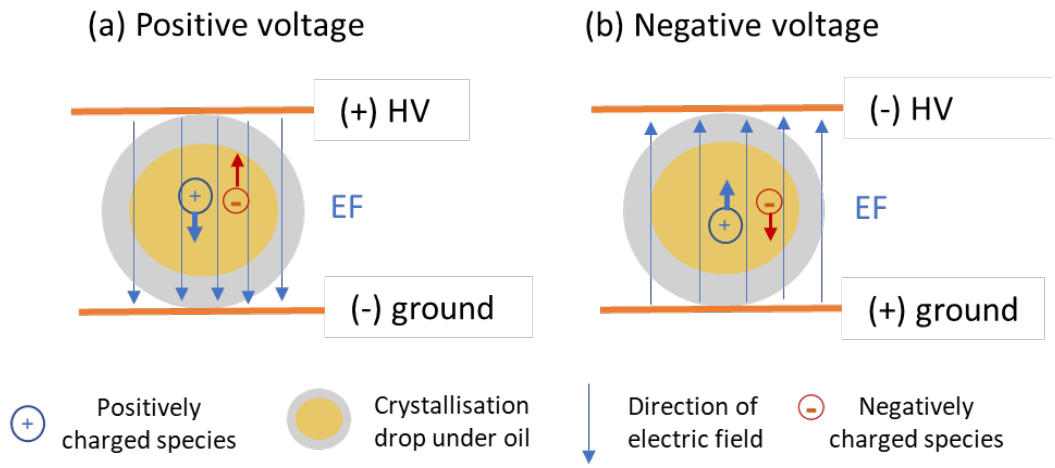

Figure 5.1. The configuration and direction of electric field at (a) positive voltage polarity, and (b) negative voltage polarity. A charged species moves against or towards the high voltage electrode, depending on the polarity of the high voltage.

When applying a positive voltage, a molecule with a positive charge (e.g. protein molecule) is moved away from the high voltage electrode (anode) in the direction of the electric field by the force of repulsion. Concurrently, negative ions (e.g., Cl-) are attracted towards the anode. In contrast, applying a negative voltage causes the positively charged protein molecules to move towards the high voltage electrode (cathode) by attraction force while repelling the Chlorine ions away from the cathode. As the force of attraction is known to be stronger due to the decreasing distance between opposite charges, the extent of electromigration of protein molecules may be higher at negative voltage conditions.

In addition, It is well known that the ionic strength and pH of the solution affect how well lysozyme binds chloride ions [53, 145]. At acidic conditions (pH 4), the high voltage generates large dipoles, which alter the electric double layer around the protein and the critical nuclei by partially neutralising the protein's positive charges, suppressing the growth of the crystals, and encouraging further nucleation.

Ei Ei et al. studied the adsorption of lysozyme and β-lactoglobulin in a metal surface with high potential at different polarities [156]. The adsorption of ß-lactoglobulin, with an overall negative charge in acidic solution, was significantly reduced by applying a negative potential to the adsorption surface. Conversely, negligible adsorption of the HEWL occurred at positive potential (Figure 5.2). These findings indicate that protein migration can be regulated by manipulating the electric potential and the net charge on the protein [156].

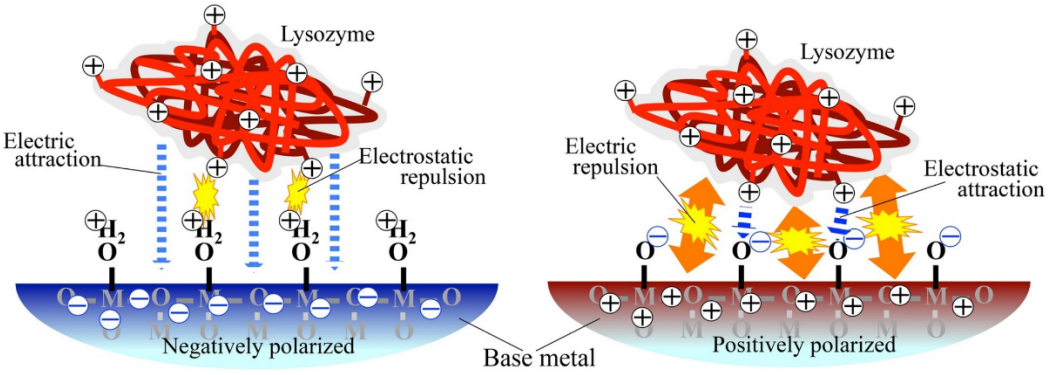

Figure 5.2. Adsorption of HEWL on a metal surface with negative (left) and positive potentials (right) (copied from [156]).

A different approach was used by Nanev et al., studying the effect of changing the direction of the electric field to examine the interaction between gravity and the electric field. In their study, the cathode was placed at the top or bottom of the all-glass quasi-two-dimensional crystallisation cells without changing the polarity of the high voltage [53]. The study showed that the majority of HEWL crystals (97–99%) were found on the glass plate in contact with the

cathode, even when positioned above the cell, compared to the control, where 66 to 75% of the crystals grew on the bottom plate, with the rest on the top [53].

5.4. Implications of experimental results in the field of crystallisation

Electric-field-assisted crystallisation can be utilised in various applications due to the ability to control and enhance the crystallisation of different materials, including macromolecules. This approach has several applications in multiple fields, such as structural biology, pharmaceuticals, and materials science.

5.4.1. Structural biology

The application of an electric field has the potential to yield larger, highly ordered crystals, which are particularly suitable for structural investigation using single-crystal X-ray crystallography. Conversely, the formation of smaller, more homogeneous crystals of superior quality, as observed in this research, is advantageous for structural studies employing microelectron diffraction (microED). This thesis has successfully demonstrated the production of crystals with these desired characteristics – smaller in size yet higher in homogeneity and quality. Such crystals maybe suited for MicroED analysis, offering a promising avenue for detailed structural elucidation. The ability to tailor crystal properties through electric field application not only broadens the scope of structural analysis techniques that can be employed but also enhances the precision of the structural information that can be obtained.

The experimental setup for in situ diffraction studies (Setup III) can be an effective tool for enhancing crystal quality for structural studies. This is primarily because analyses occur at room temperature, eliminating the need for traditional harvesting and cryoprotection steps. Data collection from multiple crystals involves systematically merging and integrating datasets, a method that enhances the reliability and accuracy of structural data. This approach allows for gathering comprehensive diffraction data directly from the crystallisation plates, thereby preserving the native state of the protein crystals. Furthermore, this technique facilitates the analysis of dynamic structural changes under various conditions, offering valuable insights into the functional mechanisms of proteins. Integrating these datasets provides a more complete and nuanced understanding of protein structures, significantly contributing to advancements in structural biology and related fields.

5.4.2. **Drug design and delivery**

Electric-field-assisted crystallisation aids in determining structural features of disease-related proteins and in designing targeted drugs capable of binding and modifying their activities [157]. Structural information can elucidate structure-activity relationships, demonstrates binding modes and bioactive conformations, and uncovers new binding pockets or allosteric binding sites. It also facilitates various drug discovery approaches, including in silico screening, creating targeted chemical libraries, and developing novel ligand scaffolds [158]. Thus, effective structure-based drug design requires reliable, fast, and predictable ways to acquire an atomically resolved target structure, essential for creating highly effective drug candidates [157, 159].

Most commercially available pharmaceuticals are composed of molecular crystals [160]. An electric field may be used to obtain uniform crystals of the targeted drugs, which enhances the process of producing drug formulations. Moreover, the crystalline properties of drugs determine their properties, such as stability and solubility. Understanding the crystalline structure of a drug is essential for various aspects of the pharmaceutical industry since it

influences characteristics, including solubility, stability, dissolution rate, bioavailability, and tabletability [160, 161]. For example, the pharmacological, toxicological, pharmacodynamic, and pharmacokinetic properties of opposite enantiomers and racemates of a chiral drug can differ substantially [160]. Electric fields can be used to obtain crystals suitable for biophysical studies, such as X-ray crystallography.

5.4.3. Material science and nanotechnology

Crystallisation is essential for creating advanced materials with specific characteristics. The electric field can be used to regulate the crystallisation of macromolecules in thin films, nanoparticles, and other nanostructured materials. Researchers can control crystalline structures' size, shape, orientation, and alignment by adjusting the applied electric field parameters, resulting in materials with improved mechanical, optical, electrical, and magnetic properties.

Macromolecules are widely used in various applications, including biomedical and biotechnology industries [162]. Protein thin biofilms are used in many applications such as biochips, biomaterials, and biosensors [163]. Electric field has been used to promote the alignment of the protein GlnB-Hs films in a favoured direction [163], which may aid in understanding of how protein biofilms are formed in the presence of electric fields.

In addition, protein crystal scaffolds have garnered considerable interest as potential biotemplating materials due to their exceptionally porous regular configuration [162]. Biotemplating is the process by which biological scaffolds including proteins, can assist in regulating the size and shape of inorganic nanostructures. Electric field can affect spatial arrangement of proteins that are adsorbed in the scaffolds, potentially resulting in alterations to their functions [164].

5.4.4. Food technology

Freezing food products reduces their water activity and protects them from microbial development, enzymatic activities, and chemical degradation processes [100]. By reducing the food deterioration rate, freezing aids in preserving it for more extended periods. During freezing, water crystallises, potentially damaging the solute's microstructure [161]. The control of the crystallisation of water has been a focus of many researchers to prevent food damage. Several researchers have drawn attention to the positive impacts of static electric fields in preventing freezing damage to food. This is attributed to decreased free energy, enhancing nucleation rate through the realignment of water molecules and creating a more organised cluster structure [48]. Freezing under an electric field creates smaller ice crystals in food, which reduces freeze damage, minimises cell disruption, decreases drip loss, lessens protein denaturation, and preserves the texture of fresh food after thawing [100].

5.5. Future directions

The findings of this research open avenues for further research to deepen our understanding of the crystallisation process under electric fields and explore its practical applications in various scientific and industrial domains. The following sections outline potential areas where future studies could build upon the work presented in this thesis, addressing both theoretical and practical aspects to further the field of protein crystallisation and its related applications.

Electric-field-assisted crystallisation can be investigated further in various ways to continue the work done in this thesis. For example, a wider range of experimental conditions can be used to further understand the mechanism and kinetics of electric field effects. Electric fields can be used of various types (AC and DC), configurations (uniform and non-uniform, external and internal), electric field strength (weak and strong electric fields), and direction (in-plane

or perpendicular with the crystallisation drop plane). High-resolution microscopes can aid in determining accurate induction time measurements and real-time data collection.

The setups can also be used to investigate a broader range of proteins with different isoelectric points to enhance their nucleation, as they are easy to use and incorporated in crystallisation screening experiments. Using this approach may lead to further understanding of the behaviour of proteins at various experimental conditions when an electric field is applied. However, the bottleneck to these experiments is establishing automated data collection programs to extract information from the micrographs and make instant measurements of nucleation and growth parameters. This opens another window for further research.

The setups can be modified and improved by decreasing the distance between the electrodes and minimising the dielectric media between the droplet and the electrodes. This step ensures that a substantial and uniform electric field reaches the crystallisation droplet. In the current setup, this is limited by the topography of the crystallisation plates. This can be achieved by designing and 3D printing a platform for electrode insertions focused on each well while considering the ease of real-time monitoring.

The in situ crystallisation setup can be improved by modifying the shape and configuration of electrodes. An example is introducing plate electrodes at the top and bottom of the crystallisation well. This can strengthen the effect of the electric field, as real-time monitoring is not essential. Another approach is to design electrode plate sealing films incorporating electrode arrays that can be connected and disconnected from the crystallisation well as needed. Alternatively, to improve the in situ diffraction analysis, using automation when preparing the plates and performing the electric field experiments at the synchrotron facility can aid in avoiding damage and improving the quality of diffraction data.

Concluding remarks

This thesis has successfully developed and implemented four innovative, low-cost experimental setups to probe the effects of electric fields on protein crystallisation, utilising computer-aided design (CAD) and 3D printing technologies. These setups were precisely fabricated and rigorously tested for their efficacy, using HEWL as a model for crystallisation under the influence of external DC electric fields. The experimental investigations revealed that the application of electric fields significantly alters the crystallisation dynamics of HEWL, leading to notable changes in nucleation rates and crystal morphology. This work contributes to the fundamental understanding of electric-field-mediated protein crystallisation. It paves the way for future studies aiming to harness electric fields for enhanced crystal quality, potentially developing methods in structural biology and related fields.

The setups were utilised for the electric-field-assisted crystallisation of HEWL using different techniques, high voltage polarities, pH and protein concentrations. The microbatch and vapour diffusion crystallisation of HEWL enhanced nucleation, producing higher numbers of crystals with smaller, more homogenous sizes. In situ XRD analysis allowed the investigation of a large number of crystals due to the elimination of harvesting step, which demonstrated improved HEWL crystal quality under electric fields, which is evident from the lower mosaic spread and better internal order in the crystal lattice.

The findings presented in this thesis show that the electric field affects the nucleation and growth of protein crystals by modifying the system's chemical potentials and diffusion coefficients. Traditionally, these changes were explained by theories mainly focusing on the physicochemical aspects of crystallisation, such as supersaturation, temperature, and solution composition. The findings highlight the need for a deeper understanding of how

electric fields interact with protein molecules at a molecular level. This includes exploring how electric fields influence molecular dipoles, disrupt or enhance electrostatic interactions, and affect the energy landscape of protein nucleation and growth.

The research suggests that electric fields can alter the nucleation and growth processes, potentially by influencing the formation of critical nuclei size or modifying the nucleation energy barriers. This could lead to new theoretical models that describe nucleation in the presence of electric fields. These findings could have broader implications beyond protein crystallisation, impacting material sciences and nanotechnology. The principles discovered could be applied to the crystallisation of other materials, leading to new material synthesis and design techniques.

The need for computational models that can simulate the effects of electric fields on crystallisation processes is evident. Such models would be invaluable in predicting crystallisation outcomes, designing experiments, and furthering our understanding of this complex phenomenon.

In conclusion, the research conducted in this thesis opens new avenues for theoretical exploration and model development in the field of crystallisation, with potential applications extending far beyond protein crystallography.

References

1. Nanev, C.N., *Recent insights into the crystallization process; protein crystal nucleation and growth peculiarities; Processes in the Presence of Electric Fields.* Crystals, 2017. **7**(10): p. 310.
2. Hekstra, D.R., *Emerging Time-Resolved X-Ray Diffraction Approaches for Protein Dynamics.* Annu Rev Biophys, 2023. **52**: p. 255-274.
3. Pusey, M.L. and R.S. Aygün, *Data analytics for protein crystallization*. 2017: Springer.
4. Gicquel, Y., et al., *Microfluidic chips for in situ crystal X-ray diffraction and in situ dynamic light scattering for serial crystallography.* JoVE (Journal of Visualized Experiments), 2018(134): p. e57133.
5. Su, X.-D., et al., *Protein crystallography from the perspective of technology developments.* Crystallography reviews, 2015. **21**(1-2): p. 122-153.
6. Yeates, T.O. and S.B.H. Kent, *Racemic Protein Crystallography.* Annual Review of Biophysics, 2012. **41**(1): p. 41-61.
7. Rosenberger, F., *Protein crystallization.* Journal of crystal growth, 1996. **166**(1-4): p. 40-54.
8. Kurochkina, N., *Proteins and Protein Structure*, in *Protein Structure and Modeling*, N. Kurochkina, Editor. 2019, Springer Singapore: Singapore. p. 1-52.
9. Kauzmann, W., *Some Factors in the Interpretation of Protein Denaturation11The preparation of this article has been assisted by a grant from the National Science Foundation*, in *Advances in Protein Chemistry*, C.B. Anfinsen, et al., Editors. 1959, Academic Press. p. 1-63.
10. McPherson, A., *Protein crystallization.* Protein crystallography: Methods and protocols, 2017: p. 17-50.
11. Rashid, M., F. Khatib, and A. Sattar, *Protein preliminaries and structure prediction fundamentals for computer scientists.* http://arxiv.org, 2015.
12. Alberts, B., et al., *The shape and structure of proteins*, in *Molecular Biology of the Cell. 4th edition*. 2002, Garland Science.
13. Ahmad Mir, R., S. Mansoor Shafi, and S.M. Zargar, *Chapter 1 - Undestanding the OMICS techniques: an introduction to genomics and proteomics*, in *Principles of Genomics and Proteomics*, R. Ahmad Mir, S. Mansoor Shafi, and S.M. Zargar, Editors. 2023, Elsevier. p. 1-28.
14. Ouellette, R.J. and J.D. Rawn, *14 - Amino Acids, Peptides, and Proteins*, in *Principles of Organic Chemistry*, R.J. Ouellette and J.D. Rawn, Editors. 2015, Elsevier: Boston. p. 371-396.
15. Mu, X., et al., *An Overview of Microcrystal Electron Diffraction (MicroED).* Annual Review of Biochemistry, 2021. **90**(1): p. 431-450.
16. Fu, Z.-Q., H.L. Sha, and B. Sha, *AI-Based Protein Interaction Screening and Identification (AISID).* International Journal of Molecular Sciences, 2022. **23**(19): p. 11685.
17. Li, J. and J. Sun, *Application of X-ray Diffraction and Electron Crystallography for Solving Complex Structure Problems.* Accounts of Chemical Research, 2017. **50**(11): p. 2737-2745.
18. Ramos, N.G., et al., *The reproducible normality of the crystallographic B-factor.* Analytical Biochemistry, 2022. **645**: p. 114594.
19. Holcomb, J., et al., *Protein crystallization: Eluding the bottleneck of X-ray crystallography.* AIMS biophysics, 2017. **4**(4): p. 557-575.

20. Nannenga, B.L. and T. Gonen, *The cryo-EM method microcrystal electron diffraction (MicroED).* Nature Methods, 2019. **16**(5): p. 369-379.
21. Clabbers, M.T.B. and H. Xu, *Microcrystal electron diffraction in macromolecular and pharmaceutical structure determination.* Drug Discovery Today: Technologies, 2020. **37**: p. 93-105.
22. Khakurel, K.P., B. Angelov, and J. Andreasson, *Macromolecular nanocrystal structural analysis with electron and X-rays: A comparative review.* Molecules, 2019. **24**(19): p. 3490.
23. Clegg, W., *Space groups – the final frontier: a tutorial guided tour of some entries in International Tables for Crystallography Volume A.* Crystallography Reviews, 2023. **29**(4): p. 228-246.
24. Clegg, W., *41Space-group determination*, in *Crystal Structure Analysis: Principles and Practice*, W. Clegg, et al., Editors. 2009, Oxford University Press. p. 0.
25. Sheldrick, G., *SHELXT - Integrated space-group and crystal-structure determination.* Acta Crystallographica Section A, 2015. **71**(1): p. 3-8.
26. Kimura, F., et al., *Single-Crystal X-ray Diffraction Study of a Magnetically Oriented Microcrystal Array of Lysozyme.* Crystal Growth & Design, 2011. **11**(1): p. 12-15.
27. Cheng, R., et al., *In situ crystallography as an emerging method for structure solution of membrane proteins: the case of CCR2A.* The FEBS journal, 2020. **287**(5): p. 866-873.
28. Mazzorana, M., E.J. Shotton, and D.R. Hall, *A comprehensive approach to X-ray crystallography for drug discovery at a synchrotron facility — The example of Diamond Light Source.* Drug Discovery Today: Technologies, 2020. **37**: p. 83-92.
29. Sanchez-Weatherby, J., et al., *VMXi: a fully automated, fully remote, high-flux in situ macromolecular crystallography beamline.* Journal of synchrotron radiation, 2019. **26**(1): p. 291-301.
30. Mikolajek, H., et al., *Protein-to-structure pipeline for ambient-temperature in situ crystallography at VMXi.* IUCrJ, 2023. **10**(4): p. 420-429.
31. Garman, E., *Cool data: quantity AND quality.* Acta Crystallogr D Biol Crystallogr, 1999. **55**(Pt 10): p. 1641-53.
32. Garman, E., *'Cool' crystals: macromolecular cryocrystallography and radiation damage.* Current Opinion in Structural Biology, 2003. **13**(5): p. 545-551.
33. Gorrec, F., *A beginner's guide to macromolecular crystallization.* The Biochemist, 2021. **43**(1): p. 36-43.
34. Rodríguez-Romero, A., et al., *Crystal Growth of High-Quality Protein Crystals under the Presence of an Alternant Electric Field in Pulse-Wave Mode, and a Strong Magnetic Field with Radio Frequency Pulses Characterized by X-ray Diffraction.* Crystals, 2017. **7**(6): p. 179.
35. Abe, M., et al., *Evaluation of crystal quality of thin protein crystals based on the dynamical theory of X-ray diffraction.* IUCrJ, 2020. **7**(4): p. 761-766.
36. Rubin, E., C. Owen, and V. Stojanoff, *Crystallization under an external electric field: A case study of glucose isomerase.* Crystals, 2017. **7**(7): p. 206.
37. Pareja-Rivera, C., et al., *Recent advances in the understanding of the influence of electric and magnetic fields on protein crystal growth.* Crystal Growth & Design, 2017. **17**(1): p. 135-145.
38. Iwai, W., et al., *Crystallization and evaluation of hen egg-white lysozyme crystals for protein pH titration in the crystalline state.* J Synchrotron Radiat, 2008. **15**(Pt 3): p. 312-5.

39. Dubach, V.R.A. and A. Guskov, *The Resolution in X-ray Crystallography and Single-Particle Cryogenic Electron Microscopy.* Crystals, 2020. **10**(7): p. 580.
40. Cheraghian Radi, H., B. Hajipour-Verdom, and F. Molaabasi, *Macromolecular crystallization: basics and advanced methodologies.* Journal of the Iranian Chemical Society, 2021. **18**(3): p. 543-565.
41. Wang, Z., et al., *A new strategy for protein crystallization : Effect of ionic liquids on lysozyme crystallization and morphology.* Korean Journal of Chemical Engineering, 2014. **31**(6): p. 919-923.
42. Russo Krauss, I., et al., *An Overview of Biological Macromolecule Crystallization.* International Journal of Molecular Sciences, 2013. **14**(6): p. 11643-11691.
43. Shao, Y., et al., *Practical techniques for protein crystallization: additive assistance and external field intensification.* CrystEngComm, 2024.
44. Li, J., et al., *In Situ Atomic-Scale Study of Particle-Mediated Nucleation and Growth in Amorphous Bismuth to Nanocrystal Phase Transformation.* Advanced Science, 2018. **5**(6): p. 1700992.
45. Karthika, S., T.K. Radhakrishnan, and P. Kalaichelvi, *A Review of Classical and Nonclassical Nucleation Theories.* Crystal Growth & Design, 2016. **16**(11): p. 6663-6681.
46. Dimitrov, I.L., *Narrow size distribution of lysozyme crystals in a reverse vapor diffusion set-up.* CrystEngComm, 2023. **25**(10): p. 1471-1478.
47. Adrjanowicz, K., M. Paluch, and R. Richert, *Formation of new polymorphs and control of crystallization in molecular glass-formers by electric field.* Physical Chemistry Chemical Physics, 2018. **20**(2): p. 925-931.
48. Dalvi-Isfahan, M., et al., *Recent advances of high voltage electric field technology and its application in food processing: A review with a focus on corona discharge and static electric field.* Journal of Food Engineering, 2023. **353**: p. 111551.
49. Alexander, L.F. and N. Radacsi, *Application of electric fields for controlling crystallization.* CrystEngComm, 2019. **21**(34): p. 5014-5031.
50. Evgeniya, R., O. Christopher, and S. Vivian, *Crystallization under an External Electric Field: A Case Study of Glucose Isomerase.* Crystals, 2017. **7**(7): p. 206.
51. Taleb, M., et al., *Crystallization of proteins under an external electric field.* Journal of Crystal Growth, 1999. **200**(3-4): p. 575-582.
52. Taleb, M., et al., *Equilibrium kinetics of lysozyme crystallization under an external electric field.* Journal of crystal growth, 2001. **232**(1-4): p. 250-255.
53. Nanev, C.N. and A. Penkova, *Nucleation of lysozyme crystals under external electric and ultrasonic fields.* Journal of Crystal Growth, 2001. **232**(1-4): p. 285-293.
54. Saban, K., et al., *Thermodynamics of crystal nucleation in an external electric field.* Crystal Research and Technology: Journal of Experimental and Industrial Crystallography, 2002. **37**(11): p. 1188-1199.
55. Nanev, C.N. and A. Penkova, *Nucleation and growth of lysozyme crystals under external electric field.* Colloids and Surfaces A: Physicochemical and Engineering Aspects, 2002. **209**(2-3): p. 139-145.
56. Mirkin, N., et al., *The influence of an internal electric field upon protein crystallization using the gel-acupuncture method.* Acta Crystallographica Section D: Biological Crystallography, 2003. **59**(9): p. 1533-1538.
57. Charron, C., et al., *TheOctopus' plate for protein crystallization under an electric field.* Journal of applied crystallography, 2003. **36**(6): p. 1482-1483.

58. Sazaki, G., A. Moreno, and K. Nakajima, *Novel coupling effects of the magnetic and electric fields on protein crystallization.* Journal of crystal growth, 2004. **262**(1-4): p. 499-502.
59. Aber, J.E., et al., *Strong dc electric field applied to supersaturated aqueous glycine solution induces nucleation of the γ polymorph.* Physical review letters, 2005. **94**(14): p. 145503.
60. Al-haq, M.I., et al., *Protein crystallization under an electric field.* Crystallography Reviews, 2007. **13**(1): p. 29-64.
61. Al-Haq, M.I., et al., *An apparatus for electric-field-induced protein crystallization.* Journal of Applied Crystallography, 2007. **40**(1): p. 199-201.
62. Al‐Haq, M.I., et al., *An apparatus for electric‐field‐induced protein crystallization.* Journal of Applied Crystallography, 2007. **40**(1): p. 199-201.
63. Koizumi, H., K. Fujiwara, and S. Uda, *Control of nucleation rate for tetragonal hen-egg white lysozyme crystals by application of an electric field with variable frequencies.* Crystal Growth and Design, 2009. **9**(5): p. 2420-2424.
64. Koizumi, H., et al., *Control of effect on the nucleation rate for hen egg white lysozyme crystals under application of an external ac electric field.* Langmuir, 2011. **27**(13): p. 8333-8338.
65. Koizumi, H., et al., *Nucleation rate enhancement of porcine insulin by application of an external AC electric field.* Journal of crystal growth, 2012. **352**(1): p. 155-157.
66. Pan, W., et al., *The influence of low frequency of external electric field on nucleation enhancement of hen egg-white lysozyme (HEWL).* Journal of Crystal Growth, 2015. **428**: p. 35-39.
67. Li, F. and R. Lakerveld, *Electric-field-assisted protein crystallization in continuous flow.* Crystal Growth & Design, 2018. **18**(5): p. 2964-2971.
68. Walter, T.s.K., et al., *Use of Protein Thin Film Organized by External Electric Field as a Template for Protein Crystallization.* ACS omega, 2018. **3**(8): p. 8683-8690.
69. Ogata, M., et al., *The role of an applied electric field in protein crystallization at low temperature.* Japanese Journal of Applied Physics, 2019. **58**(11): p. 110903.
70. Tanaka, D., R. Hijiya, and T. Wakamatsu, *The effects of applying an alternating electric field to lysozyme solutions during the initial crystallization stage.* Journal of Crystal Growth, 2021. **573**: p. 126288.
71. Wu, H., et al., *Investigation of Dipolar Response of the Hydrated Hen-Egg White Lysozyme Complex under Externally Applied Electric Fields: Insights from Non-equilibrium Molecular Dynamics.* The Journal of Physical Chemistry B, 2022. **126**(4): p. 858-868.
72. Lychev, A.P., Y.S. Rudenko, and A.I. Cheremisin, *Effect of an electric field on crystallization.* Soviet Physics Journal, 1977. **20**(4): p. 441-444.
73. Uda, S., X. Huang, and S. Koh, *Transformation of the incongruent-melting state to the congruent-melting state via an external electric field for the growth of langasite.* Journal of Crystal Growth, 2005. **281**(2): p. 481-491.
74. Koizumi, H., et al., *Crystallization of high-quality protein crystals using an external electric field.* Journal of Applied Crystallography, 2015. **48**(5): p. 1507-1513.
75. Kudryavtsev, A., et al., *The effect of ordering of internal water in thaumatin and lysozyme crystals as revealed by Raman method.* Journal of crystal growth, 2000. **219**(1-2): p. 102-114.

76. Li, W.W., et al., *Solid Separation from a Mixed Suspension through Electric‐Field‐Enhanced Crystallization.* Angewandte Chemie International Edition, 2016. **55**(52): p. 16088-16091.
77. Huda, N. and A.K. Bhuyan, *Protein Crystallization in Very Weak DC Electric Field.* Crystal Growth & Design, 2023. **23**(9): p. 6570-6577.
78. Moreno, A. and G. Sazaki, *The use of a new ad hoc growth cell with parallel electrodes for the nucleation control of lysozyme.* Journal of crystal growth, 2004. **264**(1-3): p. 438-444.
79. Koizumi, H., K. Fujiwara, and S. Uda, *Role of the electric double layer in controlling the nucleation rate for tetragonal hen egg white lysozyme crystals by application of an external electric field.* Crystal Growth and Design, 2010. **10**(6): p. 2591-2595.
80. Chayen, N.E., *The role of oil in macromolecular crystallization.* Structure, 1997. **5**(10): p. 1269-1274.
81. Hirao, A., et al. *Protein Crystallization in Microdroplets with the Aid of Electrically Induced Microbubbles*. in *2021 IEEE 34th International Conference on Micro Electro Mechanical Systems (MEMS)*. 2021. IEEE.
82. Flores-Hernández, E., et al., *An electrically assisted device for protein crystallization in a vapor-diffusion setup.* Journal of applied crystallography, 2013. **46**(3): p. 832-834.
83. Koizumi, H., et al., *Improvement of crystal quality for tetragonal hen egg white lysozyme crystals under application of an external alternating current electric field.* Journal of Applied Crystallography, 2013. **46**(1): p. 25-29.
84. Koizumi, H., et al., *Control of subgrain formation in protein crystals by the application of an external electric field.* Crystal growth & design, 2014. **14**(11): p. 5662-5667.
85. Hou, D. and H.-C. Chang, *AC field enhanced protein crystallization.* Applied Physics Letters, 2008. **92**(22): p. 223902.
86. Sui, S., et al., *A graphene-based microfluidic platform for electrocrystallization and in situ X-ray diffraction.* Crystals, 2018. **8**(2): p. 76.
87. Kumar, P. and S. Sharma, *An overview of purification methods for proteins.* Ijar, 2015. **1**(12): p. 450-459.
88. Jha, P.K., et al., *A review on effect of DC voltage on crystallization process in food systems.* Innovative Food Science and Emerging Technologies, 2017. **42**: p. 204-219.
89. Wolff, A.M., et al., *Comparing serial X-ray crystallography and microcrystal electron diffraction (MicroED) as methods for routine structure determination from small macromolecular crystals.* IUCrJ, 2020. **7**(Pt 2): p. 306-323.
90. McPHERSON, A., *Current approaches to macromolecular crystallization.* European Journal of Biochemistry, 1990. **189**(1): p. 1-23.
91. Bergfors, T.M., *Protein crystallization*. 2009: Internat'l University Line.
92. Chayen, N.E., *Crystallization with oils: a new dimension in macromolecular crystal growth.* Journal of Crystal Growth, 1999. **196**(2-4): p. 434-441.
93. D'Arcy, A., A. Mac Sweeney, and A. Haber, *Practical aspects of using the microbatch method in screening conditions for protein crystallization.* Methods, 2004. **34**(3): p. 323-328.
94. Chayen, N.E., *Protein crystallization for genomics: throughput versus output.* Journal of structural and functional genomics, 2003. **4**(2): p. 115-120.
95. Tomita, Y., et al., *Control of Gibbs free energy relationship between hen egg white lysozyme polymorphs under application of an external alternating current electric field.* Journal of Applied Crystallography, 2012. **45**(2): p. 207-212.

96. Chayen, N.E., *A novel technique for containerless protein crystallization.* Protein Engineering, Design and Selection, 1996. **9**(10): p. 927-929.
97. Koizumi, H., et al., *Technique for high-quality protein crystal growth by control of subgrain formation under an external electric field.* Crystals, 2016. **6**(8): p. 95.
98. Koizumi, H., et al., *Effect of an External Electric Field on the Kinetics of Dislocation-Free Growth of Tetragonal Hen Egg White Lysozyme Crystals.* Crystals, 2017. **7**(6): p. 170.
99. Koizumi, H., et al., *Effect of various precipitants on the nucleation rate of tetragonal hen egg-white lysozyme crystals in an AC external electric field.* Journal of crystal growth, 2010. **312**(23): p. 3503-3508.
100. Jha, P.K., et al., *A review on effect of DC voltage on crystallization process in food systems.* Innovative Food Science & Emerging Technologies, 2017. **42**: p. 204-219.
101. Singer, W., H. Rubinsztein-Dunlop, and U. Gibson, *Manipulation and growth of birefringent protein crystals in optical tweezers.* Optics Express, 2004. **12**(26): p. 6440-6445.
102. Kashchiev, D., *Nucleation*, in *Nucleation*, D. Kashchiev, Editor. 2000, Butterworth-Heinemann: Oxford. p. ix-xii.
103. Yuan, Z., et al., *Protein crystal regulation and harvest via electric field-based method.* Current Opinion in Chemical Engineering, 2022. **36**: p. 100744.
104. Nieto-Mendoza, E., et al., *Investigations on electromigration phenomena for protein crystallization using crystal growth cells with multiple electrodes: effect of the potential control.* Journal of Crystal Growth, 2005. **275**(1-2): p. e1437-e1446.
105. Tao, R. and H. Tang, *Reducing viscosity of paraffin base crude oil with electric field for oil production and transportation.* Fuel, 2014. **118**: p. 69-72.
106. Chen, X., et al., *Influence of electric field on the viscosity of waxy crude oil and micro property of paraffin: A molecular dynamics simulation study.* Journal of Molecular Liquids, 2018. **272**: p. 973-981.
107. D'Arcy, A., et al., *A novel approach to crystallising proteins under oil.* Journal of Crystal Growth, 1996. **168**(1): p. 175-180.
108. Judge, R.A., et al., *The effect of temperature and solution pH on the nucleation of tetragonal lysozyme crystals.* Biophys J, 1999. **77**(3): p. 1585-93.
109. Langenburg, G.M., *Pilot-Study: A Statistical Analysis of the ACE-V Methodology - Analysis Stage.* Journal of Forensic Identification, 2004. **54**(1): p. 64-79.
110. Penkova, A., et al., *Enhancement and suppression of protein crystal nucleation due to electrically driven convection.* Journal of Crystal Growth, 2005. **275**(1-2): p. e1527-e1532.
111. Rayment, I., *Small-scale batch crystallization of proteins revisited: an underutilized way to grow large protein crystals.* Structure, 2002. **10**(2): p. 147-151.
112. Dessau, M.A. and Y. Modis, *Protein crystallization for X-ray crystallography.* J Vis Exp, 2011(47).
113. Chayen, N.E., *Comparative studies of protein crystallization by vapour-diffusion and microbatch techniques.* Acta Crystallographica Section D: Biological Crystallography, 1998. **54**(1): p. 8-15.
114. Sauter, C., et al., *Vapour-diffusion methods.* 2012.
115. Sun, C. and D. Xue, *Crystallization: A phase transition process driving by chemical potential decrease.* Journal of Crystal Growth, 2017. **470**: p. 27-32.
116. Vekilov, P.G., *Nucleation.* Crystal Growth & Design, 2010. **10**(12): p. 5007-5019.

117. Nanev, C., *On some aspects of crystallization process energetics, logistic new phase nucleation kinetics, crystal size distribution and Ostwald ripening.* Journal of Applied Crystallography, 2017. **50**(4): p. 1021-1027.
118. Penkova, A., et al., *Nucleation of protein crystals under the influence of solution shear flow.* Annals of the New York Academy of Sciences, 2006. **1077**(1): p. 214-231.
119. Jen, A. and H.P. Merkle, *Diamonds in the Rough: Protein Crystals from a Formulation Perspective.* Pharmaceutical Research, 2001. **18**(11): p. 1483-1488.
120. Wukovitz, S.W. and T.O. Yeates, *Why protein crystals favour some space-groups over others.* Nature Structural Biology, 1995. **2**(12): p. 1062-1067.
121. Stubbs, M.T., *Protein Crystallography*, in *Reference Module in Chemistry, Molecular Sciences and Chemical Engineering*. 2013, Elsevier.
122. Shmueli, U., H. Flack, and J. Spence, *Methods of space-group determination.* 2016.
123. Fecher, G.H., J. Kübler, and C. Felser, *Chirality in the solid state: Chiral crystal structures in chiral and achiral space groups.* Materials, 2022. **15**(17): p. 5812.
124. Johnson, L.N., *The structure and function of lysozyme.* Science Progress (1933-), 1966. **54**(215): p. 367-385.
125. Blake, C.C.F., et al., *On the Conformation of the Hen Egg-White Lysozyme Molecule.* Proceedings of the Royal Society of London. Series B, Biological Sciences, 1967. **167**(1009): p. 365-377.
126. Artymiuk, P.J., et al., *The structures of the monoclinic and orthorhombic forms of hen egg-white lysozyme at 6 A resolution.* Acta Crystallographica Section B, 1982. **38**(3): p. 778-783.
127. Ewing, F., E. Forsythe, and M. Pusey, *Orthorhombic lysozyme solubility.* Acta Crystallographica Section D, 1994. **50**(4): p. 424-428.
128. Harata, K. and T. Akiba, *Structural phase transition of monoclinic crystals of hen egg-white lysozyme.* Acta Crystallographica Section D, 2006. **62**(4): p. 375-382.
129. Zhang, T., et al., *Electron density map evaluation functions for determining the quality of protein crystal structures.* Radiation Detection Technology and Methods, 2018. **2**(2): p. 42.
130. Maeki, M., et al., *Real-Time Measurement of Protein Crystal Growth Rates within the Microfluidic Device to Understand the Microspace Effect.* ACS Omega, 2020. **5**(28): p. 17199-17206.
131. Chernov, A.A., *Protein crystals and their growth.* Journal of Structural Biology, 2003. **142**(1): p. 3-21.
132. Tait, S., E.T. White, and J.D. Litster, *Mechanical Characterization of Protein Crystals.* Particle & Particle Systems Characterization, 2008. **25**(3): p. 266-276.
133. le Maire, A., et al., *In-plate protein crystallization, in situ ligand soaking and X-ray diffraction.* Acta Crystallographica Section D, 2011. **67**(9): p. 747-755.
134. Aller, P., et al., *Application of In Situ Diffraction in High-Throughput Structure Determination Platforms*, in *Structural Proteomics: High-Throughput Methods*, R.J. Owens, Editor. 2015, Springer New York: New York, NY. p. 233-253.
135. Pusey, M.L. and A. Nadarajah, *A Model for Tetragonal Lysozyme Crystal Nucleation and Growth.* Crystal Growth & Design, 2002. **2**(6): p. 475-483.
136. Annunziata, O., A. Payne, and Y. Wang, *Solubility of Lysozyme in the Presence of Aqueous Chloride Salts: Common-Ion Effect and Its Role on Solubility and Crystal Thermodynamics.* Journal of the American Chemical Society, 2008. **130**(40): p. 13347-13352.

137. Karplus, P.A. and K. Diederichs, *Linking crystallographic model and data quality.* Science, 2012. **336**(6084): p. 1030-1033.
138. Lorber, B., et al., *Crystal growth of proteins, nucleic acids, and viruses in gels.* Progress in biophysics and molecular biology, 2009. **101**(1-3): p. 13-25.
139. Kisselman, G., et al., *X-CHIP: an integrated platform for high-throughput protein crystallization and on-the-chip X-ray diffraction data collection.* Acta Crystallographica Section D: Biological Crystallography, 2011. **67**(6): p. 533-539.
140. Axford, D., et al., *In situ macromolecular crystallography using microbeams.* Acta Crystallographica Section D, 2012. **68**(5): p. 592-600.
141. Parks, C., et al., *Molecular Dynamics Electric Field Crystallization Simulations of Paracetamol Produce a New Polymorph.* Crystal Growth & Design, 2017. **17**(7): p. 3751-3765.
142. Wondratschek, H., *Classifications of space groups, point groups and lattices*, in *International Tables for Crystallography Volume A: Space-group symmetry*, T. Hahn, Editor. 2002, Springer Netherlands: Dordrecht. p. 726-731.
143. Sharma, P., et al., *Characterization of heat induced spherulites of lysozyme reveals new insight on amyloid initiation.* Scientific Reports, 2016. **6**(1): p. 22475.
144. Rosenberger, F., et al., *Nucleation and crystallization of globular proteins — what we know and what is missing.* Journal of Crystal Growth, 1996. **168**(1): p. 1-27.
145. Kuehner, D.E., et al., *Lysozyme net charge and ion binding in concentrated aqueous electrolyte solutions.* The Journal of Physical Chemistry B, 1999. **103**(8): p. 1368-1374.
146. Durbin, S.D. and G. Feher, *PROTEIN CRYSTALLIZATION.* Annual Review of Physical Chemistry, 1996. **47**(1): p. 171-204.
147. Judge, R.A., et al., *The Effect of Temperature and Solution pH on the Nucleation of Tetragonal Lysozyme Crystals.* Biophysical Journal, 1999. **77**(3): p. 1585-1593.
148. Reguera, D. and J.M. Rubí, *Homogeneous nucleation in inhomogeneous media. II. Nucleation in a shear flow.* The Journal of Chemical Physics, 2003. **119**(18): p. 9888-9893.
149. Nicholson, S.T., et al., *Characterization of Mass Transfer within the Crystal-Solution Boundary Layer of l-Alanine {120} Faces Using Laser Interferometry during Growth and Dissolution.* Crystal Growth & Design, 2023. **23**(4): p. 2755-2769.
150. Moreno, A. and M.E. Mendoza, *31 - Crystallization in Gels*, in *Handbook of Crystal Growth (Second Edition)*, P. Rudolph, Editor. 2015, Elsevier: Boston. p. 1277-1315.
151. Tanaka, H., et al., *Diffusion coefficient of the protein in various crystallization solutions: The key to growing high-quality crystals in space.* Microgravity - Science and Technology, 2006. **18**(3): p. 91-94.
152. McPherson, A. and L.J. DeLucas, *Microgravity protein crystallization.* npj Microgravity, 2015. **1**(1): p. 15010.
153. Talapatra, S.K., et al., *Design, 3D printing and validation of a novel low-cost high-capacity sitting-drop bridge for protein crystallization.* Journal of Applied Crystallography, 2019. **52**(1): p. 171-174.
154. Mathew Thomas, K. and R. Lakerveld, *An Airlift Crystallizer for Protein Crystallization.* Industrial & Engineering Chemistry Research, 2019. **58**(44): p. 20381-20391.
155. Marchenkova, M.A., et al., *3D Printed Microfluidic Cell for SAXS Time-Resolved Measurements of the Structure of Protein Crystallization Solutions.* Crystals, 2023. **13**(6): p. 938.

156. Ei Ei, H., et al., *Adsorption of lysozyme on base metal surfaces in the presence of an external electric potential.* Colloids and Surfaces B: Biointerfaces, 2016. **147**: p. 9-16.
157. Grey, J.L. and D.H. Thompson, *Challenges and opportunities for new protein crystallization strategies in structure-based drug design.* Expert Opinion on Drug Discovery, 2010. **5**(11): p. 1039-1045.
158. Rondeau, J.-M. and H. Schreuder, *Protein crystallography and drug discovery*, in *The practice of medicinal chemistry*. 2008, Elsevier. p. 605-634.
159. Derewenda, Z.S., *Protein crystallization in drug design: towards a rational approach.* Expert Opinion on Drug Discovery, 2007. **2**(10): p. 1329-1340.
160. Datta, S. and D.J. Grant, *Crystal structures of drugs: advances in determination, prediction and engineering.* Nature Reviews Drug Discovery, 2004. **3**(1): p. 42-57.
161. Adrjanowicz, K. and R. Richert, *Control of crystallization pathways by electric fields*, in *Crystallization as Studied by Broadband Dielectric Spectroscopy*. 2020, Springer. p. 149-167.
162. Hartje, L.F. and C.D. Snow, *Protein crystal based materials for nanoscale applications in medicine and biotechnology.* Wiley Interdisciplinary Reviews: Nanomedicine and Nanobiotechnology, 2019. **11**(4): p. e1547.
163. Ferreira, C.F.d.G., P.C. Camargo, and E.M. Benelli, *Formation of Organized Protein Thin Films with External Electric Field.* The Journal of Physical Chemistry B, 2015. **119**(39): p. 12561-12567.
164. Pehlivanova, V., et al., *The role of alternating current electric field for cell adhesion on 2D and 3D biomimetic scaffolds based on polymer materials and adhesive proteins.* Journal of Materials Research, 2013. **28**(16): p. 2180-2186.

Supplementary Materials

Table S1. The parameters used for printing the experimental setups

Material	PLA
Nozzle diameter	0.4 mm
Layer Height	0.2 mm
Profile	Fine - 0.1mm
Infill Pattern	Triangles
Infill Density	20 %
Print Speed	55 mm/s
Printing Temperature	235 °C
Build Plate Temperature	70 °C
Fan Speed	20 %
Support	No
Build Plate Adhesion	Skirt
Wall Thickness	1.3 mm
Wall Line Count	4
Top/Bottom Thickness	1.2 mm
Top Thickness	1.2 mm
Top Layers	6
Bottom Thickness	1.2 mm
Bottom Layers	6
Horizontal Expansion	0 mm